UNIVERSITY OF OKLAHOMA

GRADUATE COLLEGE

Atomic Layer Deposition Seeded ZnO Nanowires in Hybrid Carbon Fiber Composites: Synthesis, Characterization and Multifunctionality

A DISSERTATION

SUBMITTED TO THE GRADUATE FACULTY

in partial fulfillment of the requirements for the

Degree of

DOCTOR OF PHILOSOPHY

By

JINGYU WANG
Norman, Oklahoma
2019

Atomic Layer Deposition Seeded ZnO Nanowires in Hybrid Carbon Fiber Composites: Synthesis, Characterization and Multifunctionality

A DISSERTATION APPROVED FOR THE
SCHOOL OF AEROSPACE AND MECHANICAL ENGINEERING

BY THE COMMITTEE CONSISTING OF

Dr. Yingtao Liu, Chair

Dr. M. Cengiz Altan

Dr. Mrinal Saha

Dr. Zahed Siddique

Dr. Bin Wang

Dr. Binbin Weng

Table of Contents

Abstract

Recent advances of zinc oxide (ZnO) nanowires have attracted extensive interests due to their multifunctional properties. In this dissertation, well-aligned ZnO nanowires were synthesized as the interfacial enhancement in carbon fiber reinforced composites using atomic layer deposition (ALD) and hydrothermal methods. Optimal synthesis of ZnO seed layers on silicon substrate was first studied to understand the impact of growth parameters in ALD process including H2O/DiethylZinc (DEZn) dose ratio, background pressure, and temperature. Aligned ZnO nanowires on silicon substrate were grown from the ZnO seeds deposited by ALD treatment. Then, the developed ZnO nanowire synthesis methods were employed to grow aligned ZnO nanoarrays on carbon fiber fabrics for structural composite applications. The effects of key ALD parameters on the morphologies of ZnO nanowires were studied. In addition, the effect of temperature, growth time and concentration of zinc nitrate hydrate and hexamethylenetetramine (HMTA) during the hydrothermal treatment was characterized. Critical ZnO properties, such as morphologies, crystal phase and element identification, were characterized using field emission scanning electron microscope (FESEM), energy-dispersive X-ray spectroscopy (EDX), X-ray diffraction (XRD) and thermogravimetric analysis (TGA). Experimental results demonstrated that the properties of ZnO nanowires could be controlled by adjusting the key parameters during ALD and hydrothermal syntheses. Single fiber tensile test and single fiber fragmentation test (SFFT) were carried out to verify the influence of ZnO nanowires on carbon fiber properties as an interphase between carbon fiber and polymer matrix. The tensile strength of carbon fiber with ZnO nanowires preserved as the maximum temperature in growth process was only 200 °C. Single fiber fragmentation test revealed that the interfacial shear strength (IFSS) in epoxy composites improved by 286%. The experimental results indicated that the hierarchical carbon fibers enhanced by aligned ZnO

nanowires in epoxy composites were effective to improve IFSS. Surface energy and wetting properties of carbon fiber fabrics with aligned ZnO nanostructures were also explored. It was found that controlling the morphology of ZnO nanowires could result in significant change of surface energy of carbon fiber fabrics, changing their surface properties from hydrophobicity to hydrophilicity.

The impact of aligned ZnO nanowires on the interfacial properties in carbon fiber reinforced composites were systematically studied in this dissertation. Carbon fiber composite laminates were manufactured by vacuum assisted resin transfer molding (VARTM) with external pressure with incorporation of ZnO nanowires. Dynamic mechanical analysis (DMA), 3-point bending test and short beam 3-point bending test were conducted using hybrid carbon fiber composites to investigate the effects of different morphologies of ZnO nanowires on the interfacial properties in composites. Experimental results showed that the employment of ZnO nanowires has leaded to a maximum reinforcement in both flexural strength and interlaminar shear strength (ILSS) by up to 45.6% and 31.1%, respectively.

In summary, this dissertation developed a novel approach to synthesize well-aligned ZnO nanowires on carbon fiber fabrics using the combined ALD and hydrothermal methods. The successful development and characterization of ZnO nanowires enhanced structural composites have great potential to lead to the new generation of lightweight materials with increased mechanical properties for broad mechanical and aerospace engineering applications.

Dedication

To all the people accompany me in this journey.

Acknowledgments

I would like to express my highest respect and sincere appreciation to my advisor Dr. Yingtao Liu who creates an excellent research environment and training platform that greatly improve my scientific research ability. Dr. Liu is knowledgeable and enthusiastic, always giving me tremendous supports, positive feedbacks and constant encouragements during my research exploring. Many problems have been solved after the creative and patient discussions with him which benefit my academic career greatly. Without his valuable guidance and insights, this work would not be completed.

I also appreciate Dr. Binbin Weng for training me to use the atomic layer deposition system and other facilities in clean room, helping me to replace the precursors and teaching me how to conquer the obstacles in research. I would like to thank Dr. Mrinal Saha and Dr. M. Cengiz Altan for the usage of their laboratory apparatus and instruction of manufacturing carbon fiber composites. Thank Dr. Zahed Siddique and Dr. Bin Wang for being my committee member and giving me precious suggestions. Thank Dr. Preston Larson for offering the training and usage of scanning electron microscopy and atomic force microscopy.

I am also grateful for all stuffs in aerospace and mechanical engineering department including Billy Mays, Greg Williams, Bethany Burklund, Melissa Foster, Ellen McKenzie, Martina Ferguson and Rebeka Morales. I appreciate them for their assistance and support during my time at OU.

Thank Drs. Maya Pishvar, Mehrad Amirkhosravi, M Akif Yalcinkaya and Gorkem E. Guloglu for their advice and help in manufacturing composites. I would like to thank my lab mates Wanru Shang, Yi Hsu, Mark Olima, Chowdhury Shoieb, Wenyuan Luo, Parisa Marashizadeh and

Blake Herren. Thank you all for the companionship and friendship which have made my study time unforgettable. I wish you all the success and bright future. I also thank the people who are unnamed here that knowing you is the best luck in my life.

Thank all my family members for their understanding and support for me. Their selfless tolerance, care and dedication have always warmed me and inspired me to move forward. It is their love that makes me break through the difficulties in my life and move towards a better tomorrow.

Table list

Figure list

Chapter 1 Introduction

1.1 Interfacial treatments

The interphase of carbon fiber composites transfers shear stress between carbon fiber and polymer matrix. Debonding of carbon fiber to the matrix which causes the failure of composites will occur when the regional shear stress exceeds the interfacial shear strength of carbon fiber composites. In order to improve the better performance of composites, various methods of modifying the surface of carbon fiber attract numerous interests mainly composed of surface functionalization and roughening, and building secondary interphase.

1.1.1 Surface functionalization and roughening

The interaction between carbon fiber and polymer matrix can be improved by functionalizing and roughening the surface of carbon fiber. High reactivity of functional groups can be created on the surface of carbon fiber to increase the wetting and adhesion of carbon fiber to the polymer matrix, and the roughed surface of carbon fiber can mechanically interlock with polymer matrix by removing the smooth outer layers of carbon fiber. These treatments can improve the adhesion between carbon fiber and polymer matrix, but in-plane mechanical properties such as tensile strength of carbon fiber will decrease due to the damage in these processes. The common methods in these treatments include acidic and basic oxidation[1], plasma oxidation[2], electrochemical oxidation[3] and high energy irradiation[4].

N. Li et al.[1] treated the carbon fiber with aqueous ammonia etching, nitric acid oxidation and combined aqueous ammonia/nitric acid. Oxygen-containing functional groups were created on carbon fiber surface by nitric acid and the roughness was improved by aqueous ammonia. Better wettability of carbon fiber was obtained and the tensile strength of carbon fiber slightly loosed. The maximum improvement of IFSS was 43.36% compared to bare carbon fiber.

S. Erden et al.[2]used the continuous atmospheric plasma oxidation to treat the surface of carbon fiber. Polar oxygen-containing groups were introduced to the surface of carbon fiber and the wettability was improved. The single fiber fragmentation test showed that the IFSS was improved from 40 to 83 MPa when the carbon fiber was exposed under the plasma for 4 minutes.

D.K. Kim et al.[3] investigated the influence of electrochemical oxidation on carbon fiber. Oxygen functional groups were created and the fiber roughness was increased. Micro-bond method was used to evaluate the interfacial shear strength. It was found that the adhesion between carbon fiber and epoxy resin was greatly increased and the IFSS was increased up to 144% compared to the pristine carbon fiber.

L. Xing et al.[4] showed that high energy irradiation could be an effective way to improve the IFSS between domestic aramid fiber and epoxy chloropropane. The number of polar groups were created on the fiber surface, and the roughness and wettability of carbon fiber were improved. When the irritation energy was 400kGy, the IFSS was 68.57MPa which was increased by 45.17% compared to domestic aramid fiber composites without treatment.

1.1.2 Building secondary interphase

Building secondary interphase between fiber and polymer matrix was also an effective method to increase the IFSS as the new interphase can increase the adhesion, improve the load transfer and enlarge the contact area of fiber surface. The secondary interphase on carbon fiber includes thin film of sizing[5] and nanostructures such as carbon nanotubes[6] and ZnO nanowires[7]. The sizing layer will have a better adhesion to the polymer matrix compared to the fiber directly bonds with matrix. The sizing was compatible with both fiber and polymer. Nanostructured interfaces such as aligned carbon fiber nanotubes and ZnO nanowires have a much larger surface

contact area and the nanostructures inserted into the polymer matrix will work as mechanical interlocking.

Z.H. Dai et al.[5] studied the interfacial adhesion of sized and desized T300B and T700SC carbon fibers to evaluate the effect of sizing. The polar surface energy of desized carbon fiber was lower and the concentration of activated carbon atoms was smaller compared to the two commercial carbon fibers. It concluded that the IFSS of carbon fiber composites depended on both chemical bonding and physically adhesive interaction.

Carbon nanotubes have excellent mechanical properties that can reinforce both in-plane and out-plane properties of composites. The employment of carbon nanotubes can significantly increase the IFSS as the aligned carbon nanotubes can improve the load transfer. Chemical vapor deposition (CVD) was usually used to synthesized carbon nanotubes. However, the high temperature and involvement of catalyst in CVD process will result in the degradation of carbon fiber and formation of defects in composites.

R.J. Sager et al.[6] used CVD to grow radially aligned and randomly oriented carbon nanotubes on T650 carbon fiber. The tensile strength of carbon fiber reduced by 37% and 30% for each morphologies of carbon nanotubes. The thermal degradation and surface oxidation during CVD process were believed to add the surface defects resulting in the reduced mechanical properties of carbon fiber. Based on the results of single fiber fragmentation test, the IFSS of both were improved by 71% and 11% for randomly oriented and aligned carbon nanotubes. The presence of nanotubes increased the interphase shear yield strength and adhesion of matrix to the fiber.

To overcome the disadvantages of growing carbon nanotubes by CVD, Y. Lin et al.[7] proposed a novel approach using two-step hydrothermal method to grow ZnO nanowires on carbon fiber to increase the IFSS. The tensile properties of carbon fiber preserved due to low temperature during growth. The rigid ZnO nanowires penetrated into the polymer matrix and improved the load transfer. The incorporation of ZnO nanowires significantly increased the IFSS by 113%.

S.A. Song et al.[8] modified Lin's method, using electrochemical deposition method to deposit seed layers of ZnO nanoparticles in the first step of hydrothermal growth. Microwave radiation was used to boost the growth of ZnO nanorods in the second step of growth. The growth time of ZnO nanowires was greatly reduced by 95.8% due to the employment of microwave. The dense and uniform ZnO nanorods increased the IFSS by up to 56.2%.

1.2 ZnO nanowires growth

Zinc oxide (ZnO) is a significant semiconductor material due to its direct wide band gap (~3.3 eV at 300 K) and large exciton binding energy (~60 meV)[9]. Zinc oxide also has excellent chemical and thermal stability, nontoxicity, biocompatibility, antibacterial, and piezoelectric properties[9-11]. These multifarious properties of ZnO make it as one of the most multi-functional materials, so extensive interest has been attracted in variable applications such as solar cells[12], ultraviolet lasers[13], light emitting diodes[14], gas sensors[15], photo detectors[16], photo catalysts[17], piezoelectric nano-generators[10], interface strength enhancement[7] and others.

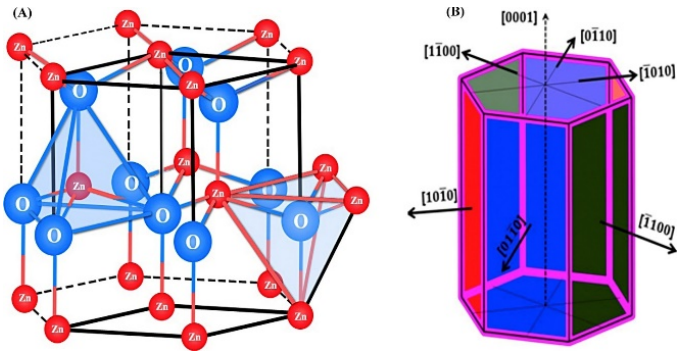

Figure 1-1 (a) Hexagonal wurtzite crystal structure of ZnO, (b) Hexagonal prism of ZnO crystal showing different crystallographic faces[18].

ZnO is a direct wide bandgap semiconductor material with piezoelectric and optoelectronic properties that belongs to the hexagonal line with wurtzite crystal structure which is shown in Figure 1-1. For its lattice constant, a= 0.32495 nm, c= 0.52069 nm, the ratio of c/a is 1.602 which is less than 1.633 (for ideal hexagonal structure)[19]. The crystal structure shows that in its unit cell, each zinc is originally tetrahedral with four oxygen atoms. Viewing from the (0001) direction, ZnO is densely deposited from Zn surface and O surface. This arrangement leads to ZnO with a Zn polarized surface (generally noted as (0001)) and an O-polarized surface (generally noted as $(000\bar{1})$)[19]. These two types of polarized surfaces have different properties in experiments showing that the Zn surface is smoother than the O surface. The crystallographic structure of ZnO also determines that the crystal prefers growth in c-axis orientation, which is suitable for the growth of high-quality oriented epitaxial films.

The key to the application of nanomaterials is to build them into a highly aligned nanoarray structure in a wide range, so fabrication of uniform alignment of nanoarray has become the focus of scientists all over the world. The methods of fabrication of ZnO nanoarray mainly are vapor-liquid-solid (VLS), vapor-solid (VS), template and wet chemical growth.

1.2.1 Vapor-Liquid-Solid (VLS)

Synthesis of one-dimensional ZnO nanostructured materials have been reported more and more based on the VLS growth mechanism of the catalytic reaction. In 2001, P.D. Yang [13] used VLS method to fabricate ZnO nanowire arrays on sapphire substrates with Au nanoparticles as catalyst. The specific growth method is that first, a layer of Au film was grown on the substrate, then an equal amount of ZnO powder and graphite powder were mixed as starting materials and put in the center of the boat in furnace. The substrates and starting materials were heated up to 800 °C to 905 °C in an Ar flow. Zn vapor was generated by carbothermal reduction of ZnO and transported to the substrates where ZnO nanowires grew. ZnO nanowires arrays perpendicular to the substrate surface along the (002) orientation could be fabricated by controlling the proper conditions and be made as ZnO nanowire laser.

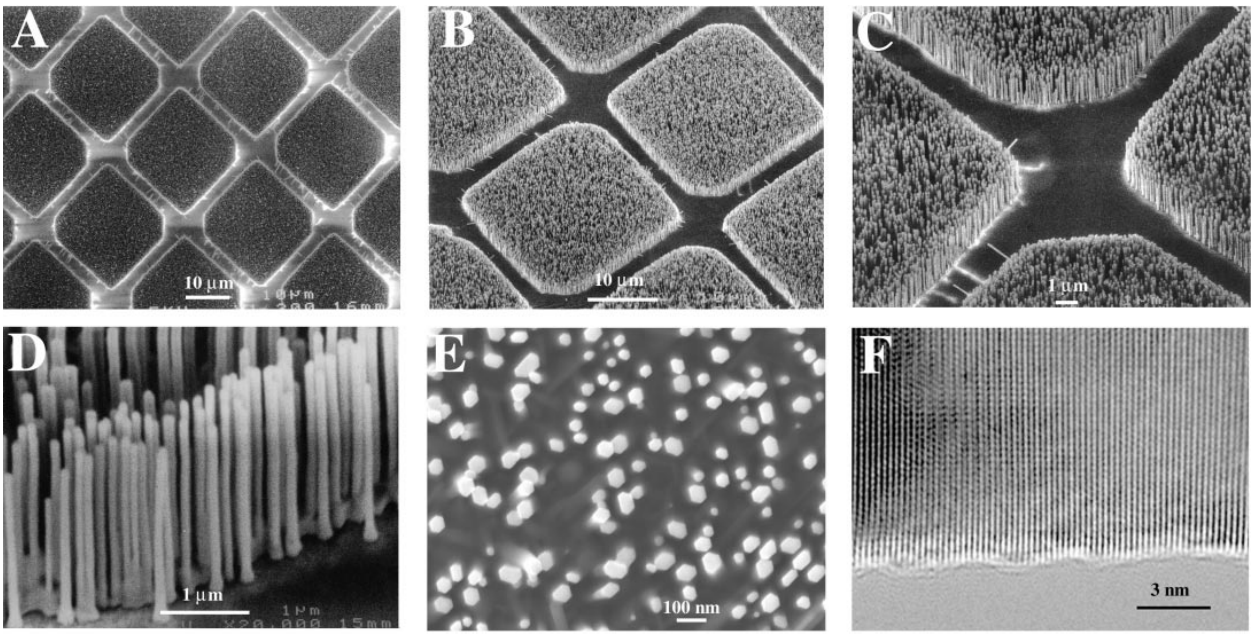

Figure 1-2 SEM images of ZnO nanowire arrays grown on sapphire substrates[13].

As shown in Figure 1-2, (a) to (e) are SEM images of ZnO nanowire arrays grown on sapphire substrates, (f) is TEM image of single ZnO nanowire. The results showed that the

nanowires only grew in the area with Au covered, and the top of each nanowire was covered with Au-Zn alloy group.

1.2.2 Vapor-Solid (VS)

In addition to the VLS mechanism, another VS mechanism is often used to prepare one-dimensional nanowires. During the growth process in vapor-solid, gas vapor is produced by thermal evaporation, chemical reduction and gas phase reaction, then the gas is transported and deposited on the substrate. This pattern of growth is often interpreted as the growth of one-dimensional materials centered on microscopic defects (dislocations, twins, etc.) at the liquid and solid interfaces. However, for most whisker growth, it is the key to control the supersaturation of the preferential coagulation, because evidence shows that supersaturation will directly determine the morphologies of the crystal growth. Supersaturation is closely related to the original growth morphologies (whiskers, lumps, powders). Low supersaturation corresponds to the whisker growth. Moderate supersaturation corresponds to the formation of massive crystals. At very high supersaturation, the powder is formed by uniform nucleation. Therefore, the size of whiskers can be controlled by supersaturation, nucleation size and growth time. One-dimensional nanomaterial can be synthesized by this method. The advantage of this preparation method is that no catalyst is required, but the disadvantage is that the growth temperature is higher.

In 2001, Z.L. Wang [20] synthesized a series of semiconductor oxide nanoribbons such as ZnO for the first time. ZnO nanobelts were synthesized by vapor-solid method at high temperature with ZnO powder (99.99%) as raw material. These ribbon structures were ideal single crystal sheet structures and the cross section is a narrow rectangular structure with width of 30 ~ 300nm, thickness of 5 to 10 nm, and the length up to a few millimeters. This was a new type of functional oxide of one-dimensional nanomaterial system after the fabrication of nanowires and nanotubes.

It was significant in the discovery of a new form with a unique defect-free oxide semiconductor system which was very important in nano-physical research and nano-device application.

1.2.3 Template method

Template method is one of the most common methods with a wide range of applications. The template can be prepared with a variety of materials, such as metal, alloy, semiconductor, conductive polymer, oxide and other material. Its superiority cannot be replaced by any other method. The outstanding advantage of this method is the fabrication of nanowire array. The nanowire array can remain in the holes of the template, or the nanoarray structures are obtained by removing the part of template when the nano structure films are fixed on certain substrates

The properties of the nanostructures can be regulated based to the composition of materials being assembled in template and the change of aspect ratio of nanowires and tubes. This has broad applications in the field of electronics. The template is a prerequisite for the synthesis of nanostructure arrays. Anodic alumina, polymer and metal templates are most commonly used in the synthesis of nanostructure arrays. The desired nanowire or tube arrays can be obtained by electrochemical deposition, sol-gel, chemical polymerization, chemical vapor deposition and other methods.

H.Q. Wu[21] used carbon nanotubes as templates to induce the growth of ZnO nanorods. They stirred the zinc nitrate solution and the appropriate amount of nitric acid treated MWNTs for 48 h. The obtained samples were filtered, washed, dried and then heat-treated at 500 ℃ for 6 h in Ar atmosphere. The samples were calcined in air at 750 ℃ for 2h to burn off the multi-walled carbon nanotubes. After burning, ZnO nanorods were obtained with diameter of 20 ~ 40nm and length of 250 ~ 1000nm.

1.2.4 Wet chemical growth method

The reaction mechanism of preparing aligned nanowire, nanorod and nanotube arrays on solid substrate by this method is that the activation energy of heterogeneous nucleation in solution is much lower than the activation energy of homogeneous nucleation[22, 23]. Therefore, the reaction particles are more likely to form fine nuclei on the solid substrate immersed in the solution. The nucleation of nuclei on the substrate is much faster than the formation in solution. In this way, it is possible to ensure that a large number of crystal nuclei with higher density and smaller grains exist on the substrate and grow along a certain crystal plane. In order to improve the orientation of prepared nanoarrays, substrate can be pre-modified with a suitable nanoparticle films, then grown with nanoarrays. Vayssieres, L.[24, 25] and Govender, K.[26] used hydrothermal method to prepare well oriented ZnO nanorods in solution.

Hydrothermal method is composed of substrates pre-treatment (ZnO particle seeding) and chemical bath deposition process (ZnO nanowire growth)[27]. Various methods have been involved to prepare the seed layers of ZnO including ,magnetron sputtering[28], spin coating [27], dip-coating [29] and atomic layer deposition[30].

P.N. Mbuyisa et al.[28] used direct current magnetron sputtering to prepare ZnO template thin films on silicon substrate with a Zn target of 99.995% purity at room temperature. Hydrothermal growth solution was prepared by the solution of zinc chloride and aqueous ammonia. Highly crystalline miniature nanorods were obtained and the mean diameter of ZnO nanorods decreased when the deposition pressure in sputtering increased.

L.L. Yang et al.[27] employed a high speed spin coater to deposit ZnO nanoparticles on silicon substrates. Then aqueous solution of zinc nitrate hexahydrate and methenamine was used

for the growth of ZnO nanowires. The influence of substrate pre-treatments, pH, angel between substrate and beaker, and growth time were studied.

Y. Lin et al.[29] prepared the dip-coating solution by dissolving the zinc acetate dihydrate and sodium hydroxide in ethanol. The carbon fiber tows were dipped into solution and dried with heating for several times. After ZnO particles formed on the surface, conventional zinc nitrate hexahydrate and hexamethylenetetramine was used to grow ZnO nanowires.

Q.C. Li et al[30] firstly introduced the atomic layer deposition in two-step hydrothermal growth. A uniform thin layer of ZnO film was deposited on different substrates including silicon wafers, polyethylene terephthalate and sapphire. The successful growth of ZnO nanorods proved that ALD was an effective method to deposit ZnO thin films on multiple substrates and offered more options in synthesizing one dimensional nanostructures.

1.3 Mechanism and characterization methods of composite interface

1.3.1 Mechanism of composite interface

A variety of theories have been established so far for the mechanism of the interface. Various theories have experimental support, but it is difficult to completely describe the interface effects and explain various experimental results simply by one theory as many roles are mutually reinforcing the interface. Interphase mechanism can be briefly summarized by the followings:

Infiltration theory considers that the combination of two phases in the interface is mechanical bonding and wetting adsorption, and the adhesion force is mainly van der Waals force. It starts from the basis of thermodynamics, considering the correlation between the energies of two surface and the resulting interfacial energy. This theory cannot explain the chemical bond interface[31].

Chemical bond theory was the earliest interface theory. It is considered that the interface mainly consists of two chemical phases which react with each other through chemical functional groups, and the binding force is mainly the action of primary bond[32].

Friction theory considered that the bond between the substrate and the reinforcement is based on the friction effect, and the coefficient of friction between the reinforcement and the substrate determines the strength of the composites. The important role of coupling agent is to increase the coefficient of friction between the resin matrix and the reinforcement[33].

1.3.2 Characterization methods

The mechanical properties of the fiber reinforced resin matrix composites are significantly affected by the bond strength between the fiber and the matrix. Therefore, most researchers use a variety of micro-mechanical testing techniques to measure the shear strength between the matrix and fiber in composites. The earliest reports were based on the interfacial strength measurements of fiber-reinforced metals proposed by Kelly, A[34] in the 1960s. This research has led to a boom in the interface research of composite materials.

According to the test principle and material failure modes, the methods of interface bonding strength test can be divided into two categories: non-destructive and destructive. Non-destructive method is to use chemical, physical or energy analysis to measure the bond strength between fiber and resin, such as spectral analysis[35], X-ray diffraction spectra[36], acoustic emission[37], Raman spectroscopy[38]. The salient feature of these methods is that they will not cause material damage during the measurement. It does not require a large number of repeated destruction experiments to achieve the test purpose. However, using these measurement methods and techniques for interfacial research requires highly sophisticated experimental equipment, and the relevant theoretical explanations pose great challenges to the researchers.

Destructive methods generally use micro-mechanical testing methods, which includes a Single Fiber Pull-out Test[39], Micro de-bonding Test[40] , Fiber Pullout and Pushout Tests[41], and Single Fiber Fragmentation Test[42]

1.4 Dissertation objective and outline

The main goal of this dissertation is to employ ALD to deposit ZnO nanoparticles as seed layers for the hydrothermal growth of ZnO nanowires on carbon fiber, then to manufacture hybrid carbon fiber composite laminates to verify the enhancement effect of ZnO nanowires.

Chapter 1 provides a literature review in different methods of fabricating ZnO and composite interface theory. Chapter 2 focuses on developing a thermal ALD process to optimize the morphology and structural properties of as-grown ZnO thin films on silicon substrate. Chapter 3 demonstrates the effect of ZnO nanoparticles grown by differing ALD parameters including temperature and growth cycles as seed layers to fabricate ZnO nanowires on carbon fabric. Chapter 4 investigates the effect of reaction temperature and concentration of chemical reagents in the second step hydrothermal method on the properties of ZnO nanowires on carbon fabric using the same recipe of ALD. Chapter 5 studies the influence of hydrothermal process time and reagent concentrations on the properties of ZnO nanowires on the substrate of carbon fabric based on the same growth parameters of ALD process.

Chapter 6 presents the optimal synthesis and characterization of aligned zinc oxide (ZnO) nanowires on carbon fibers for the development of hybrid composites with increased interfacial strength. Atomic layer deposition method was first employed to uniformly deposit nanoscale ZnO seeds on the carbon fiber surface. Then, low temperature hydrothermal method was used to grow

the ZnO seeds into aligned nanowires for composite applications. Critical properties of aligned ZnO nanowires, such as morphology and chemical compositions, were characterized.

Chapter 7 shows that the enhanced mechanical properties of carbon fiber composites including flexural strength and ILSS by introducing vertically aligned ZnO nanowires on the surface of carbon fibers were examined. The ZnO nanowires were synthesized by a two-step hydrothermal method. In the first step of growth, ALD was involved to deposit fine ZnO nanoparticles as nucleation site for the fabrication of ZnO nanowires in second step. The morphologies, elemental composition, crystal orientation and mass ratio of ZnO on carbon fabric were characterized. Carbon fiber composite laminates were manufactured by vacuum assisted resin transfer molding (VARTM) with external pressure.

Chapter 8 summarizes the major finding of this dissertation for the hybrid carbon fiber composites with the decoration of ZnO nanowires and proposes recommendations for the potential future work

Chapter 2 Growth Process Optimization of ZnO Thin Film using ALD

2.1 Introduction

In recent years, ZnO is one of the most intensively investigated semiconductor materials due to its wide direct bandgap (~3.3 eV), large exciton binding energy (~60 meV), and excellent piezoelectric properties[43]. Significant interest has been attracted in view of its broad range of research and industrial applications, including light emitting diodes[44], UV laser diodes[45, 46], photon detectors[47], solar cells[48], pressure sensors[49], transparent conductive materials[50], and also interfacial coatings for fiber strength enhancement[7].

Common techniques used to grow relatively good quality ZnO thin films are physical vapor deposition (PVD) systems, such as magnetron sputtering[51, 52], e-beam evaporation[53], and pulsed laser deposition[54]. However, these high energy PVD methods typically result in broad material interface damage, significant stoichiometric non-uniformity in films, and commonly existing structure imperfections including micro pin-holes and point-defects. With the continual trend towards scaling modern novel electronic devices down to micro- and nano-scale levels, such issues become even more severe and degrade the material quality tremendously. In contrast to these PVD methods, ALD is well-known as a promising alternative deposition method with numerous advantages, such as good uniformity and conformality, atomic-scale thickness controllability, perfect stoichiometric uniformity and low impurity contamination at lower growth temperatures from 400 °C down to as low as 50 °C[55, 56]. In addition to the improvement of the structural property, this technique also has strong capabilities to enhance the electric, optical and mechanical characteristics[57, 58] of the ALD derived thin films, including Hall mobility, electrical resistivity, light transparency, photoluminescence, hardness and Young's modulus. Moreover, in recent years, rapidly growing research attention has been paid to growing semiconductor thin films onto

lightweight, flexible and mechanically strong plastic films[59]. Generally, such organic substrates cannot withstand high processing temperature (e.g. PET ≤ 150 °C[60], Kapton Polyimide ≤400 °C[61]).

Therefore, it becomes increasingly advantageous to study ZnO thin film growth using ALD at lower temperature ranges under these considerations. It is noted that there are a few efforts that have already been made in this area, with different research emphasis including growth rate, crystal quality, and optical and electronic properties[62, 63].

In this chapter, our efforts focus on developing a thermal ALD process to optimize the morphology and structural properties of as-grown ZnO thin films. Major growth factors including the H_2O/Diethyl Zinc (DEZn) dose ratio, background base pressure and growth temperature are investigated systematically. When some growth factors are tuned out of certain ranges, a high density of flower-like nanostructures were observed for the first time in ALD growth research works. Such limitations for using thermal ALD to deliver high quality ZnO thin films are reported in this work. It is believed that the findings reported in this chapter will offer unique and valuable guidelines for researchers to grow high quality ZnO thin films by ALD method.

2.2 Methodology

ZnO thin films were grown on (100) silicon substrates by an ALD method under various growth conditions. Prior to the growth step, all 2 × 2 cm^2 Si substrates were degreased by dipping into Trichloroethylene (TCE), Acetone, and Methanol solvents respectively for 5 min (mins) each under ultrasonic agitation, followed by cleaning the substrates under running deionized water (DI) for 10 min before finally purge-drying by ultrahigh purity (UHP) N_2 gas. A customized 3'' thermal ALD system was then used to perform the ZnO growth on the cleaned Si wafers. In the reaction process, we adopted a double-exchange chemical vapor reaction between DI water and DEZn

precursors. The dose time was controlled by computer driven pneumatic valves, and N_2 gas carried these vaporized sources to the reaction chamber. The H_2O and DEZn were alternately distributed, and a 10 s (s) UHP N_2 purge period was carried out after each dosing process. It is noted that this period was enough to ensure that the pressure returned to its base level before the next pulse.

In order to find a suitable growth window and optimize the deposition procedure, three major growth factors including H_2O/DEZn distribution ratio, background base pressure, and growth temperature were investigated. Three H_2O/DEZn dose ratios of 0.8, 1.5, and 2.0 were studied by tuning the DI H_2O pulse time while fixing the pulse for the DEZn precursor. To investigate the impact of the base pressure conditions, ZnO films were grown under 0.5, 0.4, 0.3 and 0.2 Torr respectively by adjusting the feeding UHP N_2 amount. For both H_2O/DEZn dose ratio and base pressure studies, the growth temperatures were all set at 150 °C. For the temperature impact study, the growth temperatures were adjusted from 100 °C to 300 °C, in steps of 50 °C. It is worth noting that 300 growth cycles were carried out to ensure sufficient film thicknesses for characterization.

After the series of growth processes, thin films were characterized by a high-resolution Zeiss Neon EsB FESEM with Oxford EBSD capabilities, an Asylum atomic force microscope (AFM), a KLA Tencor D500 stylus profiler, and a Rigaku powder x-ray diffraction (XRD) system.

2.3 Results and discussion

During the ALD process, precursor chemistry plays a vital role. Different precursors have different chemical properties such as volatility and thermal stability. Therefore, finding a good balance between the H_2O and DEZn precursors is the most critical step in order to achieve successful ZnO ALD growth. With this consideration, the effect of dose ratio between the H_2O/DEZn precursors was studied first. With the change of pulse time of H_2O from 0.1 s to 0.3 s,

the resulting pressure spikes (ΔP) were increased consequently, as shown in Table 2-1. The top-view morphologies of feeding ratio dependent as-grown ZnO films are demonstrated in Figure 2-1 (a)–(c). As can be seen in Figure 2-1 (a) and (b), when the H_2O source was not sufficiently supplied, nanoflower-like structures were formed on top of the thin films. Such random structures increase the surface roughness and play a role as irregular seeds that will adversely affect film quality in subsequent growth processes, such as fast growth speed, and irregular orientations of grains. It is believed that the nano-flower formation results from the unbalanced H_2O/DEZn dose ratio. With a decreasing amount of H_2O, the DEZn was overdosed relatively, which results in a process more like chemical vapor deposition (CVD) rather than an ALD process. Therefore, in order to eliminate the formation of those nano-flowers, it is necessary to keep the H_2O/DEZn dose ratio over a certain level to prevent a DEZn over-dose situation. In our system, to deliver successful ZnO growth, the H_2O dose amount needs to be close to or higher than 2 times of DEZn, as shown in Figure 2-1 (c).

Table 2-1 The relationship between pulse time and pressure spike of H_2O source.

pulse time (second)	0.1	0.2	0.3
pressure spike (ΔP mTorr)	100	180	250

Note: pulse time and pressure spike for DEZn were set at 0.3 s and 120 mTorr.

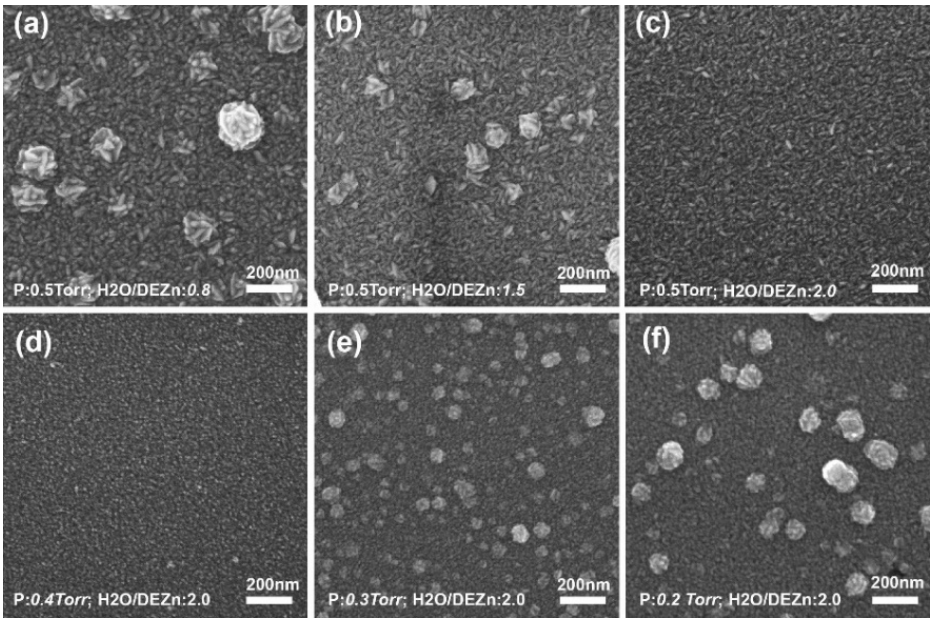

Figure 2-1 Top down SEM images for ZnO thin films deposited by ALD with various H2O/DEZn precursors dose ratio including (a)–(c) and different background pressure including (c)–(f).

ALD is a self-limiting chemical reaction process that can provide an equilibrium state between adsorption and desorption of precursors within each reaction cycles. Since background pressure is directly related to the surface adsorption or residence time of a precursor, without a suitable base pressure, the equilibrium state will be hard to maintain resulting in an uncontrollable growth process. Therefore, even if H_2O/DEZn dose ratio is at a balanced range, similar nanoflower-like random grains can still form when the base pressure falls below 0.3 Torr, as shown in Figure 2-1 (e) and (f). It is believed that a similar CVD process might be happening under this condition. Specifically, too low of a base pressure results in desorption of DEZn precursors that originally bonded on the ZnO thin film. Consequently, those precursors react with H_2O molecules and redeposit on the surface creating nanoflower-like grains. As a result, the surface roughness is found to be strongly dependent on both the H_2O/DEZn dose ratio and base pressure parameters. In order to perform a controllable and uniform ZnO ALD deposition, both dose ratio and base

pressure during the reaction process have to be tuned to a suitable window as shown in Figure 2-1 (c) and (d).

It is well known that ALD is a thermally activated process that produces self-limiting reactions on the surface of a substrate. Therefore, a suitable temperature window can be identified for ZnO thin film deposition based on the constant growth rate of the ALD process. To study the effect of deposition temperature for ZnO thin films, five different deposition temperatures were tested from 100 °C up to 300 °C as mentioned before. Other conditions followed the optimized parameters discussed in previous sections: H_2O/DEZn = 2, P_{base} = 0.5 Torr and cycle = 300.

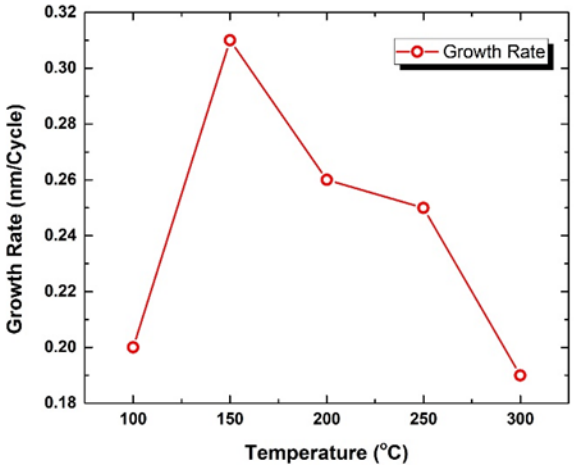

Figure 2-2 Growth temperature dependent deposition rate of ZnO thin films on Si wafers.

Figure 2-2 shows the average growth rate as a function of the growth temperature. As shown, the growth rate increases from 100 °C to 150 °C. This is due to the fact that the reactant is unable to fully overcome the necessary activation energy to chemisorb on the substrate at lower temperatures (~100 °C). It is known that H_2O is a highly polar molecule that tends to condense or physisorb on to the surface and lead to a partial CVD process with an unwanted higher growth rate. High temperature can help to minimize this issue. Therefore the growth rate decreases after the temperature rises from 150 °C to 200 °C. From 200 °C to 250 °C, a relatively stable growth rate

is achieved. The range is believed as the good ALD growth window for deposition of ZnO thin films. However, extremely high temperatures will lead to decomposition or desorption of adsorbates before the reaction. This explains why the growth rate quickly decreases from 250 °C to 300 °C.

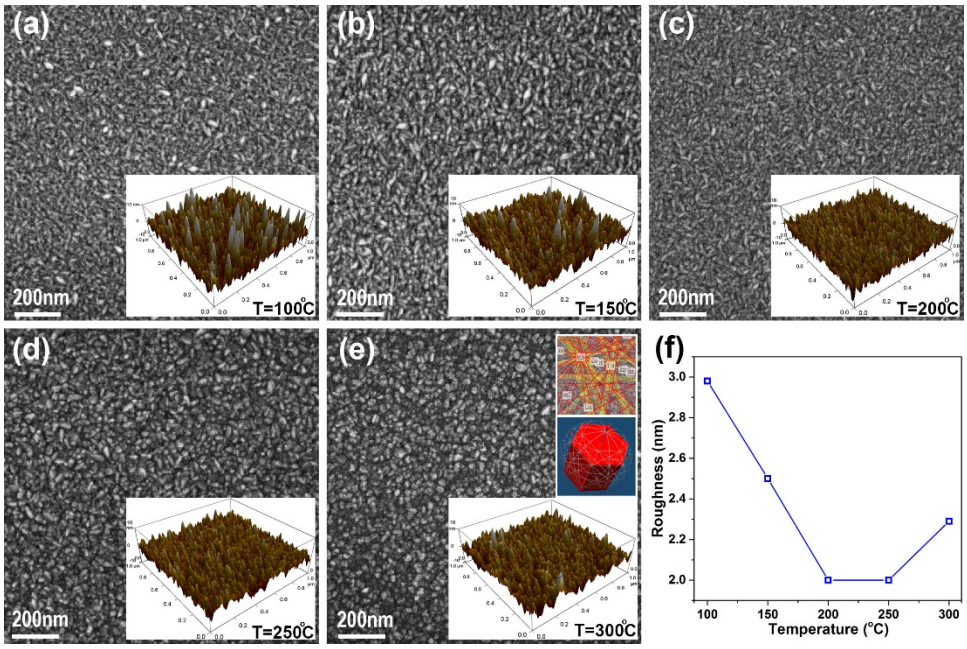

Figure 2-3 Temperature dependent morphologies of ZnO films by ALD: (a)–(e) top down SEM pictures with 3D AFM insets; (f) surface roughness as a function of growth temperature. (Note: extra small insets in (e) are indexed Kikuchi pattern and EBSD resolved wurtzite structure).

The surface morphologies of ZnO films grown under different temperatures were also characterized by SEM and AFM tools as presented in Figure 2-3 (a)–(e). The root mean square (RMS) of surface roughness was obtained from the AFM image with an accuracy of 0.1 nm. The relationship between RMS and growth temperature is also shown in Figure 2-3 (f). As shown in the 3D AFM images, with an increase in the growth temperature from 100 °C to 200 °C, the surface morphology is steadily improved. At 100 °C and 150 °C, the growth process is either due to insufficient chemisorbtion energy or involved with a partial CVD mechanism due to the H_2O

condensation issues as mentioned. Therefore, the growth is not primarily through ALD's self-limiting reaction condition and consequently we observe rough growth surfaces. This also explains why the RMS value goes up when the growth temperature increases to 300 °C, since this region can lead to very poor absorption of reactants on the substrate as explained previously. Finally, for growth temperatures at 200 °C and 250 °C, the RMS values of 2 nm suggest that the ZnO film grown by our customized ALD system is able to achieve atomic flatness under optimized growth conditions. In addition, it is worth noting that the ZnO grains have changed from rice-like to rock-shaped microstructures when the temperature goes to 300 °C, while the films grown at 250 °C is at a transition state having grains with both formations, as shown in the SEM images in Figure 2-3 (d) and (e). EBSD was used to investigate the crystallographic change of the microstructures where it was observed that rice-like grains randomly contain both zinc blende and wurtzite crystal structures. On the contrary, rock-shaped grains primarily have a wurtzite crystal structure whose indexed Kikuchi pattern and the resolved wurtzite formation are displayed as insets in Figure 2-3 (e).

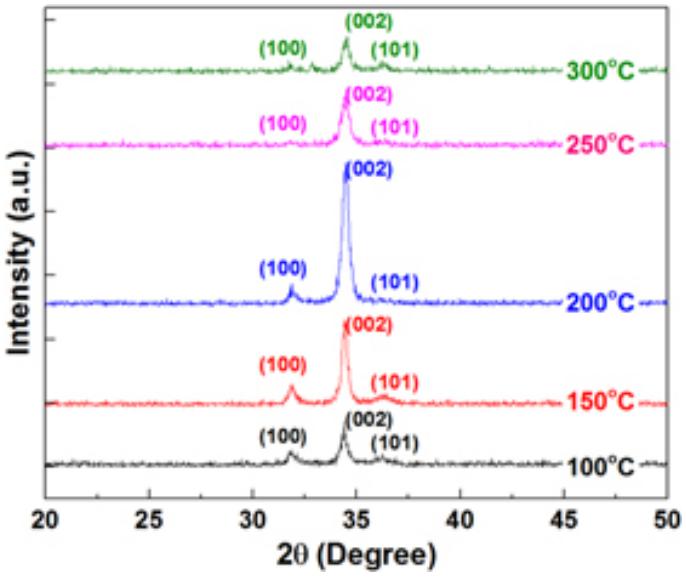

Figure 2-4 XRD patterns of ALD ZnO thin films with different growth temperatures.

Furthermore, in order to investigate the crystal quality of these films grown under different temperatures, XRD data was collected through a Rigaku powder XRD tool. XRD scans were performed from 20° to 50°, and the spectra are shown in Figure 2-4. It is found that ZnO films can be poly-crystallized even at the lowest growth temperature of 100 °C, as ZnO peaks can still be observed at this level. With an increase in temperature, we found the intensity of the (002) peak increased strongly, but the (100) and (101) peaks become weaker. The strongest (002) peak is observed at 200 °C which indicates the films were primarily grown in the c-axis orientation. However, after the temperature is over 200 °C, the (002) peak goes weaker indicating the films are no longer dominated by a c-axis. The reason could be due to the fact that crystal structures start transforming at this stage. Similar results were also observed in other studies[64, 65].

2.4 Conclusion

In this chapter, the thermal ALD growth process of ZnO thin films on silicon is systematically studied and optimized through a customized ALD system using alternating pulses of DEZn and H_2O. The impact of three ALD growth factors include H_2O/DEZn precursors dose ratio, background base pressure and growth temperature have been studied. In order to perform a controllable and uniform ZnO ALD deposition, it is found that both dose ratio and base pressure during the reaction process have to be tuned to a suitable window for highly uniform deposition: the H_2O/DEZn ratio needs to be controlled close to or above 2, and 0.4 Torr is the bottom limit base pressure for our customized ALD system. On the other hand, the study of the temperature impact suggests that the suitable temperature window for growth should stay within 200 °C – 250 °C.

Chapter 3 Effect of ALD Seeding on Growth of ZnO Nanowires on Carbon Fabrics by Hydrothermal Method

3.1 Introduction

Well aligned ZnO nanowires can be achieved by various growth techniques including vapor–liquid–solid (VLS) growth[66], chemical vapor deposition[67] and hydrothermal[68] methods. Hydrothermal synthesis is a desired option for growth due to its low growth temperature (<100 °C) and simplicity in an aqueous solution[69]. Hydrothermal method is normally composed of two steps: substrates pre-treatment (ZnO particles seeding) and chemical bath deposition process (ZnO nanowires growth)[27]. For the preparation of ZnO seed layer, various methods have been employed including dipping[70], sputtering[71], sol-gel[72] , and atomic layer deposition (ALD)[30].

Y. Lin[7] firstly synthesized the vertical ZnO nanowires on carbon fiber using dipping as first step in two-step hydrothermal method. He proved that great improvement of interfacial shear strength was obtained by introducing ZnO nanowires to the interphase between carbon fiber and polymer matrix. The tensile strength of carbon fiber preserved without degradation due to the low temperature of aqueous solution. U. Galan[73] continued Lin's work by varying the growth parameters of second step of hydrothermal method to fabricate different morphologies (length and diameter) of ZnO nanowires. He demonstrated that the enhancement of interfacial shear strength can be tailored by precise morphology control. The introduced interphase of ZnO nanowires would provide the multi-functional composites with optimal performance. The work of them offered a novel approach to make high performance composites by growing ZnO nanowires compared to conventional whiskerization method including carbon nanotubes and silicon carbide (SiC)

nanowires which would cause the degradation of carbon fiber and lower down the in-plane performance of composites.

However, dipping has some disadvantages such as uneasy controlling process, difficult deposition on some substrates and non-uniformity of seed layers. It was reported that grain size and quality of seed layers greatly affected the growth morphologies of ZnO nanowires, so a method can produce high quality with small grain size is demanded. ALD is one of the best thin film deposition method that has numerous advantages of good uniformity and conformality, atomic-scale thickness controllability, perfect stoichiometric uniformity and low impurity contamination at lower growth temperatures from 400 °C down to as low as 50 °C[74]. The high uniformity of ZnO seed layers with small grain size by ALD will lead to a favorable vertical orientation and small diameter nanowires[75]. The lower temperature of ALD will have a similar result like dipping that will preserve the tensile strength of carbon fiber and keep the in-plane properties of composites but obtain higher quality of ZnO seed layers. To investigate the parameters of ALD process will also benefit the tailored properties of ZnO nanowires for high performance composites.

By now the influence of parameters of second step of hydrothermal method on synthesizing ZnO nanowires on carbon fabric using ALD to grow the seed layer has been explored[76, 77], but the effect of ZnO nanoparticles grown by ALD as seed layers to fabricate ZnO nanowires on carbon fabric has not been studied yet. In this work, ALD was used to fabricate high quality ZnO nanoparticles as seed layer on carbon fabric. Temperature and growth cycles of ALD process were varied to investigate their influence on ZnO nanowires by hydrothermal method whose growth parameters keep unchanged. ZnO nanowires were characterized by field emission scanning electron microscope (FESEM), energy-dispersive x-ray spectroscopy (EDX), X-ray diffraction (XRD) and thermogravimetric analysis (TGA) to study their morphologies, element composition,

crystal orientation and weight ratio of ZnO on carbon fabric. The study shows that temperature from 100 °C to 300 °C has a significant effect on the morphologies and densities of ZnO nanowires, and more growth cycles will result in larger diameter of ZnO nanowires.

3.2 Experiments

3.2.1 ZnO seed layer by ALD

ALD is a self-limiting chemical reaction process in cycles that deposit materials in an equilibrium state between adsorption and desorption of precursors. A typical cycle was repeated until growth completed with following steps: self-limiting reaction of precursor A, purge to clean up the residual precursor and product, self-limiting reaction of precursor B, purge to clean up the residual precursor and product. With the growth process continuing, one layer of Zn atoms and one layer of O atom will form ZnO nanoparticles on the substrate. The self-limiting reaction makes ALD process precisely control the growth in nanoscale and easy to deposit on most substrates.

Diethylzinc (DEZn, $Zn(C_2H_5)_2$) and deionized water (DI water) were purchased from Sigma–Aldrich and used as precursors to synthesize ZnO nanoparticles as seed layers for the next step hydrothermal growth. The deposition of ZnO seed layers was carried out on a customized 3" ALD system. Carbon fabric (25 mm * 25 mm) was prepared as substrate of growth and adhered on a piece of glass slide by high temperature Kapton tape. The substrate was not cleaned due to the ultimate application in carbon fiber composites which were usually fabricated in a non-sensitive environment.

We have conducted an optimal ALD growth of ZnO thin films on Silicon substrate and obtained the results that parameters of pulse time of DEZn and water at 0.3s, vapor ratio of DEZn and water over 2, temperature at 200 °C, background pressure at 0.5 Torr and growth cycles at 300

would produce the best quality of ZnO nanoparticles. Based on these values, we will investigate the influence of substrate temperature and growth cycles which play a critical role in producing the quality of seed layers in this work. The temperature varied at 100 °C, 150 °C, 200 °C, 250 °C and 300 °C with other parameters unchanged, and the growth cycles varied at 100, 200, 300, 400 and 500 with other parameters unaltered, as shown in Table 3-1. The purge time of ultrahigh purity N_2 gas after each pulse of precursors was 20 seconds to avoid the potential CVD reaction with remained vapors.

Table 3-1 Growth parameters of ALD growth for ZnO seed layers.

	A1	A2	A3	A4	A5	A6	A7	A8	A9
Temperature (°C)	100	150	200	250	300	200	200	200	200
Growth cycles	300	300	300	300	300	100	200	400	500

3.2.2 Hydrothermal growth of ZnO nanowires

Zinc nitrate hexahydrate ($Zn(NO_3)_2 \cdot 6H_2O$) and Hexamethylenetetramine (HMTA) were purchased from Sigma–Aldrich to grow ZnO nanowires using conventional hydrothermal method. Both $Zn(NO_3)_2$ and HMTA solutions were prepared by dissolving the powers in Di water at a concentration of 25mMol/L. They were stirred by magnetic bars separately at 800 rpm and heated to 90 °C on hotplates, then mixed together in a large beaker with samples immersed inside. The beaker was put in a PolyScience water bath for 17 hours at 95 °C. After completing the growth of ZnO nanowires, samples were taken out from the beaker, rinsed by Di water for 1 minute and dried on hotplate at 125 °C for 15 minutes.

3.2.3 Materials characterization

High resolution Zeiss Neon EsB FESEM with Oxford EBSD capabilities was used to take images of ZnO nanoparticles and nanowires at a working distance of roughly 6 mm at an accelerating voltage of 5 kV by in-lens signal and to detect the elements on hybrid carbon fabric. XRD analysis was performed on a Rigaku Ultima IV diffractometer with Cu-K-alpha radiation (40 kV, 44 mA) via a Bragg-Brentano detector. TGA analysis was performed by TA Instruments Q50 with a temperature range from 35 °C to 900 °C at 10 °C/minute.

3.3 Results and discussion

The morphologies of ZnO nanoparticles as seed layers via ALD on carbon fabric were studied by SEM images as shown in Figure 3-1 (a) to (e) shows the morphologies of ZnO nanoparticles in temperature group where growth cycles are 300 but temperature range from 100 °C to 300 °C. From (a) to (c), the shape of ZnO nanoparticles seems to have a transitional growth from small rice-like to large rice-like. When the temperature goes to 250°C, the shape from rice-like to stone-like, as demonstrate in (c) and (e). When the temperature continues goes up to 300 °C, the size of stone-like ZnO particles decreases. For the growth cycles group from (f) to (j), a continuous grain size growing up was noticed. From (f) to (h), it can be seen ZnO nanoparticles transformed from stone-like to rice-like when the growth cycles increased from 100 to 300. The rice-like ZnO nanoparticles expanded its shape in plane and the density decreased quickly in (i) and (j). The orientation of rice-like ZnO nanoparticles is random with a length from 15 nm to 30 nm and width from 7 nm to 15 nm at the temperature of 200 °C for 300 growth cycles.

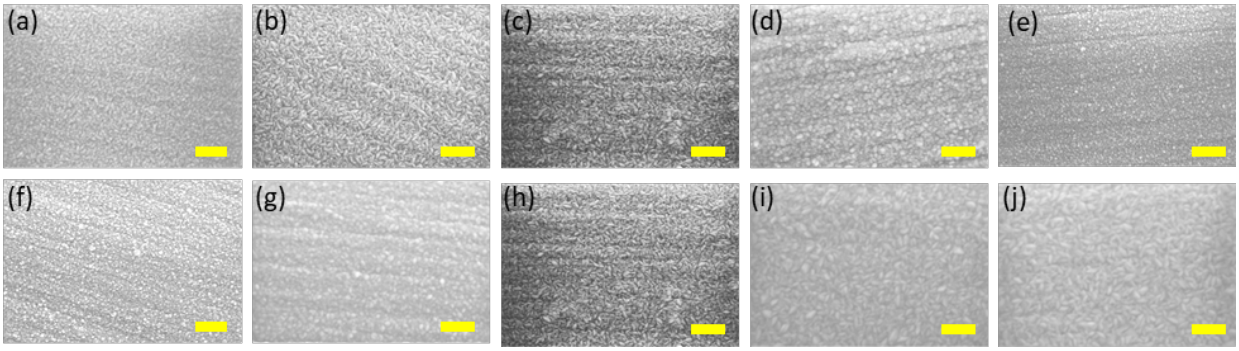

Figure 3-1 SEM images of ZnO nanoparticles: (a) 100 °C@300 cycles, (b) 150 °C@300 cycles, (c) 200 °C@300 cycles, (d) 250 °C@300 cycles, (e) 300 °C@300 cycles, (f) 100 cycles@200 °C, (g) 200 cycles@200 °C, (h) 300 cycles@200 °C, (i) 400 cycles@200 °C, (j) 500 cycles@200 °C, scale bar is 200nm.

ZnO nanowires synthesized by different ALD seeded layers of temperature and cycles group are shown in Figure 3-2. Very dense and small ZnO nanowires were obtained when the temperature was at 100 °C. Corresponding to the shape of ZnO nanoparticles that transited from stone-like to rice-like in temperature group from 100 °C to 200 °C, the diameter of ZnO nanowires increased and the density decreased. When the temperature went extremely high to 300 °C, the quantity of ZnO nanowires was very sparse in (e). For cycles group (f) to (j), there is an increasing trend for the size of ZnO nanowires when the growth cycles increase due to the nucleation of ZnO grains simultaneously grew larger. When the growth cycles were 100, the quantity of ZnO nanowires was also relatively sparse. When the growth cycles went over 400, obvious enlargement of ZnO nanowires was observed.

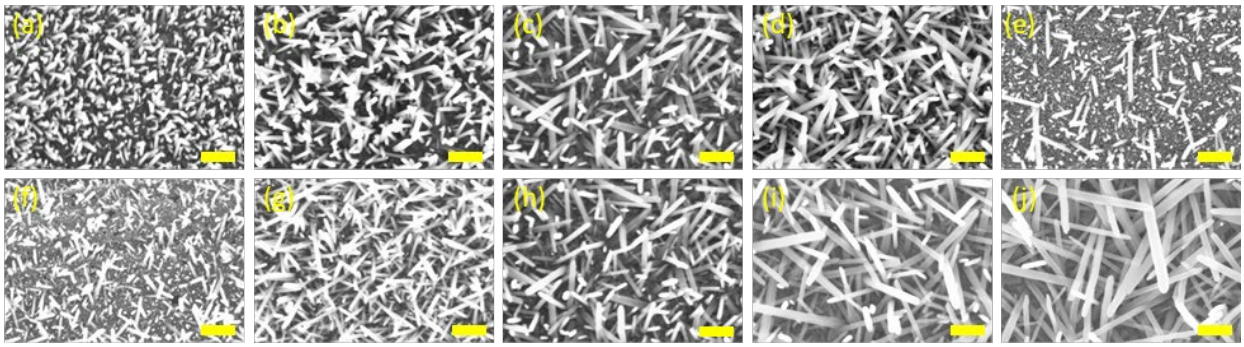

Figure 3-2 SEM images of ZnO nanowires: (a) 100 °C@300 cycles, (b) 150 °C@300 cycles, (c) 200 °C@300 cycles, (d) 250 °C@300 cycles, (e) 300 °C@300 cycles, (f) 100 cycles@200 °C, (g) 200 cycles@200 °C, (h) 300 cycles@200 °C, (i) 400 cycles@200 °C, (j) 500 cycles@200 °C, scale bar is 200nm.

The detailed information of diameter and density of ZnO nanowires for temperature and cycles group was illustrated in Figure 3-3. The diameter of ZnO nanowires for temperature group has a smooth increasing which was 17.839 ± 5.77 nm, 21.896 ± 5.968 nm, 23.862 ± 7.917 nm, 27.159 ± 7.835 nm and 33.29 ± 11.184 nm in (a). In (b), the density decreased simultaneously with the larger ZnO nanowires when the temperature goes from 100 to 200 °C. There is a jump for the density at 250 °C, but it sharply lower down when the high temperature at 300 °C which greatly reduced the quality of seed layers and finally affected the ZnO nanowires in hydrothermal process. For cycles group in (c), the increasing of the diameter of ZnO nanowires is steady when the cycles go up from 100 to 300 cycles. A jump in diameter can be seen when cycles go over 400, due to the enlargement of ZnO nanoparticles in ALD process. In (d), density of ZnO nanowires grown in 100 cycles is only 488 per um^2 which is less than the quantity in other growth cycles. When the surface of carbon fabric has been coated with ZnO nanoparticles at 200 cycles, the density of ZnO nanowires reaches the highest, then goes down with the increasing growth cycles which also brought larger size of ZnO nanowires.

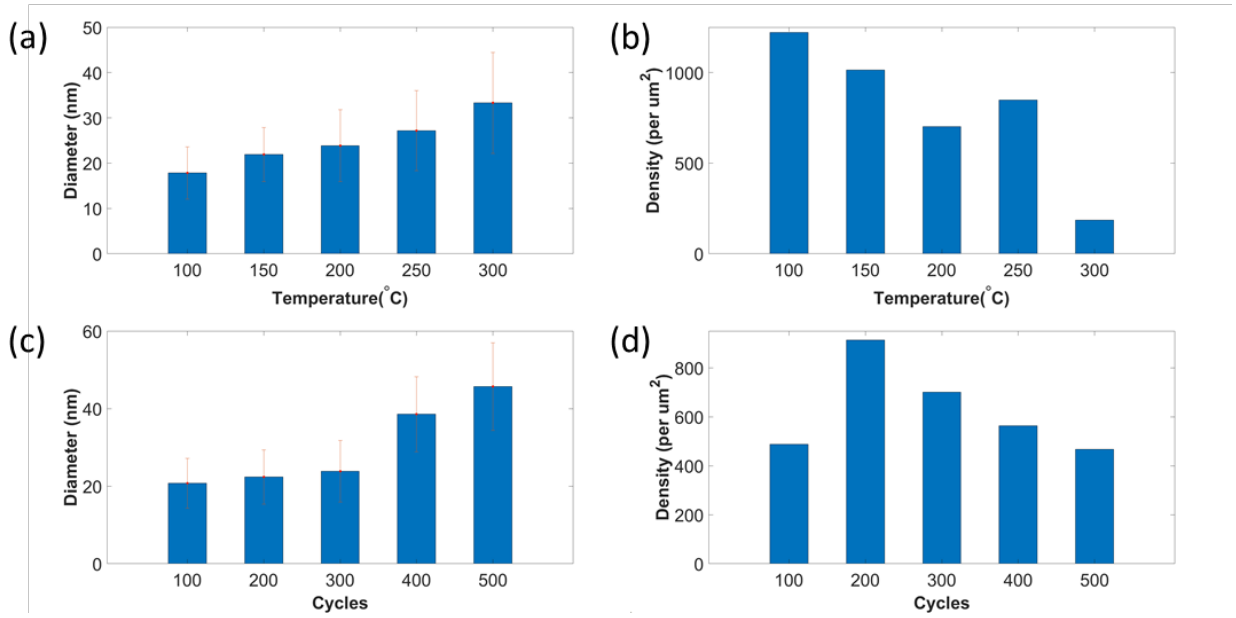

Figure 3-3 Diameter and density of ZnO nanowire: (a) diameter of temperature group, (b) density of temperature group, (3) diameter of cycles group, (d) density of cycles group.

In order to verify the element composition of nanostructures on carbon fabric, EDX analysis was carried out. Figure 3-4 manifests the EDX spectrum of ZnO nanowires by different ALD parameters of temperature and cycles group. All carbon, oxygen and zinc elements were detected for two groups, but the weight ratio and signal intensity for each vary significantly. For the temperature group in (a), the lowest weight fractionof carbon at 8.8% with highest weight ratio of zinc at 70.4% occurs when the temperature is at 150 °C. In contrast the highest weight ratio of carbon at 76.5% and lowest weight ratio of zinc at 16.2% was obtained at the temperature of 300 °C. It shows that the extremely high temperature will significantly inhibit the growth of ZnO nanowires. For the cycles group in (b), the weight fractionof all elements have a same trend when the growth cycles increase. The weight fractionof carbon lower down from 65.6% to 2.2% when the growth cycles change from 100 to 500. Oppositely, the weight ratio of oxygen increasing from 6.3% to 19.6% and zinc increasing from 28.1% to 78.1% is greatly boosted. It proved that the longer growth cycles will benefit the deposition of ZnO and lead to more weight of ZnO nanowires.

The results of EDX spectrum confirm that the nanostructure grown on carbon fabric is composed of ZnO.

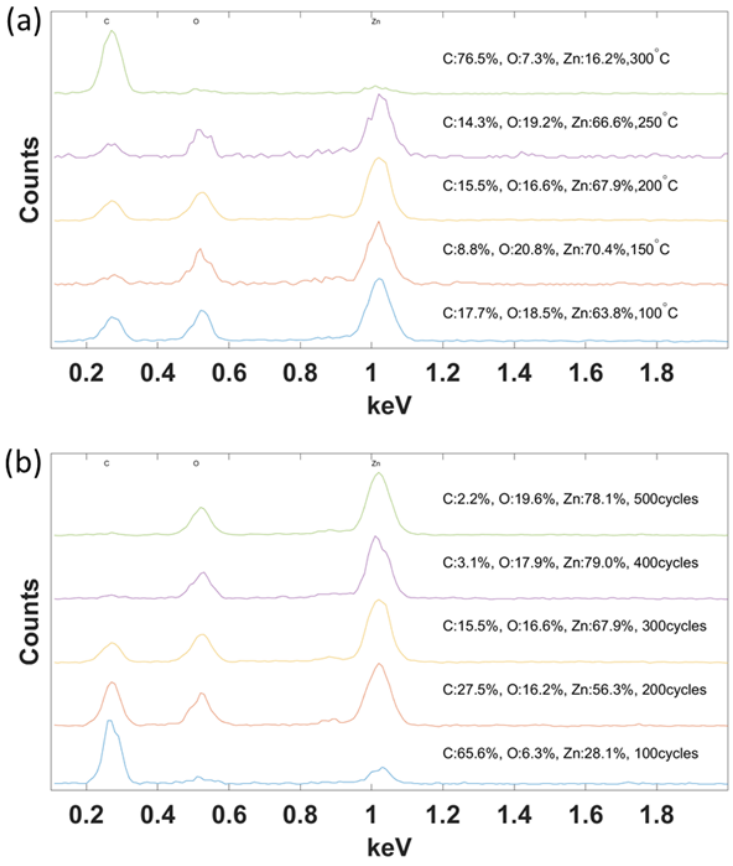

Figure 3-4 EDX spectrum of ZnO nanowires on carbon fabric: (a) temperature group, (b) cycles group.

XRD was used to study the crystal orientation of ZnO nanowires, as shown in Figure 3-5. Samples were scanned with angles from 10° and 80° at a speed of 2°/minute for a scanning step of 0.02°. For temperature group in (a), all common crystals of (100), (002), (101), (102), (110), (103) and (112) are detected except when the temperature is 300 °C. Planes of (100), (002), (101) dominate the peaks of ZnO crystals. When the temperature goes from 100 °C to 200 °C, the intensity of (100), (002), (101) becomes stronger compared to the peak of carbon. After the temperature goes over 200 °C, the intensity of these goes weaker, and (002) goes weaker compared

to the other two. As the (002) plane is the preferred growth orientation of ZnO nanowires along the c-axis direction, this explained why the alignment of ZnO nanowires is not vertical in previous SEM images. When the temperature goes to 300 °C, only the dominated three planes of (100), (002), (101) can be detected, and the others are almost gone. It can be conlcuded that high temperature will play a negative role in fabricating ZnO nanowires.

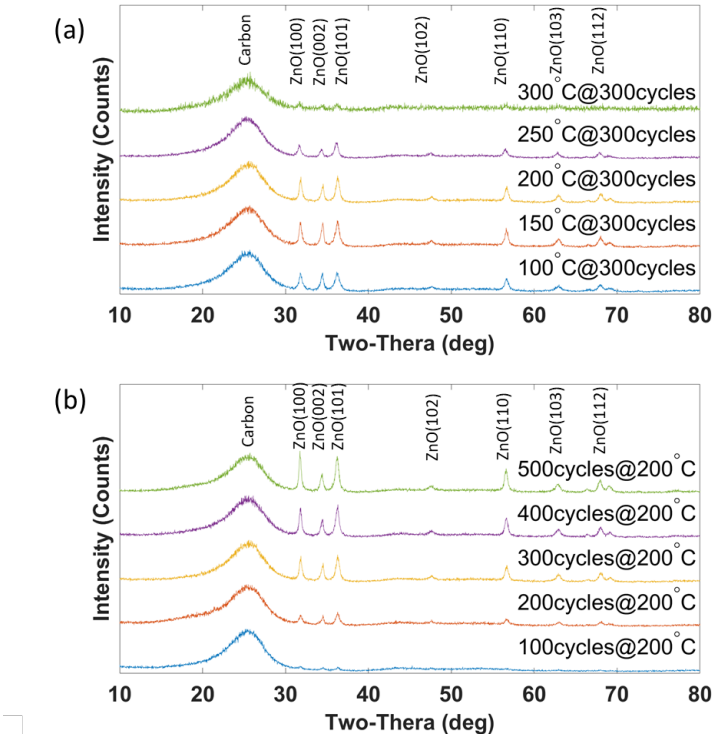

Figure 3-5 XRD diffraction of ZnO nanowires: (a) temperature group, (b) cycles group.

For cycles group in (b), the intensity of all planess increases simultaneously with the increasing of growth cycles. Intensity of plane (002) becomes weaker compared to intensity of other planes which matches the worse alignment of ZnO nanowires in previous SEM images when the growth cycles increase. When the cycles are 100, the peak of this growth has a similar situation of samples in temperature group for 300 cycles at 300 °C, that intensity of all peaks is very weak

and hard to detect. This result gave the reason why the densities of ZnO nanowires in these both growths are very sparse.

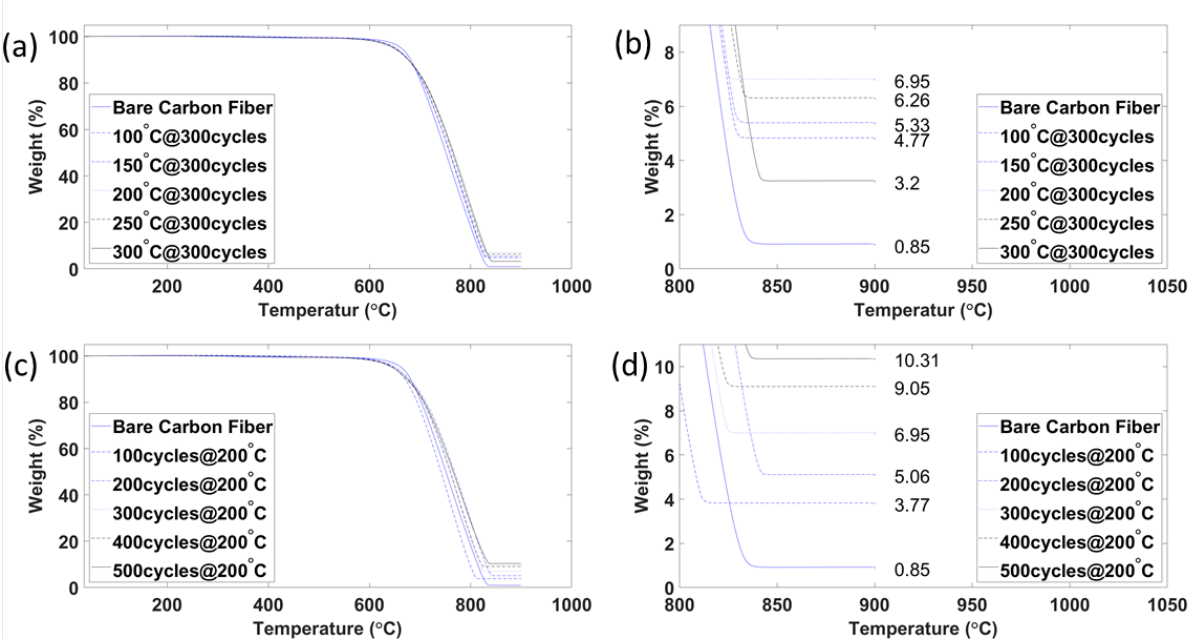

Figure 3-6 TGA of bare carbon fabric and carbon fabric with ZnO nanowires: (a) temperature group, (b) partial enlargement of (temperature group), (c) cycles group, (d) partial enlargement of cycles group.

TGA analysis was performed on temperature and cycles groups of ZnO nanowires growth to investigate how much weight is added to carbon fabric by ZnO, as shown in Figure 3-6. If the weight of ZnO is too much, it will limit the application of ZnO nanowires in carbon fiber composites as light weight composites are always desired. Air was chosen to be the gas for TGA test as the carbon fiber can be burned off in air environment before the temperature goes up to 1000°C, while the deposition temperature of ZnO is near 2000°C which is far higher than the decomposition temperature of carbon fiber.

No weight loss is found before the temperature goes to 300 °C as the carbon fabric was preserved well with no moisture inside. When the temperature was between 300 °C to 550 °C, there is about 1% weight loss which cannot be discerned in graph and is believed to be the sizing

that was burned off during this time. When the temperature reaches to 600 °C, the carbon fiber begins to burn, and finally burned off at round 850 °C, and white ZnO powder was left in burning basket.

For the temperature group in (a) and (b), the left weight ratio of ZnO nanowires increases from 4.77% to 6.95% when the temperature increase from 100 °C to 200 °C. After over 200 °C, the value drops to 3.2% at 300 °C. The weight ratio of samples at 200 °C is the highest. For the cycles group in (c) and (d), it is a linear trend for the weight ratio of ZnO when the growth cycles increase. 100 cycles have lowest with 3.77% and 500 cycles have highest with 10.31%. The TGA results give the quantitative value of weight ratio of ZnO on carbon fabric and confirm that the introducing of ZnO nanowires will not add too much weight on carbon fabric. As the highest weight fractionof ZnO in both groups is only 10.31%, ZnO will be much less when this hybrid carbon fabric is manufactured into composites. Considering the enhanced mechanical properties and other potential multi-functional properties by ZnO nanowires, growing the ZnO nanowire on carbon fabric is promising and significant.

3.4 Conclusion

In this study, we have systematically investigated the effect of ZnO nanoparticles seeded by ALD on the growth of ZnO nanowires on carbon fabric. The temperature and growth of cycles in ALD process were varied to fabricate ZnO nanowires in different morphologies. The morphologies were characterized by SEM images and studied by their diameters and densities. EDX, XRD and TGA analysis were used to investigate the element composition, crystal orientation and weight fraction of ZnO nanowires. It was found that extreme high temperature at 300 °C or lower growth cycles for 100 would inhibit the growth of ZnO nanowires. The added weight of ZnO nanowires carbon fabric was acceptable and made this application very promising.

By tailoring the morphologies of ZnO nanowires via ALD, it will give us the guide to obtain desired product which benefits its application in composites.

Chapter 4 Synthesis and Characterization of Self-Assembled ZnO Nanoarrays On Hybrid Structural Fibers

4.1 Introduction

Recently light-weight structural composite materials have attracted significant attention due to their high strength-to-weight ratio, corrosion resistance, and design flexibility[78]. Integrating nanomaterials and nanostructures within conventional fiber reinforced composites provides a promising approach to improve composite properties. Carbon felt and carbon nanotubes have been synthesized on continuous structural fiber fabric[79, 80]. Vertically aligned zinc oxide (ZnO) nanowires have been synthesized on natural fibers, such as cotton fibers[81-83] and jute fibers[84], and synthetic fibers, such as poly(acrylonitrile) fibers[85] and polyester fibers[86]. In particular, structural fibers, including carbon fibers[73, 87, 88] and aramid fibers[89-91] with vertically aligned nanowires, can result in advanced composite materials with enhanced mechanical properties due to the increased interfacial area between fiber and polymer matrix. Additionally, the piezoelectric properties of ZnO nanowires can also lead to load sensing functions for in-situ structural health monitoring and prognostics in complex composite structures[92-98].

Most current approaches to growing ZnO nanoarrays on carbon fiber fabrics are based on the dip-coating method that can only attach ZnO seeds to substrates by weak van der Waals forces in a wet chemical environment[79-86]. In addition, considering the strong hydrophobic properties and the cylindrical shape of the carbon fibers, it is challenging to deposit ZnO seeds in a good uniformity, conformity, and controlled crystal orientation using the dip-coating method.

Recently, an emerging technique called atomic layer deposition (ALD) has become popular because it offers advantages, such as high degree of conformity, atomic-scale thickness

controllability, perfect stoichiometric uniformity, low impurity contamination, and low growth temperature[99-101]. Therefore, in order to avoid the issues associated with the dip-coating method, in this chapter the ALD method was adopted to produce uniform and high-quality ZnO seed layers on carbon fiber fabrics. Then, we focused on studying the hydrothermally synthesized, vertically aligned ZnO nanoarrays on carbon fiber fabrics. Various hydrothermal growth parameters were investigated, including reaction temperature and concentration of chemical reagents, and the properties of ZnO nanoarrays coated carbon fiber fabrics were characterized using field emission scanning electron microscope (FESEM), thermogravimetric analysis (TGA) and energy-dispersive x-ray spectroscopy (EDX). We believe that the developed carbon fiber fabrics with ZnO nanoarray coatings will lead to the development of advanced composite materials with enhanced mechanical properties and potential load sensing capabilities.

4.2 Experiments

4.2.1 Materials

Unless otherwise stated, all the following listed materials and reagents were used as received. Plain weave carbon fiber fabrics were purchased from Fibre Glast. Diethylzinc and deionized water were purchased from Sigma–Aldrich and used for the ZnO seeding via ALD. Trichloroethylene (TCE, 99%), zinc nitrate hexahydrate ($Zn(NO_3)_2$, 99%) and hexamethylenetetramine (HMT, 99%) were purchased from Sigma–Aldrich and used in the hydrothermal synthesis of ZnO nanoarrays on carbon fiber fabrics.

4.2.2 Synthesis of ZnO nanoarrays on carbon fiber fabrics

A two-step synthesis approach was developed to grow vertically aligned ZnO nanowires on carbon fiber fabrics. First, the ALD method was used to deposit the ZnO seed layer on carbon fiber fabrics. Then, a low temperature hydrothermal method was employed as the second step to

synthesize ZnO nanoarrays in the forms of nanowires and nanorods. To obtain an optimal ALD procedure, the seed layer was first grown on a silicon substrate, and characterized using atomic force microscope (AFM), x-ray diffraction (XRD), and FESEM. The detailed synthesis procedure has been reported in our previous publication[74]. The identified nucleation procedure was employed to deposit the ZnO seeds on carbon fiber fabrics, followed by FESEM characterization of the seed morphology.

Table 4-1 Experimental procedures used in hydrothermal syntheses of ZnO nanoforest on carbon fiber fabrics.

Sample name	ZnO concentration (mMol/L)	HMT concentration (mMol/L)	Growth temperature (°C)
A1	25	25	70
A2	50	50	70
A3	100	100	70
B1	25	25	80
B2	50	20	80
B3	100	100	80

In the second step, carbon fiber fabrics were degreased by dipping them into TCE and methanol solvents, respectively, for 10 min under ultrasonic agitation, then washed under running deionized water for 10 min, and finally dried in an environmental oven. $Zn(NO_3)_2$ and HMT aqueous solutions were prepared. Each was stirred at 600 rpm for 10 min at 55 °C, then mixed together and stirred at 600 rpm for 10 min at 55 °C. The solution was stored in a water bath at 90 °C for 1 h to consume impurities. Finally, the carbon fiber fabrics were submerged into the prepared solution to hydrothermally synthesize ZnO nanoarrays. Detailed solution concentrations and hydrothermal growth temperature are listed in Table 4-1. The morphology of ZnO nanoarrays was studied using FESEM to characterize the average diameters and length to diameter ratio of ZnO nanoarrays. The elemental composition of the carbon fibers before and after ZnO nanoarrays coating were studied by EDX, the ZnO crystal orientation on the synthesized ZnO nanoarrays were

tested by XRD, and the decomposition property and weight ratio of the ZnO on carbon fibers were then characterized using TGA.

4.3 Results and discussion

The identification of the optimal ALD procedure to deposit a thin layer of ZnO seeds on the substrate is a critical aspect of this work. ZnO seeds were uniformly deposited on the silicon substrate, as shown in the FESEM (Figure 4-1(a)) and AFM (Figure 4-1 (b)) images. The same experimental procedure was adopted to deposit ZnO seed layer on carbon fiber fabrics. The FESEM image of the uniformly deposited ZnO seeds on a single carbon fiber was shown in Figure 4-1 (c). XRD tests were used to validate the crystal structures of the ZnO seeds and synthesized ZnO nanowires. Both the ZnO seeds grown on Si wafer (Figure 4-1 (d)) and carbon fibers (Figure 4-1 (e)) were tested first. When ZnO seeds were deposited on a flat Si wafer, the ZnO diffraction peaks in the XRD pattern proved the poly-crystalline nature of the thin film. Meanwhile, contrasting with the two weak (100) and (110) peaks, the dominant (002) diffraction peak indicated that the thin film was primarily grown in the c-axis orientation. Such optimized material quality will ensure high quality ZnO nanoarray growth in the hydrothermal growth process. When ZnO seeds were coated on carbon fiber, more diffraction peaks were detected in XRD. The (002) diffraction peak was still clear, however, the (100) and (101) diffraction peaks were also observed mainly due to the curved carbon fiber surface. The same XRD pattern was observed in ZnO nanowires compared to ZnO seeds on carbon fiber fabrics. During the hydrothermal treatment, all the ZnO diffraction peaks were enhanced, as shown in Figure 4-1 (f).

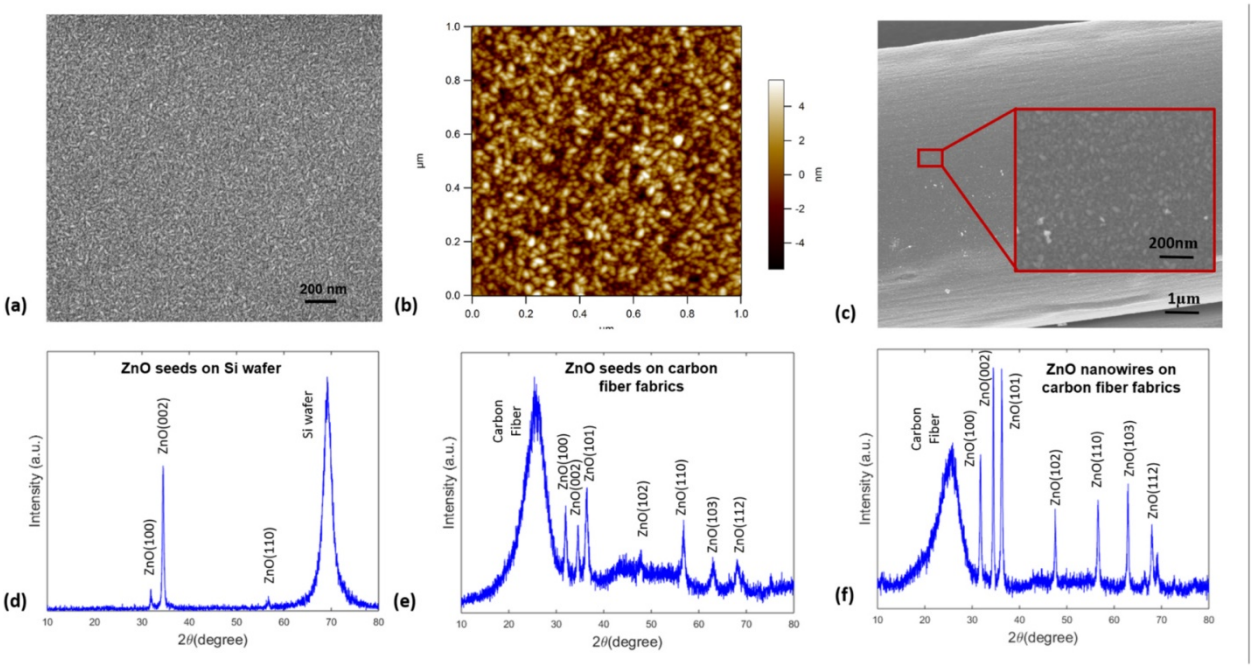

Figure 4-1 (a) FESEM image of ZnO seeds on a silicon substrate; (b) AFM image of ZnO seeds on a silicon substrate; (c) FESEM image of ZnO seeds on carbon fiber fabrics; (d) XRD pattern of ZnO nucleation on the silicon substrate; (e) XRD pattern of ZnO nucleation on carbon fiber fabrics; (f) XRD pattern of ZnO nanowires on carbon fiber fabrics.

The morphology of ZnO nanoarrays on carbon fiber fabrics was studied using FESEM, as shown in Figure 4-2. Six sets of ZnO nanoarrays were synthesized, varying the hydrothermal reaction temperature and reagents' concentrations. The hydrothermal synthesis time used was 17 h for all the experiments. It should be noted that the $Zn(NO_3)_2$ and HMT concentrations had a significant effect on ZnO morphology. As shown in Figure 4-2 (a) and (b), ZnO nanowires were obtained when 25 mMol/L of $Zn(NO_3)_2$ and HMT were used during the hydrothermal treatment. ZnO nanowires with similar morphology were obtained when the hydrothermal reaction temperature was reduced to 70 °C. However, the average diameter of ZnO nanoarrays significantly increased when 50 mMol/L of $Zn(NO_3)_2$ and HMT were used during the hydrothermal treatment. As shown in Figure 4-2 (d) and (e), ZnO nanorods were synthesized on carbon fibers. Similar ZnO nanorods were obtained when the hydrothermal reaction temperature was reduced to 70 °C, though

both the average diameter and length of ZnO nanorods were slightly reduced. The vertical alignment of ZnO nanoarrays were visualized from the side view, as shown in Figure 4-1 (c) and (f). Good ZnO alignment of both ZnO nanowires and nanorods were obtained from samples B1 and B2.

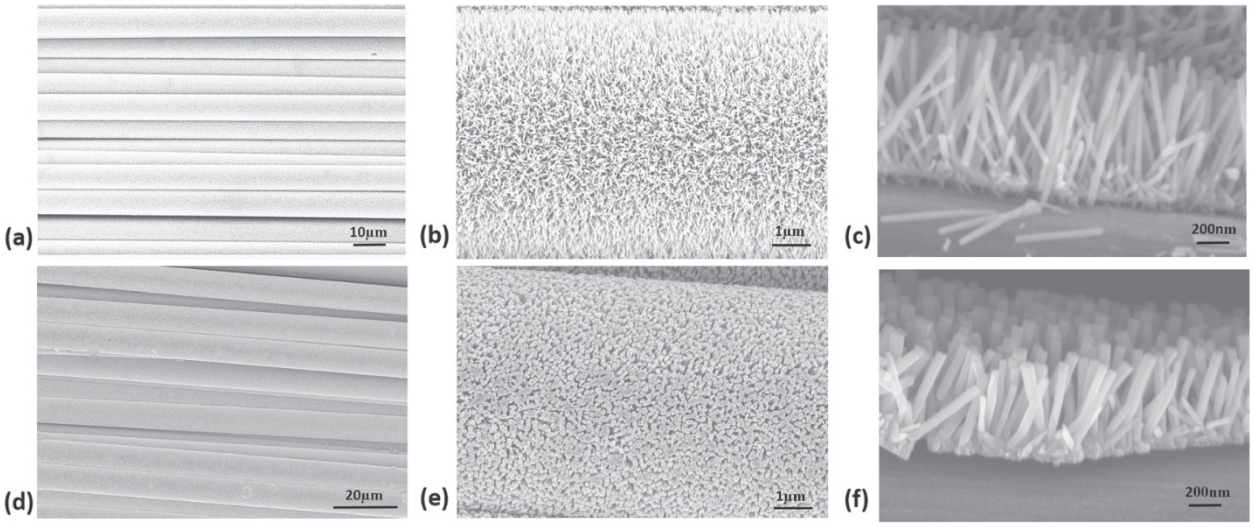

Figure 4-2 (a)–(c) FESEM images of sample B1 showing the vertically aligned ZnO nanowires on carbon fibers; (c)–(f) FESEM images of sample B2 showing the vertically aligned ZnO nanorods on carbon fibers.

When $Zn(NO_3)_2$ and HMT concentrations increased to 100 mMol/L, the diameter of ZnO nanorods increased and the ZnO nanorods were grown at an increased density. As shown in Figure 4-3, nanorods covered entire carbon fiber. Similar results were obtained from sample B3 when the hydrothermal temperature increased to 80 °C. Since this type of ZnO nanoarray coatings on carbon fibers did not significantly increase the surface area to volume ratio of carbon fibers, we did not consider those samples for interfacial strength enhancement in carbon fiber fabrics and composites.

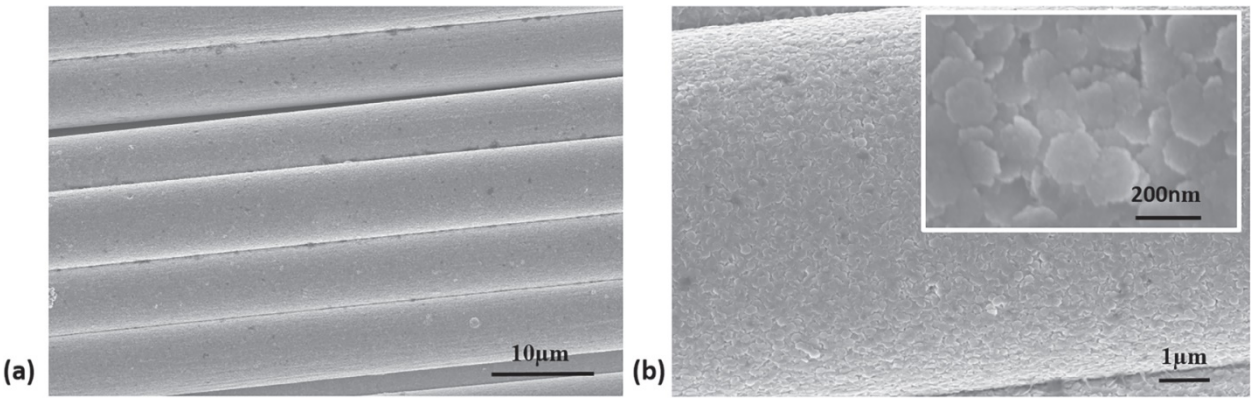

Figure 4-3 FESEM images of sample A3 showing a top view of the fully grown ZnO nanorods covering the entire carbon fiber.

The average diameters and the length to diameter ratio of ZnO are two critical parameters indicating potential mechanical property enhancement capabilities due to increased surface area on carbon fibers. As shown in Figure 4-4, the averaged diameters of ZnO nanoarrays increased from 28 nm (sample A1) to 189 nm(sample B3), and the length to diameter ratio decreased from 270 (sample A1) to 44 (sample B3), when $Zn(NO_3)_2$ and HMT concentrations increased from 25 mMol/L to 100 mMol/L. The variation of ZnO diameter and length to diameter ratio proved that the solution concentration used in hydrothermal synthesis of ZnO nanoarrays on carbon fibers was the dominant effect on the ZnO morphology.

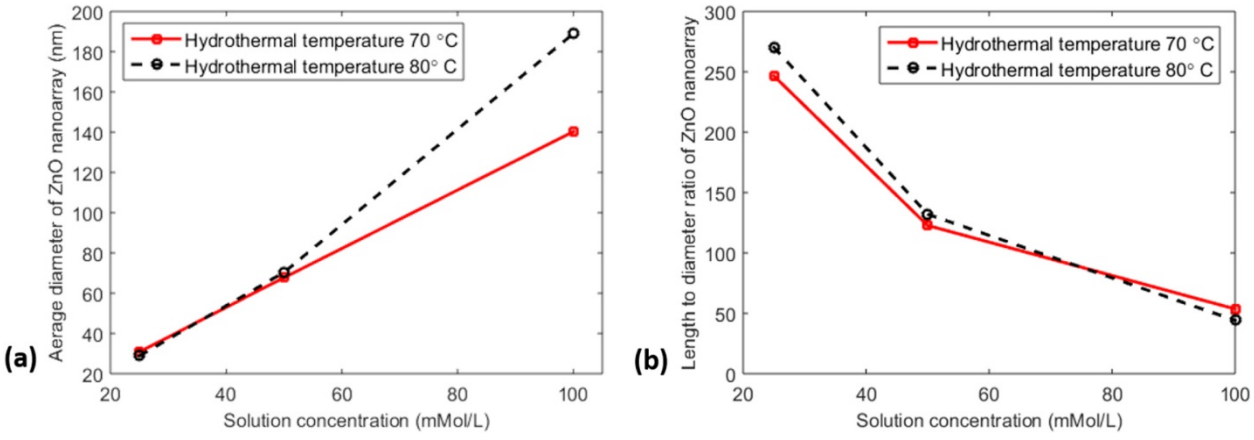

Figure 4-4 (a) Average diameters of ZnO nanoarrays with different concentrations of hydrothermal solutions; (b) average length to diameter ratio of ZnO nanoarrays with different concentrations of hydrothermal solutions.

The EDX pattern (Figure 4-5(b)) shows the elemental analysis on the ZnO nanoarrays coated carbon fiber fabrics. When carbon fibers with ZnO nanoarrays were tested using EDX, only zinc and oxygen elements were detected on the top surface, indicating the high density of ZnO nanoarrays. Although there were gaps among ZnO nanoarrays, the high length to diameter ratio of nanoarrays created full coverage of the carbon fiber surface. For comparison, when pristine carbon fibers were studied via EDX (Figure 4-5(d)), only carbon was detected.

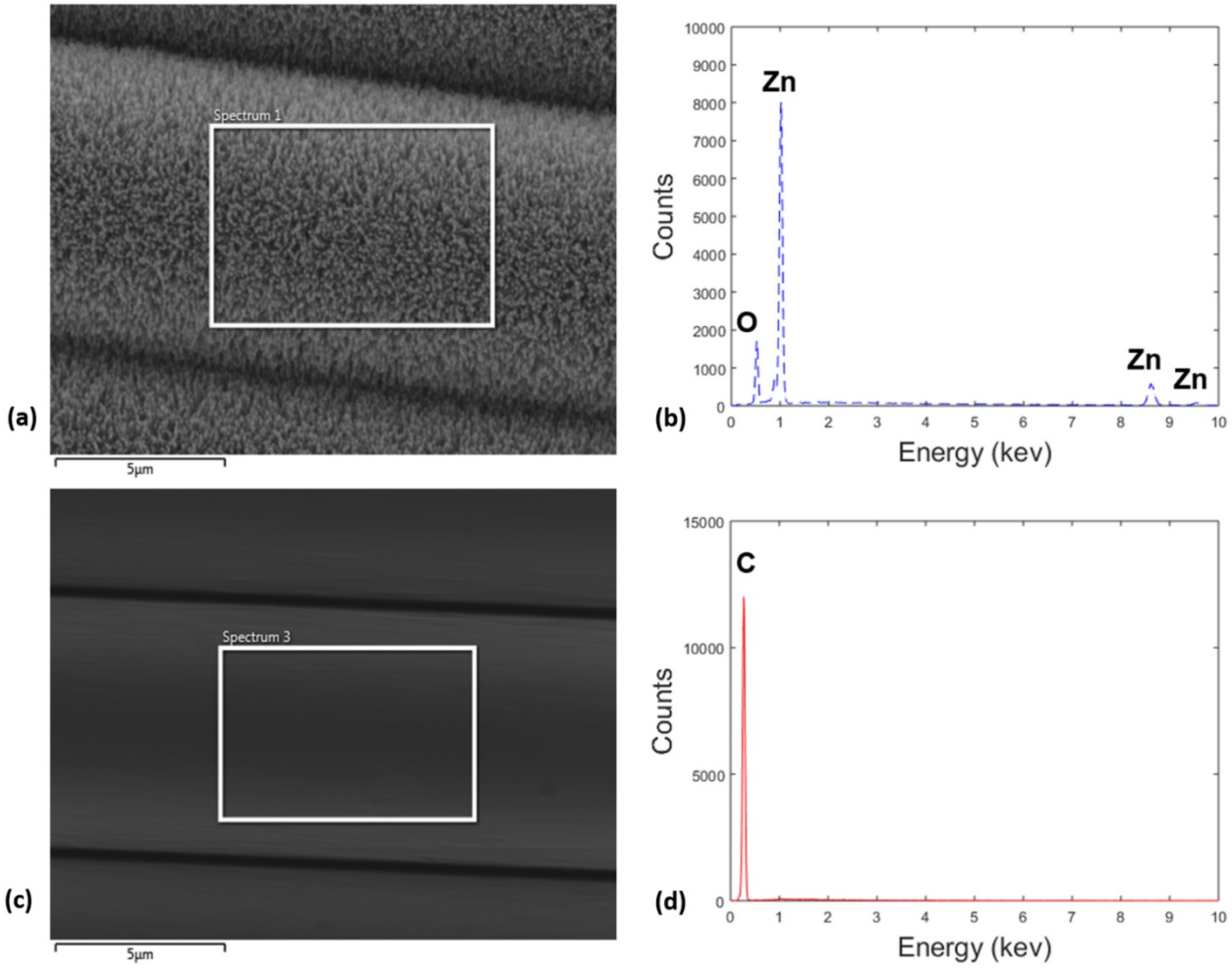

Figure 4-5 (a) FESEM image on carbon fiber with ZnO nanowires; (b) EDX graph measured from the highlighted area in (a); (c) FESEM image on bare carbon fiber; (d) EDX graph measured from the highlighted area in (c).

The weight ratios of ZnO nanoarrays on carbon fibers were investigated using TGA tests and are shown in figure 6. All the experiments were conducted by increasing the temperature by 5 °C/min. The weight of all samples began decreasing around 600 °C. ZnO modified carbon fibers reached full decomposition at 780 °C, and bare carbon fibers were fully decomposed at about 876 °C. Of the carbon fibers coated with ZnO nanoarrays, there was about 11 wt% left after the TGA tests. Since only carbon was burned off during all the TGA tests, the residual weight was considered to be only ZnO, indicating about an 11 wt% weight increase after ZnO nanoarrays synthesis on carbon fibers. In addition, the decomposition speed of bare carbon fibers was slower than the modified carbon fibers with ZnO nanowires. This is because the increased surface area to volume ratio on the modified carbon fibers increased heat transfer efficiency. Therefore, ZnO modified carbon fibers were burned off faster than their unmodified counterparts.

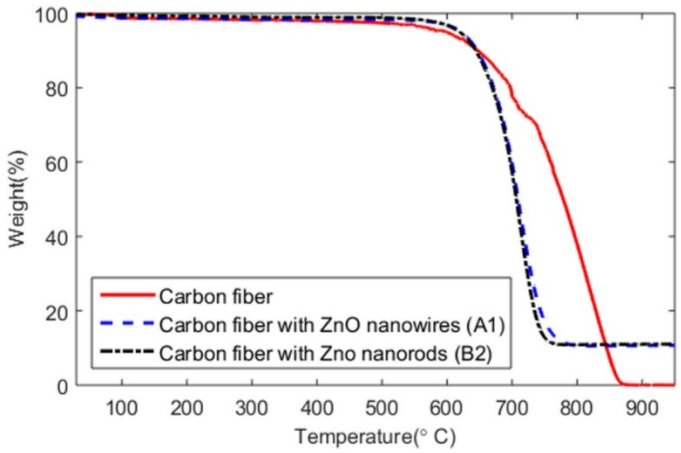

Figure 4-6 TGA graphs of carbon fiber, and carbon fiber coated with ZnO nanoarrays.

4.4 Conclusion

This chapter presents a two-step approach of vertically aligned ZnO nanoarrays synthesis on carbon fiber fabrics using the combined ALD and hydrothermal methods. The optimal ALD parameters and ZnO seeding procedure were identified using silicon substrates and adopted to

grow the ZnO seeds on carbon fiber fabrics. The hydrothermal method was used to synthesize ZnO nanoarrays. By adjusting the hydrothermal solution concentration and temperature, the average diameters of ZnO nanowires and nanorods can be controlled between 28 nm and 189 nm, and the length to diameter ratio of nanowires and nanorods can be controlled between 270 and 44. All ZnO modified carbon fibers were characterized using FESEM, EDX, and TGA. Due to the dramatic increase of surface area on the modified carbon fiber fabrics, these materials can be used to develop novel structural composites with enhanced mechanical properties. Load sensing capabilities can also be obtained due to the piezoelectric properties of the ZnO nanoarray.

Chapter 5 Synthesis and Characterization of Self-Assembled ZnO Nanoarrays On Hybrid Structural Fibers

5.1 Introduction

Advanced fiber reinforced composites have been used extensively in high-performance structural applications[102-106]. Due to weak adhesive bonding in composites, barely visible damage, such as delamination and fiber pull-out, can significantly weaken the mechanical strength of composites and even cause catastrophic structural failures[107, 108]. Hybrid fibers with nanostructured surfaces using carbon nanotubes (CNT) and zinc oxide (ZnO) nanowires have been developed to enhance interfacial mechanical properties[7, 109-111]. Due to their superior mechanical and thermal properties, well-aligned CNT nanoforests have been synthesized mainly using chemical vapor deposition (CVD) method to enhance the bonding strength and interfacial properties in fiber reinforced composite laminates[112]. However, the high CVD temperature can degrade the mechanical strength of carbon fiber fabrics in composite laminates. Due to the increased surface area to volume ratio, structural fiber fabrics coated with ZnO nanowires are expected to increase the bonding between the fiber and polymer matrix in composites. The low hydrothermal temperature of ZnO nanowires allows direct growth of ZnO nanostructures on structural fibers and used for structural composite applications. In addition, as a type of piezoelectric materials, ZnO nanowires can respond to applied external loads on composites, leading to novel functional composites with load sensing functions[113].

In recent years, increasing attention has been drawn to the advancement of synthesis technology for the growth of aligned ZnO nanoarrays in the shape of nanowires[114, 115], nanorods[116, 117], nanorings[100], nanosprings[118], and other nanostructures[119, 120] on various types

of substrates using chemical vapor deposition[121], physical vapor deposition[122], and hydrothermal[123] methods. However, most aligned ZnO nanowires on continuous structural fibers have been synthesized using a two-step method: first, the dip-coating method to generate ZnO seeds on fiber surfaces, and then the hydrothermal method for nanowire growth[29, 73]. Since the dip-coating method can hardly control the size and shape of ZnO seeds, low seeding quality affects the alignment and property of hybrid fibers with ZnO nanoarrays.

Atomic layer deposition (ALD) has been well accepted as a micro-manufacturing technology to grow thin films[55]. Since ALD is able to meet the needs for atomic layer control and conformal deposition using sequential and self-limiting surface reactions, this approach is considered to be one of the best methods to achieve high conformality, in particular, on high aspect structures. Binary metal oxides, including Al_2O_3[124], TiO_2[125], ZnO[126], and metal thin films, such as Cu[127], can be deposited on various substrates. Besides conformality, low deposition temperature is another key advantage of ALD, allowing the process of temperature sensitive materials and substrates. The employment of ALD method to grow ZnO seed layer on carbon fiber fabrics has the potential to accurately control ZnO nanoparticle size with improved uniformity. Since the mechanical properties of carbon fiber fabrics can be significantly degraded at high temperature, low deposition temperature of ALD allows to coat conformal ZnO thin films as seed layer on carbon fiber fabrics without degrading the fiber's strength. Our recent study has demonstrated the capability to grow ZnO seed layer on carbon fiber fabrics using ALD method[74, 77]. This chapter focuses on the impacts of the reagent concentrations and hydrothermal reaction time on ZnO nanoarray morphology.

In this chapter, we report an integrated approach for the morphological control of ZnO nanowire arrays on carbon fiber fabrics, using ALD to deposit ZnO seeds and the low temperature

hydrothermal method for nanowire synthesis. The unique combination of ALD and hydrothermal methods allowed to generate high ZnO seed layers on carbon fiber and to control ZnO nanoarray morphology. The nano structures of synthesized ZnO were tailored by adjusting the hydrothermal process time and reagent concentrations. Detailed properties of the fabricated hybrid fibers were characterized.

5.2 Experiments

5.2.1 Materials

Diethylzinc and deionized water were purchased from Sigma–Aldrich and used for ZnO seeding via ALD. Trichloroethylene (TCE, 99%), zinc nitrate hexahydrate ($Zn(NO_3)_2$, 99%) and hexamethylenetetramine (HMT, 99%) were purchased from Sigma–Aldrich and used in the hydrothermal synthesis of ZnO nanoarrays on carbon fiber fabrics. All the materials were used as received.

5.2.2 Synthesis procedure of hybrid fibers

In this chapter, a two-step hybrid fiber synthesis procedure, combining ALD and hydrothermal methods, was developed to synthesize ZnO nanoarrays. High quality ZnO seeds were first deposited on carbon fibers via ALD, and then grown into nanoarrays in an aqueous solution using the hydrothermal method. The schematic of synthesis procedure is shown in Figure 5-1.

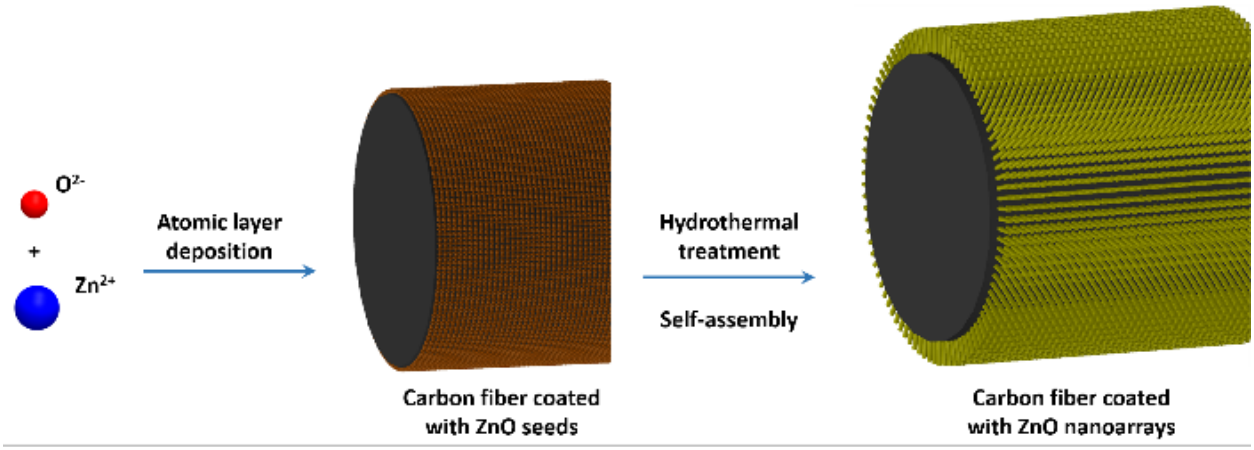

Figure 5-1 Schematic of synthesis procedure of hybrid structural fibers using combined ALD and hydrothermal methods.

Carbon fiber fabrics were first degreased by dipping them into TCE and methanol, respectively, for 10 minutes under ultrasonic agitation, washed under running deionized water for 10 minutes, and finally dried in an environmental oven. The prepared carbon fiber fabrics were used for the ALD and hydrothermal synthesis of ZnO nanoarrays on carbon fiber fabrics.

To synthesize ZnO nanoarrays on carbon fiber fabrics, a customized thermal ALD system was used to deposit ZnO seeds on the cleaned carbon fiber fabrics. In the reaction process, a double-exchange chemical vapor reaction was adopted between DI water and DEZn precursors. The dose time was controlled via computer driven pneumatic valves, and N_2 gas was used to carry these vaporized sources to the reaction chamber. The H_2O and DEZn were alternately distributed, and a 10 second ultra-high purity N_2 purge period was carried out after each dosing process. It should be noted that this period was enough to ensure the pressure returned to its base level before the next pulse.

In the second step, $Zn(NO_3)_2$ and HMT aqueous solutions were prepared for the hydrothermal process. Each was stirred at 600 rpm for 10 minutes at 55 °C, then mixed together and stirred at 600 rpm for 10 minutes at 55 °C. The solution was stored in a water bath at 90 °C

for 1 hour to consume impurities. Finally, the carbon fiber fabrics were submerged into the prepared solution to hydrothermally synthesize ZnO nanoarrays. The morphologies of synthesized nanoarrays were controlled by adjusting the hydrothermal reaction time from 5 h to 30 hours and reagent concentration from 25 mMol/L to 100 mMol/L. The ZnO nanoarrays were naturally aligned due to the self-assembly nature of ZnO nanoarrays.

5.2.3 Property characterization

The investigation of the ZnO nanoarray morphology was carried out using a field emission scanning electron microscope (FESEM) at a voltage of 20 kV. The diameters of the ZnO nanowires were measured using the commercial software ImageJ on the FESEM images, and statistical analyses were employed to study the diameter distribution of the ZnO nanoarrays. The weight concentration of ZnO in hybrid fiber was tested using the thermogravimetric analysis (TGA). The element analysis of hybrid fibers was conducted using energy-dispersive X-ray (EDX) spectroscopy. Powder X-ray diffraction (XRD) measurements were carried out using a Rigaku Ultima IV diffractometer. Cu-K-alpha radiation (40 kV, 44 mA) was used via a Bragg-Brentano detector. The hydrophobic and hydrophilic surface properties of the synthesized hybrid fibers were characterized by measuring the contact angles of water and ZnO nanoarrays. ZnO nanoarray coated carbon fiber fabrics was attached on a glass substrate and place on a flat stage in front of a camera. Water droplet was pushed out from a syringe by a motor-driven lead screw mechanism. Only one water droplet was placed on top of the ZnO nanoarray during the tests. The contact angle was measured using commercial software ImageJ from the recorded pictures.

5.3 Results and discussion

In this chapter, the morphology and microstructure of ZnO nanoarrays were controlled by tailoring the reagent concentrations and reaction time of the hydrothermal process, and were

studied via FESEM. Four types of ZnO nanoarray morphology were obtained: fine nanowires (Figure 5-2 a & b), fuzzy nanowires (Figure 5-2 c & d), fine nanorods (Figure 5-2 e & f), and compact nanorods (Figure 5-2 g & h). Both the fine nanowires and fine nanorods showed a one-dimensional (1D) microstructure of the synthesized nanoarray, with the ZnO nanowires aligned on carbon fiber fabrics. However, the fuzzy nanowires were not well-aligned due to the lack of guidance during the hydrothermal process. The ZnO compact nanorods covered the entire carbon fiber surface when the reagent concentration was 200 mMol/L or higher during the hydrothermal process. The detailed reagent concentrations, hydrothermal growth time, and obtained morphology are listed in Table 5-1. The diameter distributions of the ZnO nanoarrays obtained from the corresponding FESEM images are shown in Figure 5-3. The average diameters of the ZnO nanoarrays can be controlled at different reagent concentrations. When the reagent concentration increased from 25 to 100 mMol/L, the average diameters of the ZnO nanoarrays increased from 29nm to 65nm, correspondingly. Similar trends were obtained when the hydrothermal reaction time increased from 5 hours to 30 hours.

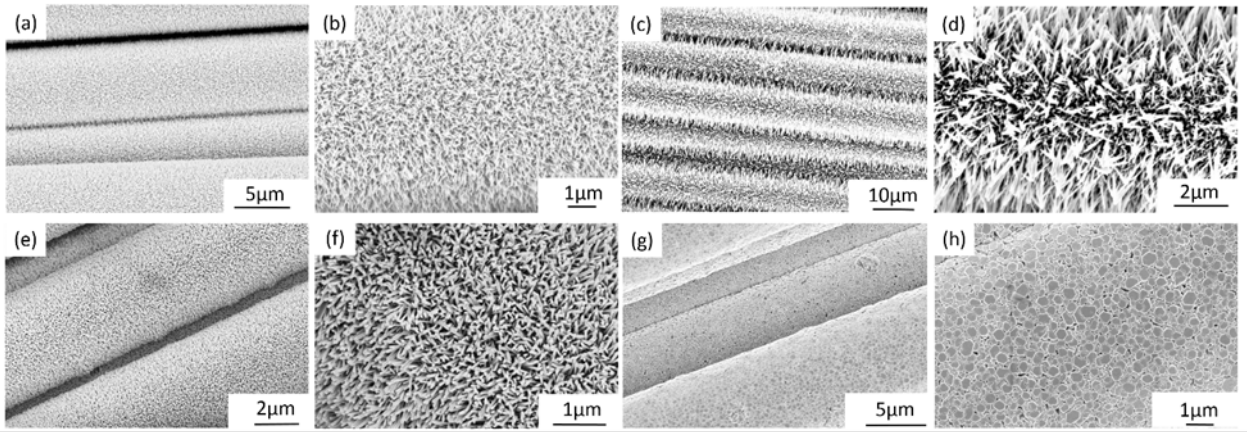

Figure 5-2 FESEM images of synthesized hybrid structural fibers: (a & b) FESEM images of ZnO fine nanowires on carbon fibers; (c & d) FESEM images of ZnO fuzzy nanowires on carbon fibers; (e & f) FESEM images of ZnO fine nanorods on carbon fibers; (g & h) FESEM images of compact nanorods on carbon fibers showing the fully coverage of carbon fiber by ZnO.

Table 5-1 Hydrothermal parameters.

Sample Name	$Zn(NO_3)_2$ (mMol/L)	HMT (mMol/L)	Growth Time (h)	Nanoarray morphology
A1	25	25	5	Fine nanowires
A2	50	50	5	Fine nanowires
A3	100	100	5	Fine nanorods
A4	200	200	5	Compact nanorods
B1	25	25	17	Fine nanowires
B2	50	50	17	Fuzzy nanowires
B3	100	100	17	Fine nanorods
B4	200	200	17	Compact nanorods
C1	25	25	30	Fine nanowires
C2	50	50	30	Fuzzy nanowires
C3	100	100	30	Fine nanorods
C4	200	200	30	Compact nanorods

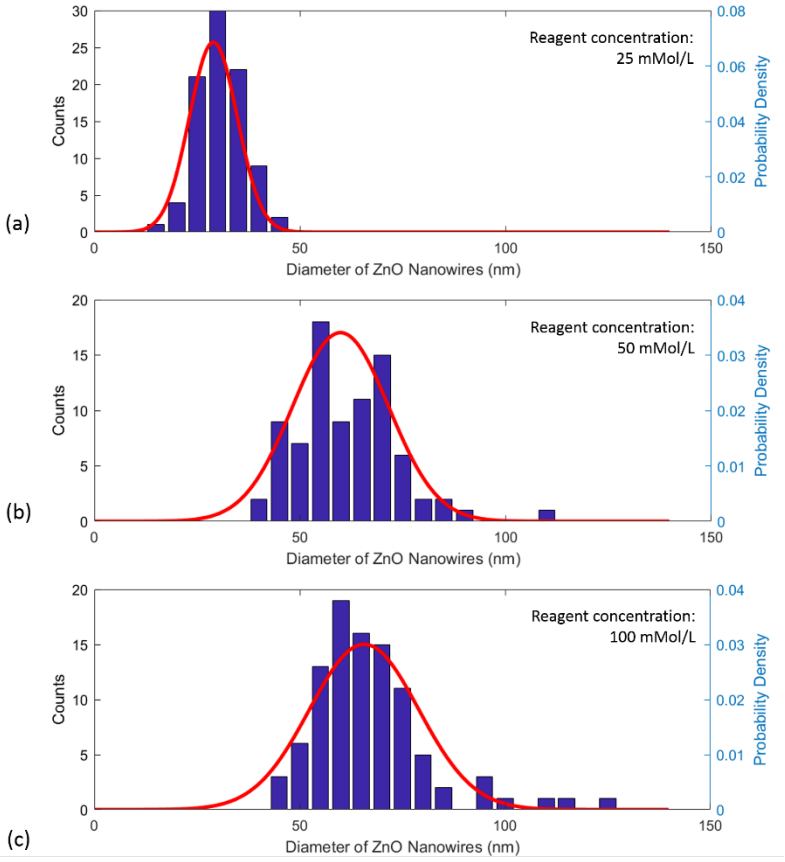

Figure 5-3 Effect of reagent concentration on diameter distributions of ZnO nanoarrays grown on carbon fiber substrates. Growth time: 5 h.

Weight concentration of aligned ZnO nanowire arrays on hybrid fiber fabrics is critical for light-weight composite applications. TGA tests were conducted to burn off all carbon fiber fabrics, and ZnO weight concentrations were calculated using the residual weight of the tested samples. As shown in Figure 5-4 (a), carbon fibers on the hybrid fiber samples A1, B1, and C1 all started decomposing at around 600˚C. Once all the carbon fibers were burned off, the residual weight concentrations of ZnO for samples A1, B1, and C1 were 5.10%, 5.68%, and 7.56%. Since the reagent concentration used for these samples was at 25 mMol/L, the TGA results proved that longer hydrothermal synthesis time results in higher ZnO concentrations and larger ZnO nanowire and nanorod diameters. Similar TGA test results were obtained using other samples. The TGA testing results of samples A2, B2, and C2 are shown in Figure 5-4 (b), and the TGA testing results of samples A3, B3, and C3 are shown in Figure 5-4 (c). The TGA results reported in the supplement materials demonstrate that longer hydrothermal synthesis time results in higher ZnO concentrations and larger ZnO nanowire and nanorods diameters. In addition to the hydrothermal treatment time, reagent concentrations also impacted ZnO weight concentrations. When the reagent concentration increased from 25 mMol/L to 100 mMol/L, the maximum ZnO weight ratio reached 11.72%. The weight concentration of ZnO of all the tested samples are listed in Table 5-2, and summarized TGA in Figure 5-4 (d).

Table 5-2 ZnO weight concentrations of hybrid fibers.

Sample Name	ZnO weight concentration	Sample Name	ZnO weight concentration	Sample Name	ZnO weight concentration
A1	5.10%	B1	5.68%	C1	7.56%
A2	5.57%	B2	7.24%	C2	9.45%
A3	7.54%	B3	10.59%	C3	11.72%

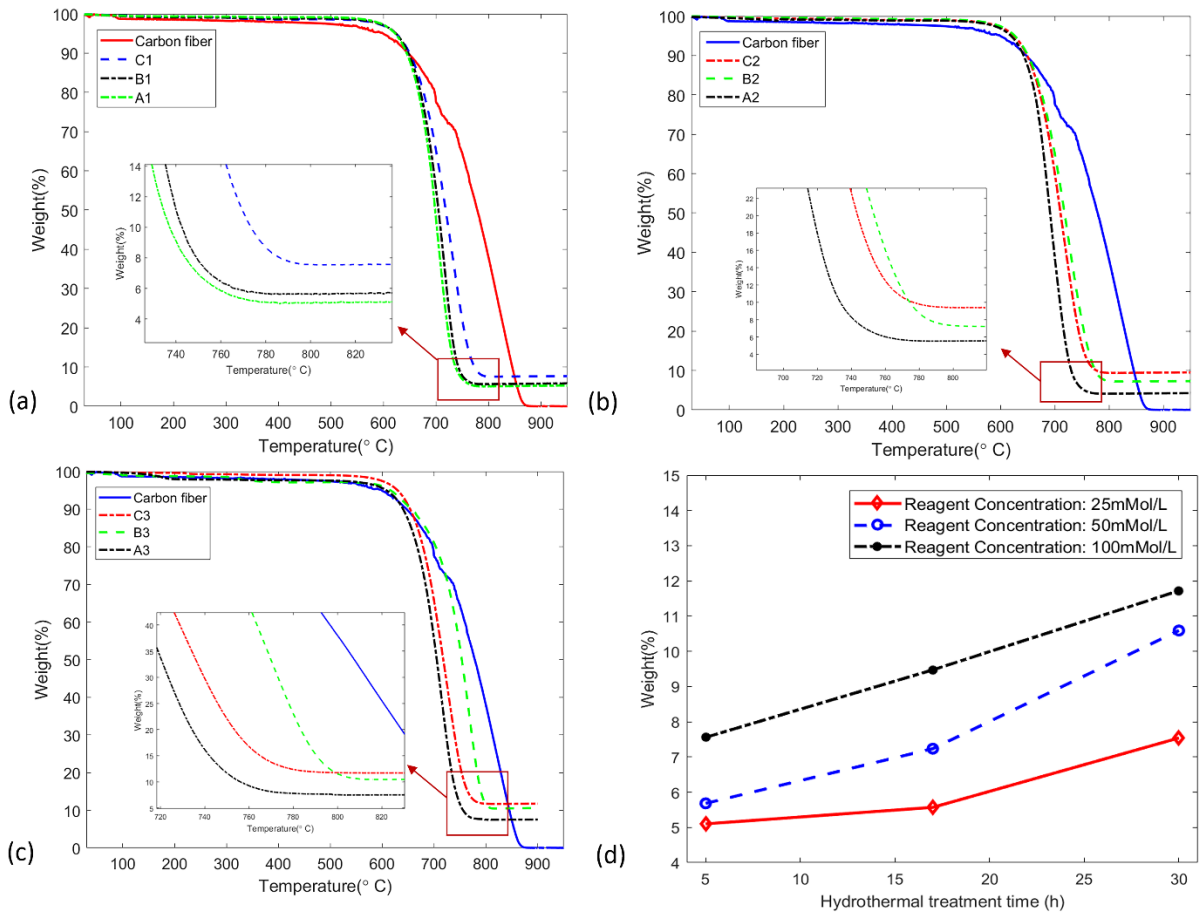

Figure 5-4 TGA characterization of ZnO weight concentrations in hybrid structural fibers.

Elemental analysis of the ZnO nanoarray coated carbon fiber fabrics was performed via EDX. Zinc, oxygen, and carbon were all detected on samples with ZnO fine nanowires. Only zinc and oxygen were detected on samples with fuzzy nanowires and fine nanorods due to the high ZnO density on the fibers (Figure 5-5). The crystal structures of ZnO nanoarrays were studied via XRD. Figure 5-6 shows that multiple diffraction peaks, including (100), (002), and (101), were recorded due to the highly cured fiber surface. Since the same XRD diffraction peaks were obtained from all the samples with different morphology, it can be concluded that the variation of reagent concentration and hydrothermal process time did not change the crystal structures of synthesized ZnO nanoarray coated carbon fiber fabrics.

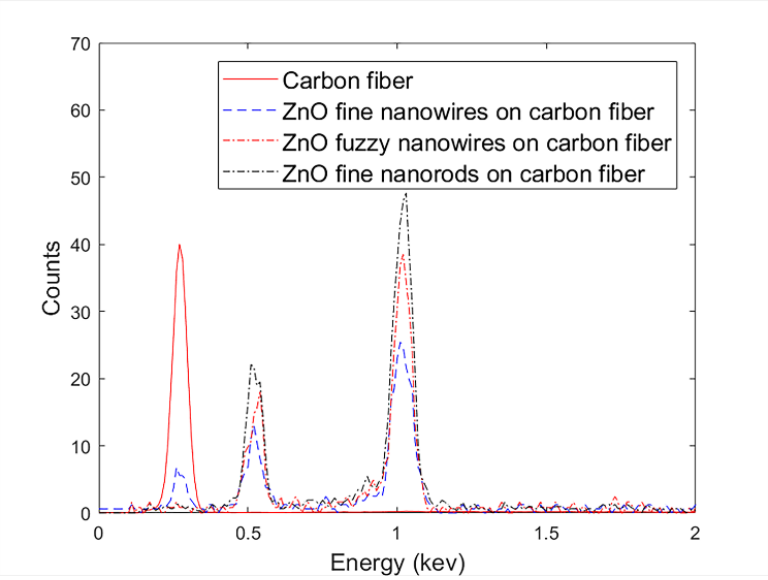

Figure 5-5 EDX spectra of ZnO nanowires on carbon fibers.

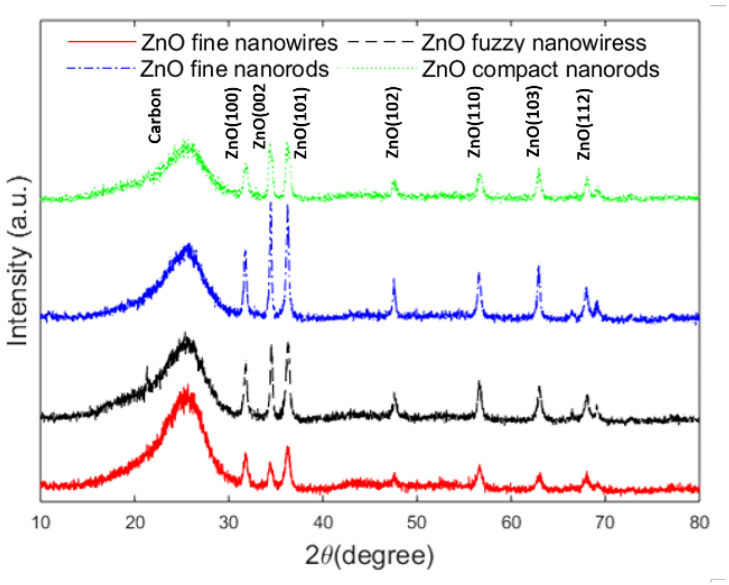

Figure 5-6 XRD diffraction of ZnO nanoarrays with different morphology.

The contact angles of water on the grown ZnO nanostructures have been measured from the synthesized hybrid fiber fabrics with four different types of ZnO morphologies. As shown in Figure 5-7, the contact angles of water on ZnO fine nanowires, fuzzy nanowires, fine nanorods, and compact nanorods were 155.7°, 144.9°, 139.0°, and 77.8°, respectively. Compared to ZnO

morphology in Figure 5-2 and the average ZnO diameters shown in Figure 5-3, it is obvious that the nanostructures of fine ZnO nanowires with good alignment and small average diameter could provide air/solid binary collaboration effect on the fabric surface, which increased the water repellence property of the fabrics. However, the hydrophobic properties were weakened when the average diameter increased and ZnO morphology converted to fuzzy nanowires and nanorods. When ZnO completely covered the entire carbon fiber and showed morphology of compact nanorods, the contact angle reduced to 77.8°, demonstrating the hydrophilic surface property of the hybrid fabrics.

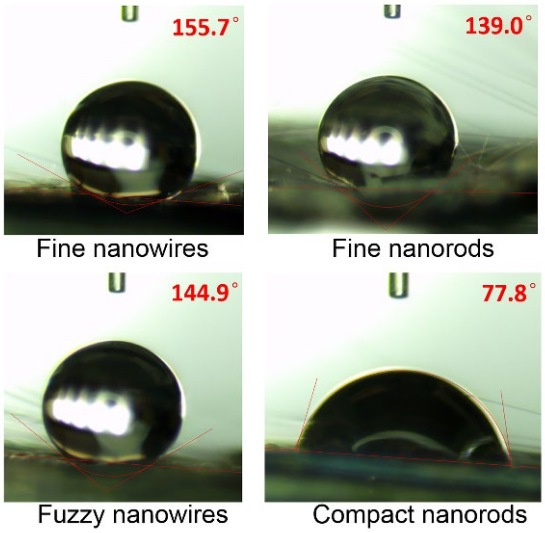

Figure 5-7 Contact angles of four types of synthesized hybrid structural fiber fabrics.

5.4 Conclusion

ZnO nanoarrays with controllable morphology were synthesized and characterized in this chapter. A two-step approach combining ALD and hydrothermal methods was developed to synthesize ZnO nanoarrays. Characterization methods, including FESEM, TGA, EDX, and XRD, were employed to study the morphology and crystal structures of ZnO. Four types of ZnO surface morphology were grown on carbon fiber fabrics: fine nanowires, fuzzy nanowire, fine nanorods,

and compact nanorods. Experimental results demonstrated that the same ZnO crystal structure was obtained regardless of the reagent concentrations and hydrothermal process time. The contact angles of the synthesized hybrid fibers were controlled by the average ZnO diameter and morphology. The developed hybrid fibers can be used to develop light-weight structural composites with enhanced interfacial properties.

Chapter 6 Enhancement of Interfacial Shear Strength in Carbon Fiber Reinforced Composite Laminates

6.1 Introduction

Advances in reinforcements fibers and polymers have led to the development of high-performance structural composites[104]. Multiple types of fibers have been applied as reinforcing materials, such as carbon fiber, glass fiber, and aramid fiber. Because the mechanical properties of composites depend not only on the constituent materials but also on the interfacial properties between fiber and polymer matrix, the research of fiber/matrix interface and load transfer mechanism have received considerable attentions. For carbon fiber reinforced polymer matrix composites, multiple surface treatment methods have been investigated to improve the bonding at the fiber/matrix interface. In general, the interfacial properties of composites are improved following three strategies: 1) enhancing the chemical interactions at the fiber/matrix interface; 2) increasing the fiber surface area for load transfer; 3) integration of both chemical interactions and increased surface area of fiber. For example, chemical oxidation can remove weak outer layers of fibers and add functional groups to generate strong chemical bonds between fiber and matrix using chemical interactions[128, 129]. Nonoxidative treatment methods, such as grafting, involve the deposition of materials on fibers, resulting in a thin layer of coating on fibers to improve the load transfer capability[130]. In addition, high energy irradiation method has been used to cure polymer matrix in composites, creating both oxygen functional groups on carbon fibers and tailoring surface roughness for increased contact area between fiber and matrix[131]. However, the surface oxidation, plasma treatment, and other chemical processing of carbon fibers can influence the graphite structures of carbon fibers and weaken the overall composite properties.

Recently, whiskerization has been a popular approach to grow high strength of nanostructures on structural fibers[132]. Various nanoparticles including aligned carbon nanotubes (CNTs), silicon carbide (SiC) nanowires, zinc oxide (ZnO) nanowires have been synthesized on carbon fibers as an interphase for the enhancement of interfacial properties[133-135]. The employment of CNTs and SiC nanowires on continuous structural fibers increases their surface area that can lead to improved mechanical interlocking and load transfer capabilities between fiber and matrix in composites. However, these approaches are challenged by the potential degradation of carbon fibers caused by the harsh nanoparticle synthesis procedures. The syntheses of CNTs and SiC nanowires using chemical vapor deposition (CVD) process are usually carried out at least 900 °C, which cause significant structural degradation of carbon fibers, thus, decreasing in-plane properties of composites[136]. In addition, catalyst used during the synthesis of CNTS can significantly lower down the tensile strength of carbon fiber[137].

To overcome these problems, Lin et al. developed a two-step hydrothermal method at low temperature (<90 °C) to vertically grow ZnO nanowires on carbon fiber [29]. He demonstrated that the IFSS was improved more than 110% when ZnO nanowires worked as an interphase without degradation of tensile strength of carbon fiber. Ehlert et al. investigated that ZnO nanowires worked as an interphase to carbon fiber and explained the chemical mechanism of adhesion[135]. He used experiment and simulation of molecule dynamics to prove that the ketone groups improve the adhesion between ZnO and graphite. Patterson et al. directly measured the adhesive force between ZnO nanoparticles and highly oriented pyrolytic graphite (HOPG) using atomic force microscopy (AFM) to investigate the interaction of ZnO nanowires and validated that ZnO was a strong interface[138]. Parisa et al. recently demonstrated a multi-scale analysis using ABAQUS to simulate the interaction of ZnO nanowires between carbon fiber and matrix [139]. She confirmed

that the existence of ZnO nanowires will enhance the load transferring between carbon fiber and matrix.

In this two-step hydrothermal method, mechanical properties of carbon fiber preserved due to this low temperature aqueous growth compared to the traditional CVD growth of CNTs [29]. The first step of seed layer growth of ZnO nanoparticles is the most important to determine the second step of ZnO nanowires growth[140]. The non-uniform ZnO seed layer will lead to a large size of ZnO nanowires and affect the morphologies of ZnO nanowires. For the first step, a dipping method was used to grow the ZnO nanoparticles which has a limitation of large grain size of ZnO nanoparticle and difficult uniformity. Compared to the dipping, atomic layer deposition (ALD) is promising for the growing of ZnO nanoparticle due to its excellent uniformity, high degree of conformity, atomic-scale thickness controllability, perfect stoichiometric uniformity, low impurity contamination, and low growth temperature which can be as low as 100 °C close to the dipping[74, 141]. ZnO nanowires synthesized on carbon fabric using ALD to grow the ZnO nanoparticles as seed layer have been reported in our previous work[76, 77].

Several techniques are used to measure the IFSS including fiber push-in test[142], pull-out test[143], micro-bond test[144] and single fiber fragmentation test (SFFT)[42]. Among them, SFFT is the most popular method as the preparation of specimen and operation of test are simple and the fail type can be visualized during process compared to the other three. In this test, a single fiber was embedded into the dog-bone shape of polymer matrix along the central axis. The specimens are applied with tensile load, and the tensile load forms the matrix which create the shear stress along the axial direction of fiber. The shear stress will also result in the normal stress of single fiber. Fiber facture occurs when the normal stress reaches to the tensile strength of fiber. The

fragmentation of fiber will reach to a saturation when the cracked fiber can no more transfer shear load.

In this chapter, ZnO nanowires grown on carbon fibers were used to develop hybrid composites. Individual carbon fibers in the diameter of several micrometers were surrounded by ZnO nanowires. Nanoscale ZnO seeds were first deposited on single carbon fiber using ALD method, then aligned 1D ZnO nanowires were synthesized using hydrothermal treatment. The synthesized ZnO nanowires on carbon fibers were characterized by field emission scanning electron microscope (FESEM), energy-dispersive x-ray spectroscopy (EDX), X-ray diffraction (XRD) and thermogravimetric analysis (TGA). The influence of this selective, nanoscale reinforcement on the mechanical properties of fiber/matrix interfaces was investigated using single fiber fragmentation test. The ZnO nanowires with optimal diameter and length to diameter ratio resulted in improved fiber/matrix interfacial load transfer capability. The improvements in interfacial strength of the ZnO nanowire-reinforced composites can potentially increase shear modulus and yield strength of polymer matrix composites.

6.2 Experiments

6.2.1 Materials

All chemicals were used as received. Diethylzinc (DEZn, $Zn(C_2H_5)_2$) and deionized water (DI water) were received from Sigma–Aldrich to grow the ZnO nanoparticles in the first step of hydrothermal method. Zinc nitrate hexahydrate ($Zn(NO_3)_2 \cdot 6H_2O$) and Hexamethylenetetramine (HMTA) were purchased from Sigma–Aldrich to synthesize the ZnO nanowires in the second step of hydrothermal method.

6.2.2 Growth of ZnO nanoparticles

Single carbon fiber was stripped from carbon fabric, fixed on a Teflon frame by carbon tape. A customized 3" ALD system was used to execute the growth of ZnO nanoparticles on single carbon fiber at the temperature of 200 °C and background pressure of 0.5 Torr for total 300 growth cycles. The vapor ratio of DI water and DEZn was about 2 and ultrahigh purity N_2 gas was purged after each dose for 20 seconds. These growth parameters were the optimized results reported in our previous publication[74].

6.2.3 Growth of ZnO nanowires

$Zn(NO_3)_2$ and HMTA powder were dissolved in DI water to prepare the growth solutions. Each solution was heated to 90 °C and stirred at 800 rpm for 10 minutes on hotplate, then combined together in a beaker. The single carbon fiber on Teflon frame was immersed in the beaker covered with wrap. The beaker was stored in a water bath at 95 °C for 17 hours. The concentration of $Zn(NO_3)_2$ and HMTA from 25 mMol/L, 50 mMol/L and 100 mMol/L at a molar ratio of 1:1 were prepared to vary the morphologies of ZnO nanowires.

6.2.4 Characterization

The FESEM was used to investigate the morphologies of ZnO nanoparticles and nanowires. The software ImageJ was used to measure the length and analyze the statistical diameters of ZnO nanowires based on the FESEM images. EDX spectroscopy was employed to conduct the elemental analysis of hybrid carbon fiber. Rigaku Ultima IV diffractometer was used to carry out the XRD measurement of ZnO structure.

6.2.5 Single fiber tensile test

Single fiber tensile test was carried out to measure the tensile strength of bare carbon fiber and carbon fiber with ZnO nanowires and to identify the effect of ZnO nanowires on carbon fiber.

It is important to obtain this value to calculate the IFSS of single fiber fragmentation test. The major benefit of growing ZnO nanowires on carbon fiber is the preserving of tensile strength of carbon fiber with little loosing. The gauge length of single bare carbon fiber and carbon fiber with ZnO nanowires is 25.4mm and 15 fibers of each concentration growth were tested by DEBEN tensile stage with a 2N load cell applying displacement rate of 0.1 mm/minute.

6.2.6 Single fiber fragmentation test

SFFT is an essential technique to determine the interfacial properties between polymer matrix and carbon fiber [42]. A dog-bone specimen embedded with single carbon fiber inside is prepared to do the tensile test under an optical microscope. Stress is transferred to the fiber in shear direction when the specimen is tensile status. Fiber fracture will occur when applied external force exceeds its tensile strength. The new segmented fiber can continue to transfer load when the tensile force increases. The number of cracked carbon fiber will increase until reaches to a saturation which means the existed fiber segment cannot transfer load to generate new fractures of carbon fiber. After saturation, the average IFSS can be calculated by following equation (1),

$$\tau = \frac{\delta_f d}{\frac{8}{3}\bar{l}} \tag{1}$$

where δ_f is the tensile strength of single carbon fiber at the critical length, d is the diameter of carbon fiber and $\bar{l}$ is the average length of fragmentation.

Single carbon fiber was clipped by two small clamps and transferred to the middle of a silicone mold (Bluesil V-340/CA-45Mold Making Silicone Rubber) before infiltrating the epoxy. Pre-tension was applied to the carbon fiber due to the shrinkage of epoxy during curing. Epon 862 and Epikure 9553 were used to prepare for the polymer matrix due to its high tensile strain over 9% which is much larger the tensile strain of carbon fiber and clear transparency after curing which

helps the observation of counting crack under optical microscope. They were mixed at a weight ratio of 100:16.9, and degassed in a vacuum tank for 3 minutes. The epoxy solution was infiltrated to the mold by a syringe to reduce the potential air bubbles before curing. Then the mold was left at room temperature for 16 hours and put in oven at 100 °C for 1 hour and 160 °C for 1 hour.

After curing, all specimens were polished by Struers with following steps. SiC foil 320 paper put on MD GEKKO was used to remove extra materials and make the specimens be the thickness of near 1.1 mm to meet the range of 200N load cell of tensile stage. Then the specimens were polished on both sides by MD LARGO with 9 micron diamond spray, MD MOL with 3 micro diameter and MD CHEM with silica suspension. Each of these three steps was polished for 3 minutes at 150 RPM under 30N. Finally, specimens with smooth and transparent surface were obtained for later SFFT.

6.3 Results and discussion

Multiple parameters including ZnO nanoparticles determined by the temperature, background pressure and cycles of ALD process, temperature, growth time and concentration of Zinc nitrate hydrate and HMTA have a critical effect on the morphologies of ZnO nanowires. Based on our previous report, lower temperature, higher growth time and higher concentration of Zinc nitrate hydrate and HMTA will lead to the larger diameter of ZnO nanowires. Undesired ZnO nanorods or nanoflakes will occur when the diameter is too large which are too dense and impossible for liquid epoxy to infiltrate in. Considering multiple parameters will results in a large group of ZnO nanostructures in different morphologies, we keep constant parameters of ALD process, and only choose concentration of $Zn(NO_3)_2$ and HMTA ranging from 25mMol/L, 50 mMol/L and 100 mMol/L at 95°C for 17 hours to investigate its effects.

The shape of ZnO nanoparticles as seed layer was rice like with random orientation, illustrated in Figure 6-1 (a). The length of ZnO nanoparticles ranged from 15 nm to 30 nm, and width ranged from 7nm to 15 nm. ZnO nanowires vertically grew on the surface of single carbon fiber with relatively uniform length and diameter, but some large nanowires can be also seen in a random distribution. When the reagent concentration increases, the morphologies of ZnO nanowires change from needle liked tip (Figure 6-1(b)) to hexagonal column (Figure 6-1(d)) and the length of ZnO nanowires varied greatly. The length of ZnO nanowires was defined as the half value of the diameter of carbon fiber with ZnO nanowires subtracting the diameter of bare carbon fiber. The diameter of bare carbon fiber was 6.972 um, so the average length of ZnO nanowires under different growth condition was 0.811 um, 1.853 um and 2.490 um, respectively.

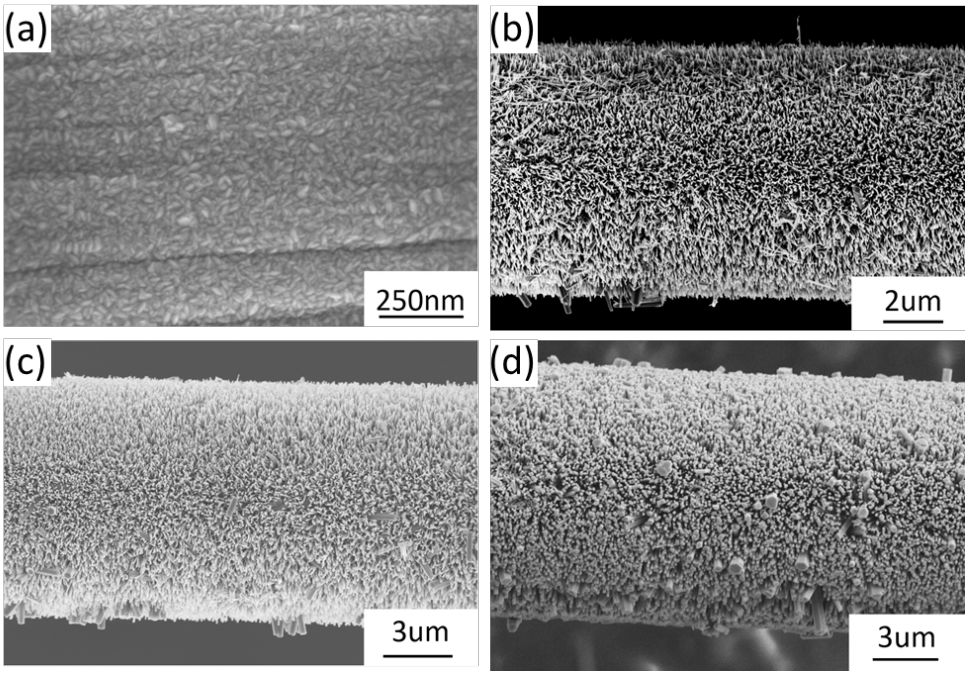

Figure 6-1 FESEM images of ZnO nanostructure on single carbon fiber (a) ZnO nanoparticles via ALD, (b) ZnO nanowires via 25mMol/L, (c) Zn nanowires via 50 mMol/L, (d) ZnO nanowires via 100 mMol/L.

Much higher magnification (30 kx to 60 kx) of FESEM images were taken and software ImageJ was used to measure the diameter of ZnO nanowires from corresponding images. The diameter distributions of ZnO nanowires under different growth conditions are manifested in Figure *6-2*(a-c). The diameters of ZnO nanowires shift in the trend of increasing of reagent concentration, so we know that the average diameter of ZnO nanowires can be controlled by reagent concentration. Diameter of each is 24 nm, 58nm and 99 nm when the reagent concentration is 25 mMol/L, 50mMol/L and 100 mMol/L. The largest diameter is almost close to 200nm which can be also in Figure 6-1(d). The statistical quantity of ZnO nanowires was more than 200 for each concentration, and the statistic is closely consistent with normal distribution. The dispersity of diameter is believed to relate to the inhomogeneous rice-like ZnO nanoparticles by ALD process. Figure *6-2* (d) shows the length to diameter ratio of ZnO nanowires under different concentration. The ratio is 33, 31 and 25 when the concentration is 25 mMol/L, 50mMol/L and 100 mMol/L. It can be seen that the increased growth concentration will result in smaller length to diameter ratio of ZnO nanowires.

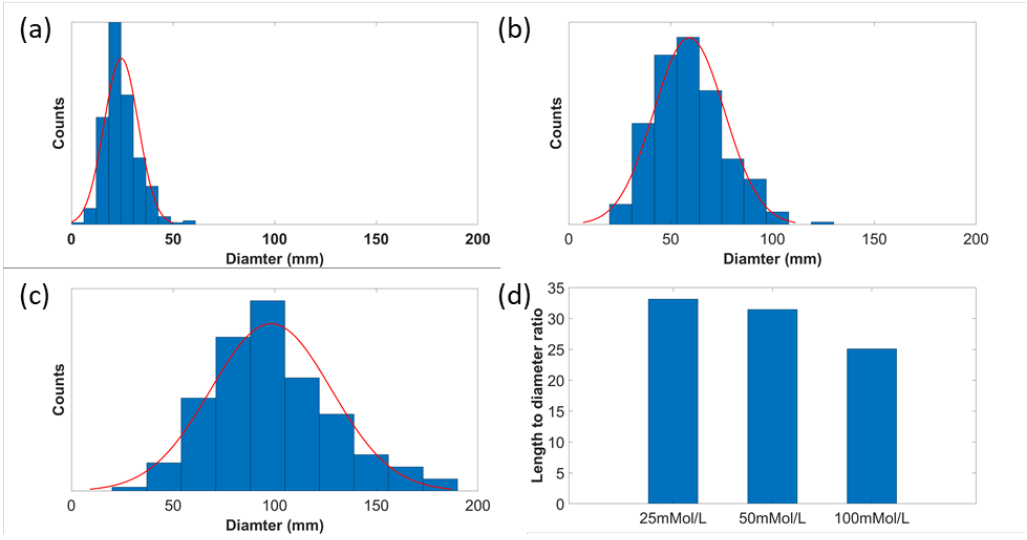

Figure 6-2 Diameter distributions of ZnO nanowires under different concentration: (a) 25 mMol/L, (b) 50 mMol/L, (c)100 mMol/L, and (d) length to diameter ratio of each concentration.

EDX analysis was performed to detect the material composition of ZnO nanowires on single carbon fiber. *Figure 6-3* (a) illustrates the EDX spectrum of ZnO nanowires on carbon fiber under different growth concentrations. It is observed that Zinc and oxygen elements were all detected for 3 groups, but carbon was almost missing when the reagent concentration was 100 mMol/L due to the high volume of ZnO with largest length and diameter on carbon fiber. The peak height of zinc increases compared to the peak height of oxygen when the growth concentrations increase, so does the relationship between oxygen and carbon. The EDX results confirme that the nanowires on carbon fiber is formed by ZnO.

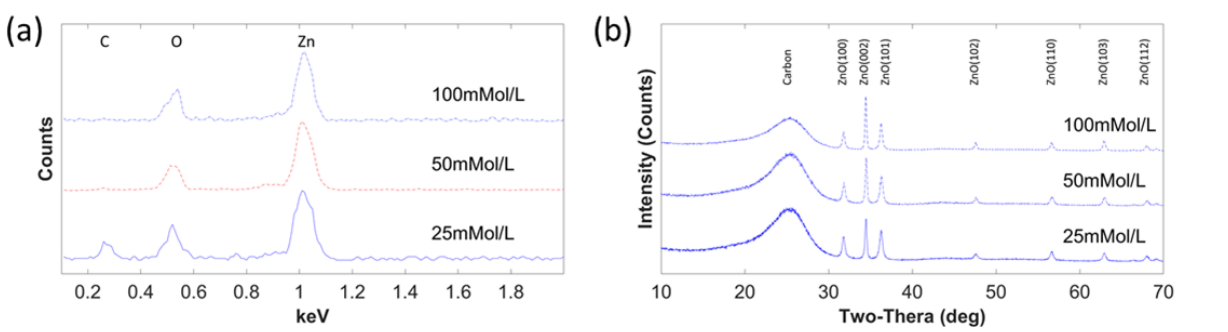

Figure 6-3 In different concentrations: (a)EDX spectrum of ZnO nanowires on single carbon fiber, (b) XRD diffraction of ZnO nanowires.

The crystal structure of ZnO nanowires was investigated by XRD, as indicated in *Figure 6-3* (b). The record range is between 10° and 70° with a speed of 2 degree/minute at a scanning step of 0.02°. For the ZnO nanowires grown in concentration of 100 mMol/L, 2θ value of 31.8°, 34.48°, 36.3°,47.6°, 56.62°, 62.88°and 67.98° are found for the diffraction peaks which are identified for (100), (002), (101), (102), (110), (103) and (112) of the ZnO planes. There is a very slight difference of 2θ peak for each concentration which is difficult to discern in graph. JCPDS card number 80-0075 was used to identify all the XRD diffraction patterns of ZnO nanowires which show that ZnO nanowires are wurtzite crystal structures. Of all the diffraction patterns,

planes of (100), (002), and (101) dominate the main crystal structures. With an increase in reagent concentration, the intensities of all ZnO peaks increase compared to the intensity of carbon. Within the three dominating peaks, peak (002) improves strongly and the peaks (100) and (101) become weaker compared to the peak (002). The intense peak of (002) plane shows that the preferred growth orientation of ZnO nanowires is along the c-axis direction.

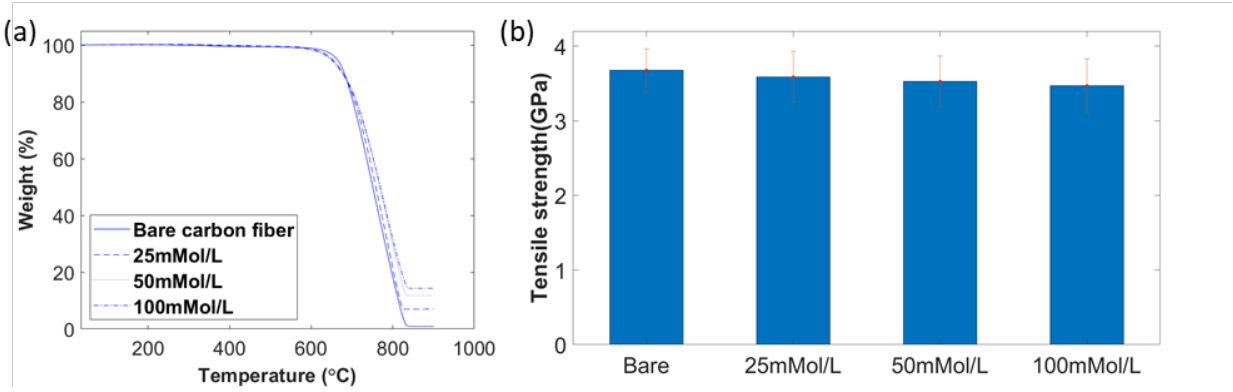

Figure 6-4 (a) TGA of bare carbon fiber and carbon fiber with ZnO nanowires, (b) Tensile strength of bare carbon fiber and carbon fiber with ZnO nanowires.

In order to identify the weight of the ZnO nanowires on carbon fiber, TGA analysis was performed, as the decomposition temperature of ZnO is about 1,974 °C [145] which is much higher than the decomposition temperature of carbon fiber that can be mostly burned off in air at the temperature less than 1000 °C. The temperature range of TGA test is from 35°C to 900 °C with a ramp of 10 °C/minute. As shown in Figure *6-4* (a), the starting decomposition temperature of all carbon fiber with ZnO nanowires is about 600 °C which is earlier than bare carbon fiber's at about 620°C. After all carbon fiber is burned off, the residual weight fractionof each is 0.92%, 7.01%, 11.82% and 14.33%, which indicates that the growth of higher reagent concentration results in higher weight fractionof ZnO. There is no weight loss before the temperature rose to 300 °C which

means no moisture was inside. Less than 1% of weight loss is found when the temperature ranges from 300 °C to 550 °C which is believed that the sizing on the carbon fiber was being burned off.

The tensile strength of single carbon fiber under different concentrations are demonstrated in Figure *6-4* (b). The tensile strength of bare carbon fiber and carbon fiber under growth concentration of 25mMol/L, 50mMol/L and 100 mMol/L was 3.676 ± 0.286GPa, 3.588 ± 0.343 GPa, 3.529 ± 0.337 GPa, 3.47 ± 0.362 GPa, respectively. As the highest temperature during the ALD processing is only 200 °C, there is no significant degradation of carbon fiber with ZnO nanowires under different growth concentrations. The slight decreasing of tensile strength is guessed to be caused by the weight of ZnO nanowires.

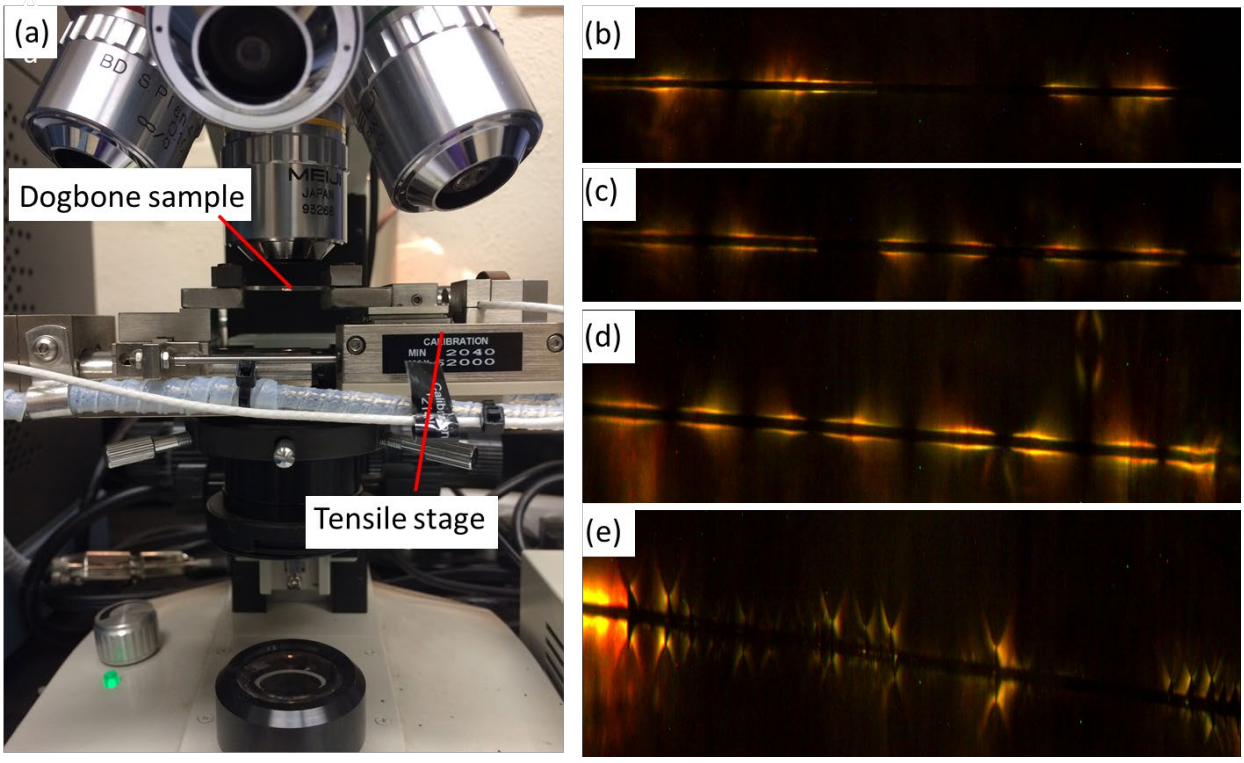

Figure 6-5 (a) Setting up of single fiber fragmentation test, crack patter of bare carbon fiber and carbon fiber with ZnO nanowires under different growth concentration, (b) bare carbon fiber, (c) 25mMol/L, (d) 50 mMol/L, (e) 100 mMol/L.

The setting up of SFFT is demonstrated in Figure *6-5* (a). The specimen was fixed on the tensile stage with a 200N load cell, and the gauge length of dog-bone specimen was 15mm applied with strain rate of 1 mm/minute. The quantity of cracked fiber was counted by the feature of birefringence under the optical scope at 10x magnification through polarized light. The quantity of fragmentations was recorded after every 0.1 mm displacement was applied until saturation was observed for multiple times. In Figure *6-5* (b), (c), (d), (e), debonding of adhesive failure can be seen. Under the similar magnification of each, 2 cracks can be seen for bare carbon fiber and more cracks for the carbon fiber with ZnO nanowires.

When the growing concentration increases, the number of cracks increases greatly, detailed in Figure *6-6* (a). The crack number of bare carbon fiber in saturation is 21, and highest number of fragmentations is 50 that can be seen for the carbon fiber with ZnO nanowires under the growth concentration of 100 mMol/L. The cracks of all specimens occur when the strain was at 3.33% which is much higher than the general tensile strain (1.7%~2.2%). This is believed that the pre-tension load during the specimen curing is not enough to keep the fiber aligned and the shrinkage of epoxy may affect it. The saturation strain for all specimens is 5.33%. After reaching to the saturation, no more cracks of carbon fiber are found when external force was applied to the strain of 6.67%.

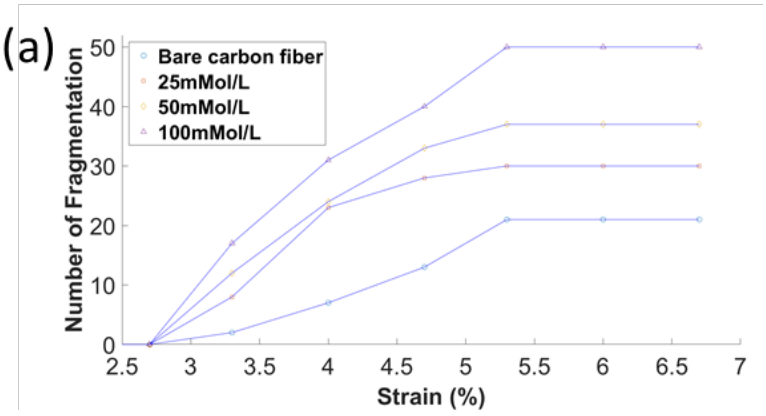

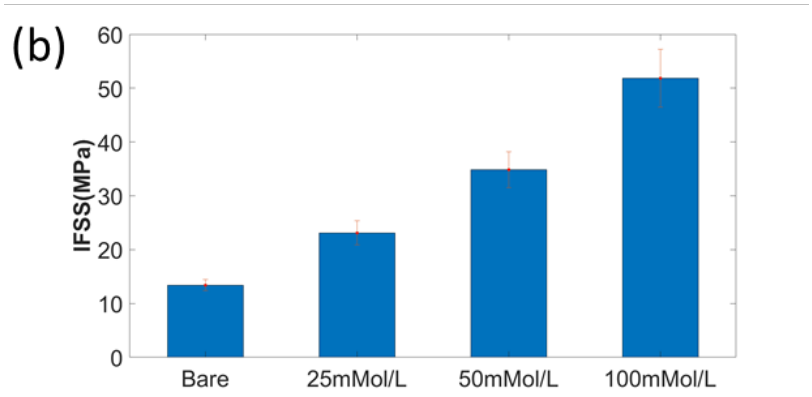

Figure 6-6 (a) number of fragmentations of carbon fiber with and without ZnO nanowires, (b) IFSS of carbon fiber without and with ZnO nanowires under different growth concentration.

By now, increased fragmentations will lead to lower average length of fragmentations $\bar{l}$, and increased length of ZnO nanowires will result in larger diameter of carbon fiber d. The tensile stress of carbon fiber changed little, based on the calculation equation of interfacial shear stress considering all these factors, so the IFSS is greatly improved, changing from 13.4 ± 1.1 MPa to 51.8 ± 5.4 MPa as demonstrated in Figure *6-6* (b). The larger and longer ZnO nanowires can have a larger volume to transfer the load and enlarge the contact area for the epoxy. The IFSS increases when the diameter and length of ZnO nanowires increases leading to an increased surface area and mechanical interlocking. ZnO nanowires work as an interphase between carbon fiber and polymer matrix to improve the bonding. Although the IFSS has a positive correlation with the reagent concentration which can be presented by larger diameter and longer length of ZnO nanowires, maximum diameter and length to cause the highest interfacial shear stress are believed. If the diameter continues increasing, the space between nanowires will be crowded and become difficult for liquid epoxy to wet, so the bonding becomes weaker and less load can be transferred.

6.4 Conclusion

In this chapter, we have investigated a novel approach to grow ZnO nanowires to be used as an enhanced interphase between carbon fiber and polymer matrix. The diameter from 24.491 nm to 99.303 nm and length from 0.811 um to 2.49um of ZnO nanowires were controlled by adjusting the growth concentration of $Zn(NO_3)_2$ and HMTA. Single fiber tensile test was performed, identifying that little influence of ZnO nanowires was on the tensile strength of carbon fiber. IFSS was great improved as much as 286% with the incorporation of ZnO nanowires under the concentration of 100 mMol/L. This result proved that ZnO nanowires as an interphase can be an effective approach to enhance the bonding between carbon fiber and polymer matrix.

Chapter 7 Reinforcement of Carbon Fiber Reinforced Composites by ALD Seeded ZnO Nanowires

7.1 Introduction

Carbon fiber composites have been playing a critical role in industry due to their high specific strength and stiffness, and flexible tailoring[104]. The performance of composites not only depends on the interfacial phase between fiber and polymer matrix which determines the in-plane properties such as interfacial shear stress (IFSS), but also on out-of-plane properties such as interlaminar shear strength (ILSS)[146]. High performance composites are always desirable, but the surface of carbon fiber is inert and smooth leading to the limitation of composites[147].

Various surface modifications of carbon fiber have been investigated to improve the overall performance of composites including surface roughening[148, 149] and designing architecture[150, 151]. The fibers are roughened to obtain a reactive surface using methods such as chemical oxidation[152], high energy radiation[153] and plasma[154]. The fiber surface will be etched by these methods, and the roughened surface will be mechanically interlocked with polymer matrix. Chemical bonds can also be generated by adding functional groups[155] to make strong connection between carbon fiber and polymer matrix. However, these methods will decrease the tensile strength of fibers resulting in the decreasing of in-plane properties[156].

Designing architecture to build high strength of nanostructures on fiber surface has been a popular method to improve delamination resistance[146]. Aligned carbon nanotubes (CNTs)[146, 157, 158] as interphases have been employed to improve the interlaminar shear strength. These interphases have a good bonding with carbon fibers and enlarge the surface area of interaction to polymer matrix. However, the synthesis of these nanostructures is usually in high temperature

environment (over 900 °C) using chemical vapor deposition (CVD)[159] process. The extremely high temperature will cause degradation of carbon fiber, and also the introduction of catalyst during the fabrication of CNTs will significantly lower down the tensile strength of carbon fiber, thus, decreasing in-plane properties of composites.

Consequently, it is very important to find a successful approach to improve the out-of-plane properties by preserving the tensile strength of in-plane properties of carbon fibers. Lin et al.[29, 160]demonstrated a designed architecture of ZnO nanowires on carbon fiber surface using a two-step hydrothermal method. The IFSS was improved more than 110% and the tensile strength of carbon fiber was preserved due to the low temperature (less than 100 °C) in hydrothermal growth process. Malakooti et al.[161] fabricated aligned ZnO nanowires on the surface of aramid fibers using the two-step hydrothermal method. He characterized the hybrid composites by tensile test and found that the elastic modulus and tensile strength of composites improved by 34.3% and 18.4%. This high strength composites can be also used for energy harvesting as ZnO is a piezoelectric material. Fei et al.[162] chemically treated the carbon fiber surface and synthesized ZnO nanorod on carbon fabric using the two-step hydrothermal method. He showed that the ILSS was improved by incorporating the ZnO nanorods in carbon fiber composites. The wet tribological properties of this composites were also studied and the wear rate decreased significantly by 81.5% compared to the carbon fiber composites without ZnO.

For the hydrothermal method the above researches used, dipping[160, 163] was the first step to form nucleation sites of ZnO nanoparticles as seed layers for the growth of ZnO nanowires in the second step of hydrothermal. However, there are some disadvantages for dipping as a step for seed layers that the process is not easy to control, some substrates are difficult to be deposited and the seed layers may not be very uniform. The morphologies of ZnO nanowires are determined by

the grain size and quality of seed layers of ZnO nanoparticles[75], so an approach that can produce high quality seed layer with smaller grain size is necessary. ALD has been one of the most popular thin film deposition methods due to its low defect density, fine control of thickness deposition, excellent uniformity and conformality, and lower deposition temperature as low as 100 °C which is close to the growth temperature of hydrothermal method[74]. A favorable vertical orientation and high quality of ZnO nanowires will be obtained by ALD seeded ZnO nanoparticles as first step in hydrothermal method[76, 77]. The tensile strength of carbon fibers will be preserved because the temperature of ALD will not be harmful for carbon fibers.

In this chapter, different morphologies of ZnO nanowires were synthesized on carbon fabric by controlling the growth parameter of hydrothermal step. Nanoscale ZnO nanoparticles were deposited on carbon fabric by ALD, working as seed layers for growth of aligned ZnO nanowires. Hydrothermally synthesized ZnO nanowires on carbon fabric were characterized by field emission scanning electron microscope (FESEM), energy-dispersive X-ray spectroscopy (EDX), X-ray diffraction (XRD) and thermogravimetric analysis (TGA). The carbon fabric coated with ZnO nanowires were stacked in different plies to manufacture the composite laminates. The mechanical properties of laminates were characterized by dynamic mechanical analysis (DMA), 3-point bending test and short beam 3-point bending test to investigate the effect of reinforcement of ZnO nanowires. The results show that carbon fiber composites decorated with ZnO nanowires as interface between filler and polymer matrix have a significant improvement in flexural strength and interlaminar shear strength.

7.2 Experiments

7.2.1 Materials

The type of carbon fabric was AGP193-P supplied by Hexcel® HexForce™. Diethylzinc (DEZn, $Zn(C_2H_5)_2$) and deionized water (DI water) were purchased from Sigma–Aldrich and worked as precursors to deposit seed layers of ZnO nanoparticles for later hydrothermal growth. Zinc nitrate hexahydrate ($Zn(NO_3)_2$ $6H_2O$) and Hexamethylenetetramine (HMTA) were received from Sigma–Aldrich to synthesize the ZnO nanowires in hydrothermal step. Resin INF-114 and hardener INF-211 were obtained from PRO-SET® to make composite laminates. All materials were used as received.

7.2.2 ZnO nanoparticles seeded by ALD

The carbon fabrics were cut into dimension of 2.75 inch by 2.75 inch and used as the substrate of ZnO nanoparticle growth. They were fixed on a glass sheet (3” * 3” * 1/8”) by high temperature Kapton tape. Considering the carbon fiber composites were usually fabricated in a non-sensitive environment, the carbon fabrics were not cleaned. A self-built 3” ALD system was used for the deposition of ZnO nanoparticles which work as nucleation sites of ZnO nanowires in later hydrothermal growth. The growth parameter of ALD process is the optimal results of our previous works. The pulse time of DEZb and water is 0.3 second leading to a vapor ratio of DEZn and water over 2. The growth temperature is 200 °C with a background pressure at 0.5 Torr and growth cycles at 300. The purging time of ultrahigh purity N_2 is 20 second after each pulse of precursors to remove the residual vapors in chamber and avoid the potential CVD reaction.

7.2.3 Hydrothermal growth of ZnO nanowires

The growth solution of ZnO nanowires in a beaker was made by combining the $Zn(NO_3)_2$ and HMTA solutions which were prepared by dissolve the powders of each in DI water. Before

mixing, each solution was heated to 90 °C and stirred by magnetic bar at 800 rpm on a hot plate. The carbon fabrics on the glass sheets coated with ZnO nanoparticles were immersed into the growth solution. The substrates were supported by a four-leg Teflon structure and faced downside in the beaker. Facing downside of growth substrate will avoid the situation that the generated ZnO in solution covers up the substrate and inhibits the ZnO nanowires growing. The beaker was transferred into a PolyScience water bath for hydrothermal growth. The temperature was set at 95 °C and the time was kept for 17 hours. After growth, the samples were moved out and flushed by Di water for 1 minute to remove the residual on surface, then dried on hotplate at 125 °C for 15 minutes. The concentration of $Zn(NO_3)_2$ and HMTA ,temperature and growth time in hydrothermal step play a critical role in determining the quality of ZnO nanowires. Larger diameter of ZnO nanowires would be obtained with lower temperature, higher growth time and higher concentration of $Zn(NO_3)_2$ and HMTA based on our previous reports. Among them, adjusting the concentration of $Zn(NO_3)_2$ and HMTA will significantly affect the quality of ZnO nanowires, so in this chapter, we controlled the both concentration of $Zn(NO_3)_2$ and HMTA at 25 mMol/L, 50 mMol/L and 100 mMol/L to verify their influence in mechanical properties of carbon fiber composites incorporated with ZnO nanowires as interface.

7.2.4 Manufacturing of carbon fiber composites

Considering the economic and labor cost, four and ten layers of carbon fiber composites with and without ZnO nanowires were fabricated by VARTM technique. 4-ply carbon fiber composite laminates were used to do the 3-point bending test and to verify the effect of ZnO nanowires in flexural strength. 10-ply composite laminates were used for the short beam 3-point bending test and to investigate its influence in interlaminar properties. Resin INF-114 and hardener INF-211 with a weight ratio of 3.65:1 were used to prepare the polymer matrix. This epoxy has

medium curing speed which provides a pot life near 2 hours. They were mixed by an overhead stirrer at 600 rpm for 5 minutes, then degassed for 50 minutes to remove the air bubbles. The infiltration time of epoxy was decreased greatly from about 5 minutes to about 2 minutes for the composite laminates with ZnO nanowires. Once the carbon fabrics were fully wetted, the laminate was compressed by the Instron universal testing system 5960 at a pressure of 1 MPa. The external pressure will result in the uniform thickness laminates with ZnO nanowires. Without external pressure, the thickness of composites modified by ZnO nanowires will increase greatly which leads to the relatively low volume fraction of carbon fiber causing lower mechanical properties of composites. The composite laminate was left at room temperature for 17 hours to be initial cured, then post cured at 80 °C for 8 hours.

7.2.5 Material characterization

The morphologies of ZnO nanoparticles and nanowires on carbon fabric were examined by high resolution Zeiss Neon EsB FESEM with Oxford EBSD capabilities at a working distance of roughly 6 mm at an accelerating voltage of 5 kV by in-lens signal. The diameters and densities of ZnO nanowires in different morphologies were analyzed by software ImageJ. The elemental analysis was conducted by EDX spectroscopy in Zeiss Neon EsB FESEM. The crystal structures of ZnO nanowires were determined by a Rigaku Ultima IV diffractometer with Cu-K-alpha radiation (40 kV, 44 mA) via a Bragg-Brentano detector. The mass fraction of ZnO nanowires on carbon fiber was investigated by TGA of TA Instruments Q50. The temperature ramp was 10 °C/min going up from 35 °C to 900 °C.

The viscoelastic properties of composite laminates were studied by DMA (TA Instruments Q800) in 3-point bending mode with 20mm span length. The loading frequency is 1Hz and the temperature ranges from 35 °C to 180 °C at a ramp of 3 °C/min. The dimension of specimens using

10-ply laminates for DMA is about 45 mm in length, 4 mm in width and 2.1 mm in thickness. The flexural strength of laminates was investigated by 3-point bending test using Instron universal testing system 5960. The specimens of 4-ply laminates were cut into dimensions of 2 in. in length and 0.5 in. in width with a thickness about 0.8mm. The span length is 1 in. and the crosshead speed is 2 mm/min. The short beam 3-point bending test following ASTM D2344 standard was performed to investigate the ILSS of 10-ply laminates at a crosshead speed of 2 mm/min. The thickness of laminates with and without ZnO nanowires was about 2.1 mm and 2.0 mm.

7.3 Results and discussion

The morphologies of ZnO nanoparticles by ALD process and ZnO nanowires by hydrothermal process under different concentration are shown in Figure 7-1 (a) to (d). ALD seeded ZnO nanoparticles seem to be long rice-like, and the orientation is random. The length of ZnO nanoparticles is 15nm to 30 nm and width is 7nm to 15 nm. The morphologies of ZnO nanowires under different concentration can be distinguished from FESEM images. When the concentration increased from 25 mMol/L to 50 mMol/L, slight changes can be seen in diameters and densities. When the growth concentration continues up to 100 mMol/L, obvious changes can be seen that hexagonal column of ZnO nanowires appear. The higher concentration offers more growing materials resulting in larger diameters. The space between ZnO nanowires is very crowed compared to the ZnO nanowires grown in lower concentration. Some larger nanowires extruded out when the concentration is lower. It is believed that the nucleation sites of ZnO nanoparticles are combined with each other leading to the larger nanowires. The length of nanowires is restricted as the space between each single fiber is limited. It seems that ZnO nanowires stop growth when the nanowires on neighbored fibers touch each other.

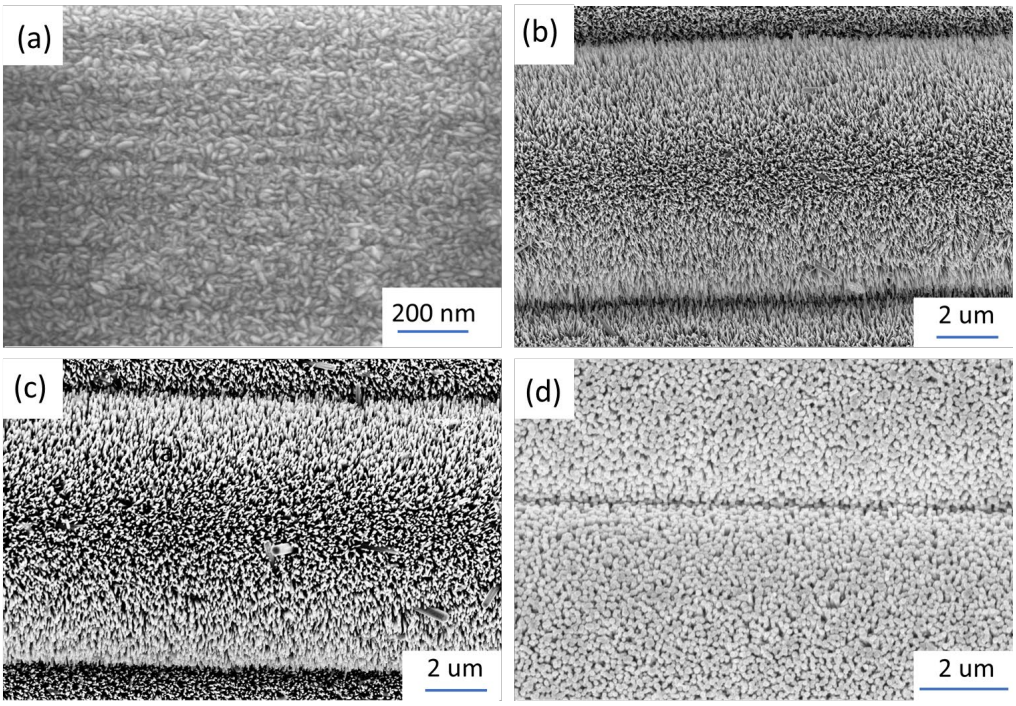

Figure 7-1 FESEM images of ZnO nanostructures on carbon fabrics (a) ZnO nanoparticles via ALD, (b) ZnO nanowires via 25mMol/L, (c) Zn nanowires via 50 mMol/L, (d) ZnO nanowires via 100 mMol/L.

The quantitative analysis of diameter distribution and densities of ZnO nanowires is demonstrated in Figure 7-2 (a) to (d). FESEM images at higher magnification of ZnO nanowires in different concentrations are used to do the statistical analysis. The distributions of ZnO nanowires are influenced by distributed size of ZnO nanoparticles, gravity and angle of images. The average diameter is used to represent the distribution of ZnO nanowires. The average dimeters of each concentration are 29.194 ± 11.034 nm, 49.804 ± 19.94 nm and 97.421 ± 24.161 nm, respectively. ALD process is believed to influence the dispersity of ZnO nanowires due to the inhomogeneous rice-like ZnO nanoparticles. It can be concluded that adjusting the growth concentration of $Zn(NO_3)_2$ and HMTA will lead to the controllable morphologies of ZnO nanowires. The average diameters shift in a larger trend when the reagent concentration increases. During the statistic of diameters, the densities of each morphologies can be also calculated. The

densities for each are 695, 580 and 400 per um^2. The decreasing of density is mainly caused by the enlargement of ZnO nanowires under higher reagent concentration.

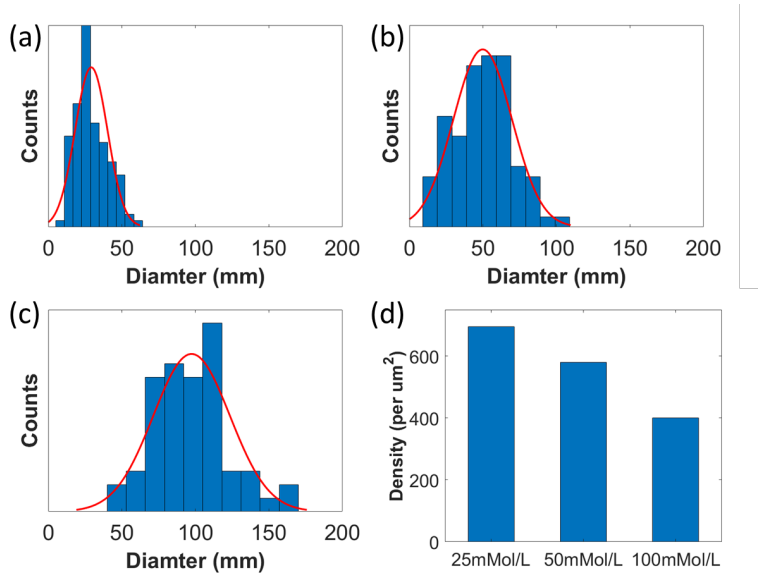

Figure 7-2 Diameter distributions of ZnO nanowires under different concentrations: (a) 25 mMol/L, (b) 50 mMol/L, (c)100 mMol/L, and (d) densities of each concentration.

The elemental composition of ZnO nanowires on carbon fabric is analyzed by EDX spectrum, indicated in Figure 7-3 (a). All peaks of carbon, oxygen and zinc elements are detected. The weight fraction of carbon decrease significantly from 13.2% to 2.8% when the growth concentration increase. However, the weight fraction of zinc increase from 69.3% to 78.1%. The change of oxygen element is steady compared to the other elements. It is believed that the higher reagent concentration will boost increased volume fraction of ZnO. It is confirmed that the nanostructures synthesized on carbon fabric is composed of ZnO by EDX results.

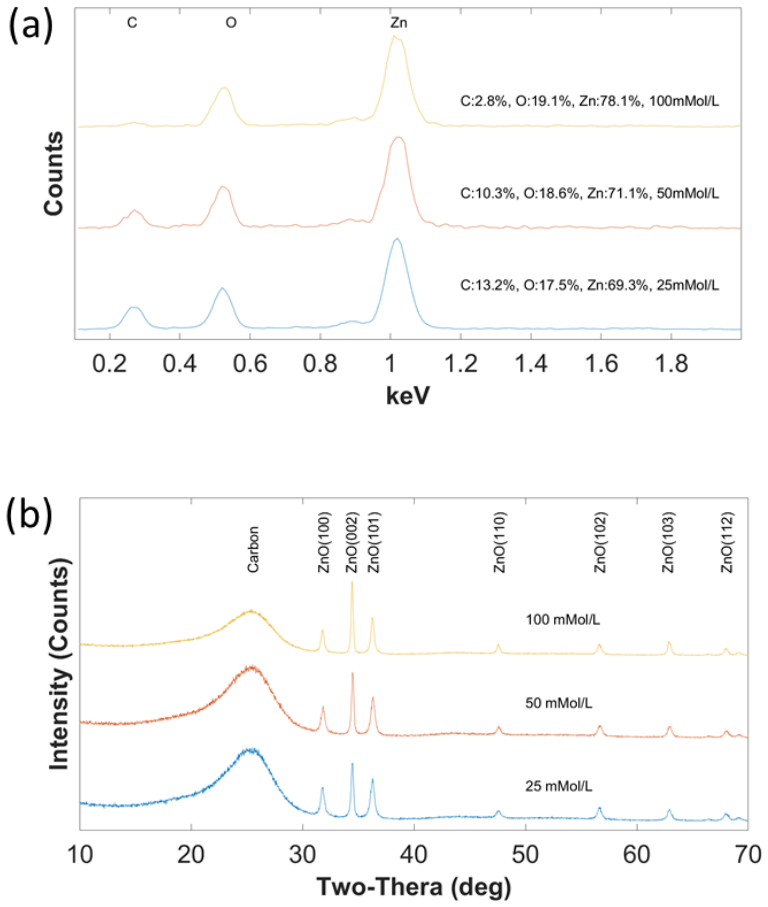

Figure 7-3 In different concentrations: (a) EDX spectrum of ZnO nanowires (b) XRD diffraction of ZnO nanowires.

The crystal orientations of ZnO nanowires are investigated by XRD analysis, shown in Figure 7-3 (b). The scanning angle was between 10° and 70° with a step of 0.02° and the scanning speed is 2°/min. Common crystals of plane (100), (002), (101), (102), (110), (103) and (112) are all detected. Plane (100), (002), (101) dominate of all crystal orientations and the intensities of them increase greatly when the reagent increase. The intensity peaks of plane (002) under different concentration is smaller than, close to and exceeded the intensity peak of carbon, when the concentrations are 25 mMol/L, 50 mMol/L and 100 mMol/L. With the increasing intensity of plane (002), the intensity of plane (100) and (101) decrease compared to plane (002). Plane (002) shows that the preferred growth orientation of ZnO nanowires is along the c-axis direction. The higher

growth concentration leads to the better vertically aligned ZnO nanowires on the radial direction of carbon fiber.

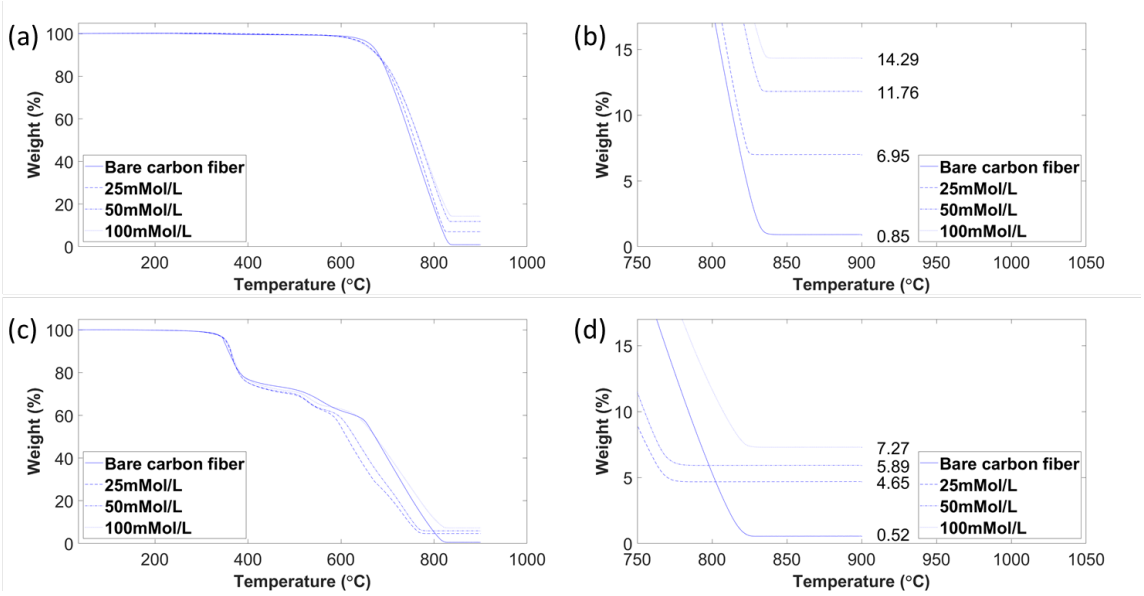

Figure 7-4 TGA for different concentation: (a) bare carbon fabric and carbon fabric with ZnO nanowires, (b) partial enlargement of (a), (c) carbon fiber composites without and with ZnO nanowires, (d) partial enlargement of (c).

TGA analysis is employed to investigate the weight ratio of ZnO nanowires on carbon fabric and in hybrid composites, as shown in Figure 7-4 (a) to (d). The deposition temperature of ZnO is very high near 2000 °C, but for carbon fiber and epoxy, the temperature is only about 620 °C and 320 °C, they can be totally burned off in air environment before the temperature goes up to 1000 °C. As light-weight is one the advantages of carbon fiber composites, the involvement of ZnO is expected not to add too much weight to the hybrid composites, so TGA analysis is necessary for burning carbon fiber coated with ZnO nanowires. In Figure 7-4 (a) and (b), no weight loss is found before the temperature reaches to 300 °C indicating no moisture inside. Then, there is about less than 1% weight loss when the temperature continues going up to 550 °C. This loss is believed to be the decomposition of sizing on fabric. Clear drops are found at 620 °C and 600 °C for carbon fabric with ZnO nanowires and bare carbon fibers. Before temperature reaches 900 °C,

all carbon fiber is burned off and white ZnO powder was left inside. The weight fraction of ZnO is 6.95%, 11.76% and 14.29% when the growth concentration is 25 mMol/L, 50 mMol/L and 100 mMol/L.

For burning the carbon fiber in hybrid carbon fiber composites enhanced by ZnO nanowires in Figure 7-4 (c) and (d), there is 25% weight loss when the temperature ranges from 300 °C to 400 °C which is the decomposition of epoxy. The epoxy is continuously burned when the temperature goes up to about 600 °C and 620 °C for the composite. When the temperature continues going up, the decomposition of carbon fiber occurs. After completing the burning, 0.52% weight is left for hybrid composites without ZnO. 4.65%, 5.89% and 7.27% are the weight fraction of ZnO in hybrid composites at each concentration. As the maximum weight fractionof ZnO is only 7.27% in composites and the multifunctional ZnO will work as a reinforcement in composites which can also be used to harvest energy, applying ZnO in carbon fiber composites is promising and significant.

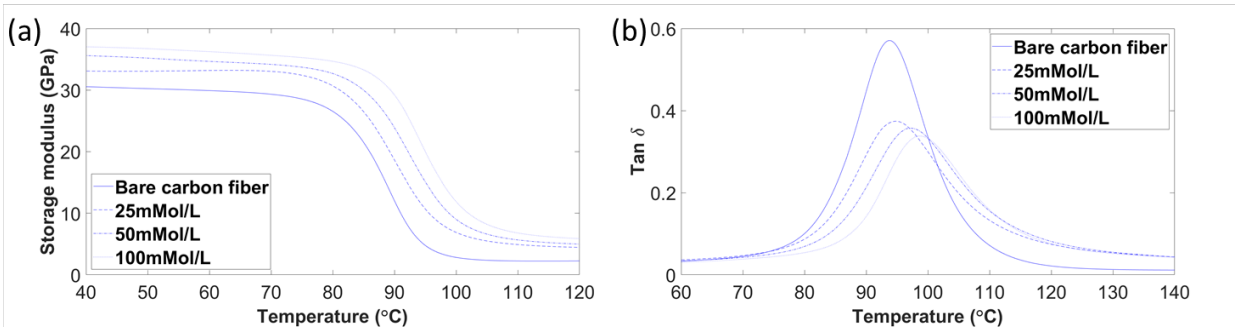

Figure 7-5 DMA results of hybrid composites: (a) storage modulus, (b) loss factor.

DMA analysis is used to the study the influence of nanostructures as an interphase on the stiffness and damping properties of composites. The effect of ZnO in composite laminates on storage modulus and loss factor is presented in Figure 7-5 (a) and (b). DMA gives the storage modulus and loss modulus of material. The storage modulus measures the stored energy which

relates to the elastic response of material. The loss modulus measures the dissipated energy as heat which relates to the viscous response of material. The ratio of loss modulus and storage modulus is the loss factor (tan delta) which means the damping properties. The storage modulus of hybrid composites with ZnO nanowires increase when the volume of ZnO is more involved. The introduction of ZnO improves the elastic properties of composites which suggests that the hybrid composites are more resistive to the shear deformation. For loss factor, the value decrease as more volume of ZnO nanowires are fabricated in composites. The aligned ZnO nanowires take up the space of interphase between carbon fiber and polymer matrix. As ZnO is rigid and stiff, it may decrease the energy dissipating in composites. The more ZnO nanowires is involved, the lower damping property is obtained when the growth concentrations increase from 25 mMol/L to 100 mMol/L. It can be also found the glass transition temperature shift in a larger direction when the growth concentration increase.

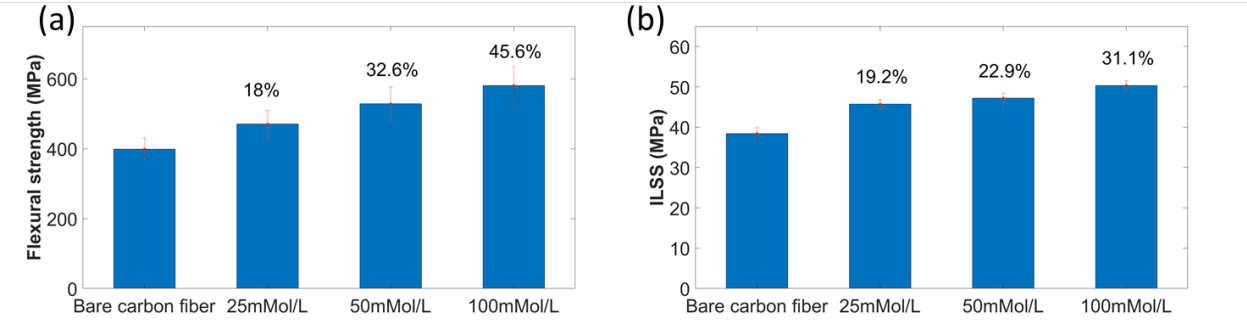

Figure 7-6 Hydrid composites: (a) flexurak strength, (b) ILSS.

The flexural properties of composites are demonstrated in Figure 7-6 (a). The flexural strength of hybrid composite laminates incorporated with Zno nanowires is all improved with a maximum enhancement of 45.6%. The improvement of flexural strength can be explained associate with the ILSS. The ILSS with and without ZnO nanowires were measured by short beam 3-point bending test in Figure 7-6 (b). All hybrid composites with ZnO exhibit an improvement in

ILSS. The ILSS of each are 38.4 ±1.5 MPa,45.8± 1.1 MPa,47.2 ± 1.23 MPa, 50.4 ± 1.1 MPa, corresponding to an increasing of 19.2%, 22.9% and 31.1%. The interfacial adhesion and boding are usually low in neat hybrid composites, as the surface carbon fiber is inert and smooth. The polymer matrix will typically separate from fiber when suffering the large shear stress. However, the decoration of ZnO nanowires on fibers will increase the interaction between fiber and polymer matrix due to the mechanical interlocking and enlarged contact area. Both interphase of composites and shear properties of polymer matrix can determine the ILSS. ZnO nanowires enhance the interphase and improve the shear resistance of polymer matrix to the crack as ZnO is stiffer and more rigid than epoxy. The initial crack and its propagation will be impeded by the existence of ZnO nanowires, which needs higher stress to crack the ZnO.

7.4 Conclusion

This chapter demonstrated a novel approach of employing ZnO nanowires as interphase in carbon fiber composites using ALD seeded hydrothermal methods. Different morphologies of ZnO nanowires were obtained by controlling the growth concentration. The diameters of ZnO nanowires are 29.194 ± 11.034 nm, 49.804 ± 19.94 nm and 97.421 ± 24.161 nm for these typical growth concentrations. Hybrid carbon fiber composite laminates were manufactured using the carbon fabric coated with these 3 morphologies of ZnO nanowires. Multiple mechanical properties of these laminates were tested including damping, flexure strength and ILSS. The results show that the larger ZnO nanowires are involved, the higher flexural strength and ILSS are improved. The maximum improvements of each are 45.6% and 31.1% for incorporating the largest ZnO nanowires at growth concentration of 100 mMol/L.

Chapter 8 Conclusions and Future Research Directions

8.1 Summary

In this dissertation, ALD replaced the conventional dipping coating to grow ZnO nanoparticles as the seed layer to fabricate ZnO nanowires using a two-step synthesis method. Multifunctional ZnO nanowires were grown on carbon fibers as the reinforced interphase in composites, resulting in novel composites with improved interfacial strength.

First, silicon wafer was chosen as the substrate to deposit ZnO seed layer using the ALD method. Key ALD parameters including H_2O/DEZn precursors dose ratio, background base pressure and growth temperature were systematically studied. The scanning electron microscopic and atomic force microscopic images revealed that the H_2O/DEZn precursors dose ratio was critical to control the morphology of ZnO nanoparticles. To achieve high uniformity, the H_2O dose amount needed to be at least twice of that of DEZn. If the background pressure drops below 400 mTorr, a large amount of nanoflower-shaped ZnO grains would emerge and significantly increase surface roughness. In addition, the temperature ranging between 200 °C and 250 °C was found to be the optimal growth window. Moreover, the crystal structures and orientations of ZnO nanoparticles were highly correlated to the synthesis temperature as proved by electron back-scattering diffraction and x-ray diffraction results.

After successfully depositing ZnO seed layer on the silicon substrates, carbon fabrics were used as new substrates to grow ALD seeded ZnO nanowires using the developed two-step synthesis method. The effects of ALD parameters including temperature and growth cycles on the hydrothermal growth of ZnO nanowires were investigated. The growth of ZnO nanowires would be inhibited when the extreme high temperature was at 300 °C or lower growth cycles was for 100.

The maximum adding weight by ZnO nanowires on carbon fabric was only 10.31% which was acceptable and made this method promising applied in reinforcement of carbon fiber composites.

As the effect of parameters of ALD process was studied, the influence of parameters of ZnO nanowires growth in second step hydrothermal process was also investigated. These parameters included temperature, growth time and concentration of Zinc nitrate hydrate and Hexamethylenetetramine (HMTA). It was found that high growth temperature, lower growth time, and lower concentration of Zinc nitrate hydrate and HMTA would result in fine ZnO nanowires. Serval morphologies of ZnO nanostructures were obtained including fine nanowires, fuzzy nanowires, fine nanorods and compact nanorods.

Completing systematical investigation of growth parameters in this two-step hydrothermal method, the carbon substrates including single carbon fiber and carbon fabric decorated with different morphologies of ZnO nanowires under different growth concentrations of Zinc nitrate hydrate and HMTA were applied into polymer matrix composites. The tensile strength and in-plane properties of single carbon fiber preserved as the maximum temperature in whole growth process was only 200 °C. Mechanical properties including IFSS, flexure shear strength and ILSS were all improved as much as 286%, 45.6% and 31.1%, respectively. The reason for these enhancements was that ZnO nanowires worked as an interphase between carbon fiber and polymer matrix to transfer the shear load. The incorporation of ZnO nanowires on the carbon fiber surface would increase the contact area and mechanically interlock with polymer matrix.

8.2 Contributions

1. For the first time, ZnO nanowires was grown by ALD synthesized ZnO nanoparticles as seed layers on the surface of carbon substrates including single carbon fiber and carbon fabric.

2. The effects of growth parameters of seed layers by ALD and nanowire growth in hydrothermal method were systematically investigated. Several morphologies of ZnO nanostructures were obtained which laid a foundation of investigating the properties determined by unique structures.
3. Single carbon fiber and carbon fabric with different morphologies of ZnO nanowires in length and diameter were manufactured into carbon fiber composites. The introducing of ZnO nanowires as an interphase in carbon fiber composites significantly improved the mechanical properties including IFSS, flexure shear strength and ILSS

8.3 Future research directions

Due to the limitation of chamber size in ALD system, the maximum size of carbon fiber composite laminates was only 2.5" by 2.5", which limited the further testing and application of the developed nanocomposites. Although using ALD to deposit the seed layers of ZnO nanoparticles offers a more option in fabricating ZnO nanowires, the current research only provides a prototype to demonstrate the possibility. A much larger ALD system is preferred to manufacture larger composite laminates. In addition, an ALD system can continuously deposit ZnO nanoparticles on continuous carbon fiber is necessary for further study and application in aerospace engineering structures. The dimension of laminates can meet the requirement of most mechanical property tests including tensile test, fracture test of mode I, II and III, and toughness tests to verify how the incorporation of ZnO nanowires will reinforce the mechanical properties of carbon fiber composites[164-168].

Since this dissertation only focused on experimental study, but the mechanism of reinforcement of ZnO nanowires as an interphase in carbon fiber composites can be studied using the modeling approach[139, 169-171]. We need to know the mechanisms that how the ZnO nanowires

bond with carbon fiber and how strong is the adhesion between carbon fiber and ZnO nanowires. In addition, it is critical to identify the relationship between the dimensions of ZnO nanowires and the reinforced mechanical properties of composites. A multiscale analysis of fiber-matrix interfacial enhancement is recommended and molecular dynamics simulations (MD) should be useful to investigate the adhesion[172-175]. Combining the experiment and simulation results, the properties of composites involved with ZnO nanowires can be tailored and designed.

This work mainly used ZnO nanowires as the reinforcement structures in the enhanced mechanical properties of carbon fiber composites. As ZnO is the multifunctional material that has piezoelectric and semi-conductive properties, more applications of this hybrid carbon fiber composites can be explored such as in-situ load and deformation sensing[98, 176-187], real-time damage state awareness and prognostics[175, 188-196], nondestructive evaluation[197-200], energy harvesting[201, 202], and temperature sensing[203]. Multifunctional carbon fiber composites of high performance are always desirable and the research trend in the future.

Reference

1. Li, N., Liu, G., Wang, Z.P., Liang, J.Y., and Zhang, X.X. (2014). Effect of Surface Treatment on Surface Characteristics of Carbon Fibers and Interfacial Bonding of Epoxy Resin Composites. *Fibers and Polymers*, 15(11), 2395-2403.
2. Erden, S., Ho, K.K.C., Lamoriniere, S., Lee, A.F., Yildiz, H., and Bismarck, A. (2010). Continuous Atmospheric Plasma Oxidation of Carbon Fibres: Influence on the Fibre Surface and Bulk Properties and Adhesion to Polyamide 12. *Plasma Chemistry and Plasma Processing*, 30(4), 471-487.
3. Kim, D.K., An, K.H., Bang, Y.H., Kwac, L.K., Oh, S.Y., and Kim, B.J. (2016). Effects of electrochemical oxidation of carbon fibers on interfacial shear strength using a micro-bond method. *Carbon Letters (Carbon Lett.)*, 19, 32-39.
4. Xing, L.X., Liu, L., Huang, Y.D., Jiang, D.W., Jiang, B., and He, J.M. (2015). Enhanced interfacial properties of domestic aramid fiber-12 via high energy gamma ray irradiation. *Composites Part B-Engineering*, 69, 50-57.
5. Dai, Z.S., Shi, F.H., Zhang, B.Y., Li, M., and Zhang, Z.G. (2011). Effect of sizing on carbon fiber surface properties and fibers/epoxy interfacial adhesion. *Applied Surface Science*, 257(15), 6980-6985.
6. Sager, R.J., Klein, P.J., Lagoudas, D.C., Zhang, Q., Liu, J., Dai, L., and Baur, J.W. (2009). Effect of carbon nanotubes on the interfacial shear strength of T650 carbon fiber in an epoxy matrix. *Composites Science and Technology*, 69(7-8), 898-904.
7. Lin, Y.R., Ehlert, G., and Sodano, H.A. (2009). Increased Interface Strength in Carbon Fiber Composites through a ZnO Nanowire Interphase. *Advanced Functional Materials*, 19(16), 2654-2660.
8. Song, S.A., Lee, C.K., Bang, Y.H., and Kim, S.S. (2016). A novel coating method using zinc oxide nanorods to improve the interfacial shear strength between carbon fiber and a thermoplastic matrix. *Composites Science and Technology*, 134, 106-114.
9. Ozgur, U., Alivov, Y.I., Liu, C., Teke, A., Reshchikov, M.A., Dogan, S., Avrutin, V., Cho, S.J., and Morkoc, H. (2005). A comprehensive review of ZnO materials and devices. *Journal of Applied Physics*, 98(4).
10. Zhou, J., Xu, N.S., and Wang, Z.L. (2006). Dissolving behavior and stability of ZnO wires in biofluids: A study on biodegradability and biocompatibility of ZnO nanostructures. *Advanced Materials*, 18(18), 2432-2435.
11. Jones, N., Ray, B., Ranjit, K.T., and Manna, A.C. (2008). Antibacterial activity of ZnO nanoparticle suspensions on a broad spectrum of microorganisms. *Fems Microbiology Letters*, 279(1), 71-76.
12. Zhang, Q., Dandeneau, C.S., Zhou, X., and Cao, G. (2009). ZnO nanostructures for dye-sensitized solar cells. *Advanced Materials*, 21(41), 4087-4108.
13. Huang, M.H., Mao, S., Feick, H., Yan, H., Wu, Y., Kind, H., Weber, E., Russo, R., and Yang, P. (2001). Room-temperature ultraviolet nanowire nanolasers. *science*, 292(5523), 1897-1899.
14. Lim, J.H., Kang, C.K., Kim, K.K., Park, I.K., Hwang, D.K., and Park, S.J. (2006). UV electroluminescence emission from ZnO light-emitting diodes grown by high-temperature radiofrequency sputtering. *Advanced Materials*, 18(20), 2720-2724.

15. Wan, Q., Li, Q.H., Chen, Y.J., Wang, T.H., He, X.L., Li, J.P., and Lin, C.L. (2004). Fabrication and ethanol sensing characteristics of ZnO nanowire gas sensors. *Applied Physics Letters*, 84(18), 3654-3656.
16. Soci, C., Zhang, A., Xiang, B., Dayeh, S.A., Aplin, D.P.R., Park, J., Bao, X.Y., Lo, Y.H., and Wang, D. (2007). ZnO nanowire UV photodetectors with high internal gain. *Nano Letters*, 7(4), 1003-1009.
17. Chakrabarti, S. and Dutta, B.K. (2004). Photocatalytic degradation of model textile dyes in wastewater using ZnO as semiconductor catalyst. *Journal of Hazardous Materials*, 112(3), 269-278.
18. Kamble, A.S., Sinha, B.B., Chung, K., Gil, M.G., Burungale, V., Park, C.J., Kim, J.H., and Patil, P.S. (2014). Effect of hydroxide anion generating agents on growth and properties of ZnO nanorod arrays. *Electrochimica Acta*, 149, 386-393.
19. Norton, D.P., Heo, Y., Ivill, M., Ip, K., Pearton, S., Chisholm, M.F., and Steiner, T. (2004). ZnO: growth, doping & processing. *Materials today*, 7(6), 34-40.
20. Pan, Z.W., Dai, Z.R., and Wang, Z.L. (2001). Nanobelts of semiconducting oxides. *Science*, 291(5510), 1947-1949.
21. Wu, H.Q., Wei, X.W., Shao, M.W., and Gu, J.S. (2004). Synthesis of zinc oxide nanorods using carbon nanotubes as templates. *Journal of Crystal Growth*, 265(1-2), 184-189.
22. Vayssieres, L., Chaneac, C., Tronc, E., and Jolivet, J.P. (1998). Size tailoring of magnetite particles formed by aqueous precipitation: An example of thermodynamic stability of nanometric oxide particles. *Journal of Colloid and Interface Science*, 205(2), 205-212.
23. Vayssieres, L., Hagfeldt, A., and Lindquist, S.E. (2000). Purpose-built metal oxide nanomaterials. The emergence of a new generation of smart materials. *Pure and Applied Chemistry*, 72(1-2), 47-52.
24. Vayssieres, L., Beermann, N., Lindquist, S.E., and Hagfeldt, A. (2001). Controlled aqueous chemical growth of oriented three-dimensional crystalline nanorod arrays: Application to iron(III) oxides. *Chemistry of Materials*, 13(2), 233-235.
25. Vayssieres, L., Keis, K., Hagfeldt, A., and Lindquist, S.E. (2001). Three-dimensional array of highly oriented crystalline ZnO microtubes. *Chemistry of Materials*, 13(12), 4395-4398.
26. Govender, K., Boyle, D.S., O'Brien, P., Binks, D., West, D., and Coleman, D. (2002). Room-Temperature Lasing Observed from ZnO Nanocolumns Grown by Aqueous Solution Deposition. *Advanced Materials*, 14(17), 1221-1224.
27. Yang, L., Zhao, Q., and Willander, M. (2009). Size-controlled growth of well-aligned ZnO nanorod arrays with two-step chemical bath deposition method. *Journal of alloys and compounds*, 469(1-2), 623-629.
28. Mbuyisa, P., Ndwandwe, O., and Cepek, C. (2015). Controlled growth of zinc oxide nanorods synthesised by the hydrothermal method. *Thin Solid Films*, 578, 7-10.
29. Lin, Y., Ehlert, G., and Sodano, H.A. (2009). Increased interface strength in carbon fiber composites through a ZnO nanowire interphase. *Advanced functional materials*, 19(16), 2654-2660.
30. Li, Q.C., Kumar, V., Li, Y., Zhang, H.T., Marks, T.J., and Chang, R.P.H. (2005). Fabrication of ZnO nanorods and nanotubes in aqueous solutions. *Chemistry of Materials*, 17(5), 1001-1006.
31. Smith, R.E., Smettem, K.R., and Broadbridge, P., *Infiltration theory for hydrologic applications*. 2002: American Geophysical Union.

32. Harrison, W.A., *Electronic structure and the properties of solids: the physics of the chemical bond*. 2012: Courier Corporation.
33. Herrerafranco, P.J. and Drzal, L.T. (1992). Comparison of Methods for the Measurement of Fiber Matrix Adhesion in Composites. *Composites*, 23(1), 2-27.
34. Kelly, A. and Tyson, W.R. (1965). Tensile Properties of Fibre-Reinforced Metals - Copper/Tungsten and Copper/Molybdenum. *Journal of the Mechanics and Physics of Solids*, 13(6), 329-350.
35. Valadez-Gonzalez, A., Cervantes-Uc, J., Olayo, R., and Herrera-Franco, P. (1999). Effect of fiber surface treatment on the fiber–matrix bond strength of natural fiber reinforced composites. *Composites Part B: Engineering*, 30(3), 309-320.
36. Rong, M.Z., Zhang, M.Q., Liu, Y., Yang, G.C., and Zeng, H.M. (2001). The effect of fiber treatment on the mechanical properties of unidirectional sisal-reinforced epoxy composites. *Composites Science and Technology*, 61(10), 1437-1447.
37. Netravali, A.N., Li, Z.F., Sachse, W., and Wu, H.F. (1991). Determination of Fiber Matrix Interfacial Shear-Strength by an Acoustic-Emission Technique. *Journal of Materials Science*, 26(24), 6631-6638.
38. Schadler, L., Giannaris, S.a., and Ajayan, P. (1998). Load transfer in carbon nanotube epoxy composites. *Applied physics letters*, 73(26), 3842-3844.
39. Takaku, A. and Arridge, R.G.C. (1973). The effect of interfacial radial and shear stress on fibre pull-out in composite materials. *Journal of Physics D: Applied Physics*, 6(17), 2038.
40. Mandell, J., Chen, J., and McGarry, F. (1980). A microdebonding test for in situ assessment of fibre/matrix bond strength in composite materials. *International Journal of Adhesion and Adhesives*, 1(1), 40-44.
41. Kerans, R.J. and Parthasarathy, T.A. (1991). Theoretical-Analysis of the Fiber Pullout and Pushout Tests. *Journal of the American Ceramic Society*, 74(7), 1585-1596.
42. Feih, S., Wonsyld, K., Minzari, D., Westermann, P., and Lilholt, H. (2004). Testing procedure for the single fiber fragmentation test.
43. Janotti, A. and Van de Walle, C.G. (2009). Fundamentals of zinc oxide as a semiconductor. *Reports on progress in physics*, 72(12), 126501.
44. Zhang, X.M., Lu, M.Y., Zhang, Y., Chen, L.J., and Wang, Z.L. (2009). Fabrication of a High-Brightness Blue-Light-Emitting Diode Using a ZnO-Nanowire Array Grown on p-GaN Thin Film. *Advanced Materials*, 21(27), 2767-2770.
45. Mitra, A., Thareja, R.K., Ganesan, V., Gupta, A., Sahoo, P.K., and Kulkarni, V.N. (2001). Synthesis and characterization of ZnO thin films for UV laser. *Appl. Surf. Sci.*, 174(3-4), 232.
46. Vanmaekelbergh, D. and Van Vugt, L.K. (2011). ZnO nanowire lasers. *Nanoscale*, 3(7), 2783-2800.
47. Liang, S., Sheng, H., Liu, Y., Huo, Z., Lu, Y., and Shen, H. (2001). ZnO Schottky ultraviolet photodetectors. *Journal of Crystal Growth*, 225(2-4), 110-113.
48. Huang, J., Yin, Z., and Zheng, Q. (2011). Applications of ZnO in organic and hybrid solar cells. *Energy & Environmental Science*, 4(10), 3861-3877.
49. Wang, X., Zhou, J., Song, J., Liu, J., Xu, N., and Wang, Z.L. (2006). Piezoelectric field effect transistor and nanoforce sensor based on a single ZnO nanowire. *Nano Lett.*, 6(12), 2768.

50. Wang, F., Chen, X.L., Geng, X.H., Zhang, D.K., Wei, C.C., Huang, Q., Zhang, X.D., and Zhao, Y. (2012). Development of natively textured surface hydrogenated Ga-doped ZnO-TCO thin films for solar cells via magnetron sputtering. *Appl. Surf. Sci.*, 258(22), 9005.
51. Gao, W. and Li, Z.W. (2004). ZnO thin films produced by magnetron sputtering. *Ceram. Int.*, 30(7), 1155.
52. Ellmer, K. (2000). Magnetron sputtering of transparent conductive zinc oxide: relation between the sputtering parameters and the electronic properties. *Journal of Physics D: Applied Physics*, 33(4), R17.
53. Agarwal, D.C., Chauhan, R.S., Kumar, A., Kabiraj, D., Singh, F., Khan, S.A., Avasthi, D.K., Pivin, J.C., Kumar, M., Ghatak, J., and Satyam, P.V. (2006). Synthesis and characterization of ZnO thin film grown by electron beam evaporation. *J. Appl. Phys.*, 99(12).
54. Tsoutsouva, M., Panagopoulos, C., Papadimitriou, D., Fasaki, I., and Kompitsas, M. (2011). ZnO thin films prepared by pulsed laser deposition. *Materials Science and Engineering: B*, 176(6), 480-483.
55. George, S.M. (2010). Atomic layer deposition: an overview. *Chem. Rev.*, 110(1), 111.
56. Leskelä, M. and Ritala, M. (2002). Atomic layer deposition (ALD): from precursors to thin film structures. *Thin solid films*, 409(1), 138-146.
57. Yen, C.Y., Jian, S.R., Chen, G.J., Lin, C.M., Lee, H.Y., Ke, W.C., Liao, Y.Y., Yang, P.F., Wang, C.T., Lai, Y.S., Jang, J.S.C., and Juang, J.Y. (2011). Influence of annealing temperature on the structural, optical and mechanical properties of ALD-derived ZnO thin films. *Appl. Surf. Sci.*, 257(17), 7900.
58. Przezdziecka, E., Wachnicki, L., Paszkowicz, W., Lusakowska, E., Krajewski, T., Luka, G., Guziewicz, E., and Godlewski, M. (2009). Photoluminescence, electrical and structural properties of ZnO films, grown by ALD at low temperature. *Semicond. Sci. Technol.*, 24(10).
59. Ju, S., Facchetti, A., Xuan, Y., Liu, J., Ishikawa, F., Ye, P., Zhou, C., Marks, T.J., and Janes, D.B. (2007). Fabrication of fully transparent nanowire transistors for transparent and flexible electronics. *Nat. Nanotechnol.*, 2(6), 378.
60. Theiss, S., Carey, P., Smith, P., Wickboldt, P., Sigmon, T., Tung, Y., and King, T.-J. *Polysilicon thin film transistors fabricated at 100/spl deg/C on a flexible plastic substrate*. in *International Electron Devices Meeting 1998. Technical Digest (Cat. No. 98CH36217)*. 1998. IEEE.
61. Hishiyama, Y., Yasuda, S., Yoshida, A., and Inagaki, M. (1988). Structure and properties of highly crystallized graphite films based on polyimide Kapton. *J. Mater. Sci.*, 23(9), 3272.
62. Guziewicz, E., Godlewski, M., Krajewski, T., Wachnicki, L., Szczepanik, A., Kopalko, K., Wojcik-Glodowska, A., Przezdziecka, E., Paszkowicz, W., Lusakowska, E., Kruszewski, P., Huby, N., Tallarida, G., and Ferrari, S. (2009). ZnO grown by atomic layer deposition: a material for transparent electronics and organic heterojunctions. *J. Appl. Phys.*, 105(12).
63. Nam, T., Kim, J.M., Kim, M.K., Kim, H., and Kim, W.H. (2011). Low-temperature atomic layer deposition of TiO2, Al2O3 and ZnO thin films. *J. Korean Phys. Soc.*, 59(2), 452.
64. Kim, H.W., Kim, K.S., and Lee, C. (2003). Low temperature growth of ZnO thin film on Si (100) substrates by metal organic chemical vapor deposition. *Journal of materials science letters*, 22(15), 1117-1118.
65. Kotha, R., Elam, D., Collins, G., Guven, N., Chabanov, A., Chen, C., and Ayon, A. *Atomic layer deposited (ALD) zinc oxide film characterization for NEMS and MEMS*. in *2010*

Symposium on Design Test Integration and Packaging of MEMS/MOEMS (DTIP). 2010. IEEE.
66. Li, S.Y., Lee, C.Y., and Tseng, T.Y. (2003). Copper-catalyzed ZnO nanowires on silicon (100) grown by vapor-liquid-solid process. *Journal of Crystal Growth*, 247(3-4), 357-362.
67. Xiang, B., Wang, P.W., Zhang, X.Z., Dayeh, S.A., Aplin, D.P.R., Soci, C., Yu, D.P., and Wang, D.L. (2007). Rational synthesis of p-type zinc oxide nanowire arrays using simple chemical vapor deposition. *Nano Letters*, 7(2), 323-328.
68. Greene, L.E., Law, M., Goldberger, J., Kim, F., Johnson, J.C., Zhang, Y.F., Saykally, R.J., and Yang, P.D. (2003). Low-temperature wafer-scale production of ZnO nanowire arrays. *Angewandte Chemie-International Edition*, 42(26), 3031-3034.
69. Tian, J.-H., Hu, J., Li, S., Zhang, F., Liu, J., Shi, J., Li, X., Tian, Z., and Chen, Y. (2011). Improved seedless hydrothermal synthesis of dense and ultralong ZnO nanowires. *Nanotechnology*, 22(24), 245601.
70. Baruah, S. and Dutta, J. (2009). Effect of seeded substrates on hydrothermally grown ZnO nanorods. *Journal of sol-gel science and technology*, 50(3), 456.
71. Wang, J.X., Sun, X.W., Yang, Y., Huang, H., Lee, Y.C., Tan, O.K., and Vayssieres, L. (2006). Hydrothermally grown oriented ZnO nanorod arrays for gas sensing applications. *Nanotechnology*, 17(19), 4995-4998.
72. Bai, S.N. and Wu, S.C. (2011). Synthesis of ZnO nanowires by the hydrothermal method, using sol-gel prepared ZnO seed films. *Journal of Materials Science-Materials in Electronics*, 22(4), 339-344.
73. Galan, U., Lin, Y.R., Ehlert, G.J., and Sodano, H.A. (2011). Effect of ZnO nanowire morphology on the interfacial strength of nanowire coated carbon fibers. *Composites Science and Technology*, 71(7), 946-954.
74. Weng, B., Wang, J., Larson, P., and Liu, Y. (2016). Growth process optimization of ZnO thin film using atomic layer deposition. *Materials Research Express*, 3(12).
75. Ladanov, M., Algarin-Amaris, P., Villalba, P., Emirov, Y., Matthews, G., Thomas, S., Ram, M.K., Kumar, A., and Wang, J. (2013). Effects of the physical properties of atomic layer deposition grown seeding layers on the preparation of ZnO nanowires. *Journal of Physics and Chemistry of Solids*, 74(11), 1578-1588.
76. Wang, J., Weng, B., Larson, P., and Liu, Y. (2019). Synthesis and characterization of self-assembled ZnO nanoarrays on hybrid structural fibers. *Surfaces and Interfaces*, 16, 188-193.
77. Wang, J., Weng, B., Larson, P., and Liu, Y. (2018). Synthesis of ZnO nanoarrays on carbon fibers using combined atomic layer deposition and hydrothermal methods. *Materials Research Express*, 5(6).
78. Mouritz, A.P., Gellert, E., Burchill, P., and Challis, K. (2001). Review of advanced composite structures for naval ships and submarines. *Composite structures*, 53(1), 21-42.
79. Le, T.X.H., Bechelany, M., and Cretin, M. (2017). Carbon felt based-electrodes for energy and environmental applications: A review. *Carbon*, 122, 564-591.
80. Liu, Z., Wang, J., Kushvaha, V., Poyraz, S., Tippur, H., Park, S., Kim, M., Liu, Y., Bar, J., Chen, H., and Zhang, X. (2011). Poptube approach for ultrafast carbon nanotube growth. *Chemical Communications*, 47(35), 9912.
81. Athauda, T.J., Hari, P., and Ozer, R.R. (2013). Tuning physical and optical properties of ZnO nanowire arrays grown on cotton fibers. *ACS Applied Materials & Interfaces*, 5(13), 6237.

82. Athauda, T.J., LePage, W.S., Chalker, J.M., and Ozer, R.R. (2014). High density growth of ZnO nanorods on cotton fabric enables access to a flame resistant composite. *Rsc Advances*, 4(28), 14582.
83. Soumya, S., Kumar, S.N., Mohamed, A.P., and Ananthakumar, S. (2016). Silanated nano ZnO hybrid embedded PMMA polymer coatings on cotton fabrics for near-IR reflective, antifungal cool-textiles. *New J. Chem.*, 40(8), 7210.
84. Arfaoui, M.A., Dolez, P.I., Dube, M., and David, E. (2017). Development and characterization of a hydrophobic treatment for jute fibres based on zinc oxide nanoparticles and a fatty acid. *Appl. Surf. Sci.*, 397, 19.
85. Kayaci, F., Vempati, S., Ozgit-Akgun, C., Biyikli, N., and Uyar, T. (2014). Enhanced photocatalytic activity of homoassembled ZnO nanostructures on electrospun polymeric nanofibers: a combination of atomic layer deposition and hydrothermal growth. *Applied Catalysis B: Environmental*, 156, 173.
86. Ashraf, M., Champagne, P., Perwuelz, A., Campagne, C., and Leriche, A. (2015). Photocatalytic solution discoloration and self-cleaning by polyester fabric functionalized with ZnO nanorods. *Journal of Industrial Textiles*, 44(6), 884.
87. Ehlert, G.J., Galan, U., and Sodano, H.A. (2013). Role of surface chemistry in adhesion between ZnO nanowires and carbon fibers in hybrid composites. *ACS Applied Materials & Interfaces*, 5(3), 635.
88. Skandani, A.A., Masghouni, N., Case, S.W., Leo, D.J., and Al-Haik, M. (2012). Enhanced vibration damping of carbon fibers-ZnO nanorods hybrid composites. *Appl. Phys. Lett.*, 101(7).
89. Zhang, L., Bai, S., Su, C., Zheng, Y.B., Qin, Y., Xu, C., and Wang, Z.L. (2015). A high-reliability kevlar fiber-ZnO nanowires hybrid nanogenerator and its application on self-powered UV detection. *Adv. Funct. Mater.*, 25(36), 5794.
90. Hwang, H.S., Malakooti, M.H., Patterson, B.A., and Sodano, H.A. (2015). Increased interyarn friction through ZnO nanowire arrays grown on aramid fabric. *Compos. Sci. Technol.*, 107, 75.
91. Hwang, H.S., Malakooti, M.H., and Sodano, H.A. (2015). Tailored interyarn friction in aramid fabrics through morphology control of surface grown ZnO nanowires. *Composites Part A: Applied Science and Manufacturing*, 76, 326.
92. Liu, Y., Mohanty, S., and Chattopadhyay, A. (2010). Condition based structural health monitoring and prognosis of composite structures under uniaxial and biaxial loading. *J. Nondestruct. Eval.*, 29(3), 181.
93. Liu, Y. and Nayak, S. (2012). Structural health monitoring: state of the art and perspectives. *JOM*, 64(7), 789.
94. Thostenson, E.T. and Chou, T.W. (2008). Real-time in situ sensing of damage evolution in advanced fiber composites using carbon nanotube networks. *Nanotechnology*, 19(21).
95. Kang, I.P., Schulz, M.J., Kim, J.H., Shanov, V., and Shi, D.L. (2006). A carbon nanotube strain sensor for structural health monitoring. *Smart Mater. Struct.*, 15(3), 737.
96. Liu, Y., Kim, S.B., Chattopadhyay, A., and Doyle, D.T. (2011). Application of system-identification techniquest to health monitoring of on-orbit satellite boom structures. *Journal of Spacecraft and Rockets*, 48(4), 589-598.
97. Liu, Y. and Chattopadhyay, A. (2013). Low-velocity impact damage monitoring of a sandwich composite wing. *Journal of Intelligent Material Systems and Structures*, 24(17), 2074-2083.

98. Zou, J., Liu, Y., Chattopadhyay, A., and Dai, L. *A self-sensing fiber reinforced polymer composite using mechanophore-based smart polymer*. in *Behavior and Mechanics of Multifunctional Materials and Composites 2015*. 2015. International Society for Optics and Photonics.
99. Elias, J., Utke, I., Yoon, S., Bechelany, M., Weidenkaff, A., Michler, J., and Philippe, L. (2013). Electrochemical growth of ZnO nanowires on atomic layer deposition coated polystyrene sphere templates. *Electrochim. Acta*, 110, 387.
100. Hughes, W.L. and Wang, Z.L. (2005). Controlled synthesis and manipulation of ZnO nanorings and nanobows. *Applied Physics Letters*, 86(4), 043106.
101. Pung, S.Y., Choy, K.L., Hou, X., and Shan, C. (2008). Preferential growth of ZnO thin films by the atomic layer deposition technique. *Nanotechnology*, 19(43), 435609.
102. Akil, H., Omar, M., Mazuki, A., Safiee, S., Ishak, Z.M., and Bakar, A.A. (2011). Kenaf fiber reinforced composites: A review. *Materials & Design*, 32(8-9), 4107-4121.
103. Bakis, C.E., Bank, L.C., Brown, V., Cosenza, E., Davalos, J., Lesko, J., Machida, A., Rizkalla, S., and Triantafillou, T. (2002). Fiber-reinforced polymer composites for construction—State-of-the-art review. *Journal of composites for construction*, 6(2), 73-87.
104. Chand, S. (2000). Review carbon fibers for composites. *Journal of materials science*, 35(6), 1303-1313.
105. Yuan, Y., Sun, Y., Yan, S., Zhao, J., Liu, S., Zhang, M., Zheng, X., and Jia, L. (2017). Multiply fully recyclable carbon fibre reinforced heat-resistant covalent thermosetting advanced composites. *Nature communications*, 8, 14657.
106. Carabba, L., Santandrea, M., Carloni, C., Manzi, S., and Bignozzi, M.C. (2017). Steel fiber reinforced geopolymer matrix (S-FRGM) composites applied to reinforced concrete structures for strengthening applications: A preliminary study. *Composites Part B: Engineering*, 128, 83-90.
107. Barbero, E.J., *Introduction to composite materials design*. 2017: CRC press.
108. Agarwal, B. and Broutman, L., *Analysis and performance of fiber composites Second edition*. 1990, John wiley & Sons.
109. Thostenson, E.T., Ren, Z., and Chou, T.-W. (2001). Advances in the science and technology of carbon nanotubes and their composites: a review. *Composites science and technology*, 61(13), 1899-1912.
110. Zhang, X. and Liu, Z. (2012). Recent advances in microwave initiated synthesis of nanocarbon materials. *Nanoscale*, 4(3), 707-714.
111. Ehlert, G.J., Lin, Y., Galan, U., and Sodano, H.A. (2010). Interaction of ZnO nanowires with carbon fibers for hierarchical composites with high interfacial strength. *Journal of Solid Mechanics and Materials Engineering*, 4(11), 1687-1698.
112. Bello, D., Wardle, B.L., Zhang, J., Yamamoto, N., Santeufemio, C., Hallock, M., and Virji, M.A. (2010). Characterization of exposures to nanoscale particles and fibers during solid core drilling of hybrid carbon nanotube advanced composites. *International journal of occupational and environmental health*, 16(4), 434-450.
113. Groo, L., Inman, D.J., and Sodano, H.A. (2018). In Situ Damage Detection for Fiber-Reinforced Composites Using Integrated Zinc Oxide Nanowires. *Advanced Functional Materials*, 28(35), 1802846.
114. Vayssieres, L. (2003). Growth of arrayed nanorods and nanowires of ZnO from aqueous solutions. *Advanced Materials*, 15(5), 464-466.

115. Yu, H., Liu, J., Fan, X., Yan, W., Han, L., Han, J., Zhang, X., Hong, T., and Liu, Z. (2016). Bionic micro-nano-bump-structures with a good self-cleaning property: The growth of ZnO nanoarrays modified by polystyrene spheres. *Materials Chemistry and Physics*, 170, 52-61.
116. Liu, Z., Ya, J., and Lei, E. (2010). Effects of substrates and seed layers on solution growing ZnO nanorods. *Journal of Solid State Electrochemistry*, 14(6), 957-963.
117. Liu, Z., Lei, E., Ya, J., and Xin, Y. (2009). Growth of ZnO nanorods by aqueous solution method with electrodeposited ZnO seed layers. *Applied Surface Science*, 255(12), 6415-6420.
118. Gao, P.X. and Wang, Z.L. (2005). High-yield synthesis of single-crystal nanosprings of ZnO. *Small*, 1(10), 945-949 %@ 1613-6810.
119. Wang, X., Summers, C.J., and Wang, Z.L. (2004). Large-scale hexagonal-patterned growth of aligned ZnO nanorods for nano-optoelectronics and nanosensor arrays. *Nano letters*, 4(3), 423-426 %@ 1530-6984.
120. Zhang, J., Liu, Z., Liu, J., Lei, E., and Liu, Z. (2016). Effects of seed layers on controlling of the morphology of ZnO nanostructures and superhydrophobicity of ZnO nanostructure/stearic acid composite films. *Materials Chemistry and Physics*, 183, 306-314.
121. Barreca, D., Bekermann, D., Comini, E., Devi, A., Fischer, R.A., Gasparotto, A., Maccato, C., Sberveglieri, G., and Tondello, E. (2010). 1D ZnO nano-assemblies by Plasma-CVD as chemical sensors for flammable and toxic gases. *Sensors and Actuators B: Chemical*, 149(1), 1-7.
122. Wang, L., Zhang, X., Zhao, S., Zhou, G., Zhou, Y., and Qi, J. (2005). Synthesis of well-aligned ZnO nanowires by simple physical vapor deposition on c-oriented ZnO thin films without catalysts or additives. *Applied Physics Letters*, 86(2), 024108.
123. Na, J.-S., Gong, B., Scarel, G., and Parsons, G.N. (2009). Surface polarity shielding and hierarchical ZnO nano-architectures produced using sequential hydrothermal crystal synthesis and thin film atomic layer deposition. *Acs Nano*, 3(10), 3191-3199.
124. Park, J., Huang, J., Yun, J., Liu, F., Ouyang, Z., Sun, H., Yan, C., Sun, K., Kim, K., and Seidel, J. (2018). The Role of Hydrogen from ALD-Al2O3 in Kesterite Cu2ZnSnS4 Solar Cells: Grain Surface Passivation. *Advanced Energy Materials*, 8(23), 1701940.
125. Singh, R., Bapat, R., Qin, L., Feng, H., and Polshettiwar, V. (2016). Atomic layer deposited (ALD) TiO2 on fibrous nano-silica (KCC-1) for photocatalysis: nanoparticle formation and size quantization effect. *ACS Catalysis*, 6(5), 2770-2784.
126. Jędrzejewska-Szczerska, M., Wierzba, P., Chaaya, A.A., Bechelany, M., Miele, P., Viter, R., Mazikowski, A., Karpienko, K., and Wróbel, M. (2015). ALD thin ZnO layer as an active medium in a fiber-optic Fabry–Perot interferometer. *Sensors and Actuators A: Physical*, 221, 88-94.
127. Yoon, H.-C., Shin, J.-H., Park, H.-S., and Suh, S.-J. (2015). The Properties of Cu Thin Films on Ru Depending on the ALD Temperature. *Journal of nanoscience and nanotechnology*, 15(2), 1601-1604.
128. Yue, Z., Jiang, W., Wang, L., Gardner, S., and Pittman Jr, C. (1999). Surface characterization of electrochemically oxidized carbon fibers. *Carbon*, 37(11), 1785-1796.
129. Montes-Moran, M.A., Martinez-Alonso, A., Tascon, J.M.D., and Young, R.J. (2001). Effects of plasma oxidation on the surface and interfacial properties of ultra-high modulus carbon fibres. *Composites Part a-Applied Science and Manufacturing*, 32(3-4), 361-371.

130. Zhang, R.L., Gao, B., Ma, Q.H., Zhang, J., Cui, H.Z., and Liu, L. (2016). Directly grafting graphene oxide onto carbon fiber and the effect on the mechanical properties of carbon fiber composites. *Materials & Design*, 93, 364-369.
131. Xu, Z.W., Huang, Y.D., Zhang, C.H., Liu, L., Zhang, Y.H., and Wang, L. (2007). Effect of gamma-ray irradiation grafting on the carbon fibers and interfacial adhesion of epoxy composites. *Composites Science and Technology*, 67(15-16), 3261-3270.
132. Kowbel, W., Bruce, C., Withers, J.C., and Ransone, P.O. (1997). Effect of carbon fabric whiskerization on mechanical properties of C-C composites. *Composites Part a-Applied Science and Manufacturing*, 28(12), 993-1000.
133. Wu, R.B., Yang, Z.H., Fu, M.S., and Zhou, K. (2016). In-situ growth of SiC nanowire arrays on carbon fibers and their microwave absorption properties. *Journal of Alloys and Compounds*, 687, 833-838.
134. Lv, P., Feng, Y.Y., Zhang, P., Chen, H.M., Zhao, N.Q., and Feng, W. (2011). Increasing the interfacial strength in carbon fiber/epoxy composites by controlling the orientation and length of carbon nanotubes grown on the fibers. *Carbon*, 49(14), 4665-4673.
135. Ehlert, G.J., Galan, U., and Sodano, H.A. (2013). Role of surface chemistry in adhesion between ZnO nanowires and carbon fibers in hybrid composites. *ACS applied materials & interfaces*, 5(3), 635-645.
136. De Greef, N., Zhang, L.M., Magrez, A., Forro, L., Locquet, J.P., Verpoest, I., and Seo, J.W. (2015). Direct growth of carbon nanotubes on carbon fibers: Effect of the CVD parameters on the degradation of mechanical properties of carbon fibers. *Diamond and Related Materials*, 51, 39-48.
137. Zhang, Q.H., Liu, J.W., Sager, R., Dai, L.M., and Baur, J. (2009). Hierarchical composites of carbon nanotubes on carbon fiber: influence of growth condition on fiber tensile properties. *Composites Science and Technology*, 69(5), 594-601.
138. Patterson, B.A., Galan, U., and Sodano, H.A. (2015). Adhesive Force Measurement between HOPG and Zinc Oxide as an Indicator for Interfacial Bonding of Carbon Fiber Composites. *Acs Applied Materials & Interfaces*, 7(28), 15380-15387.
139. Marashizadeh, P., Abshirini, M., Saha, M.C., and Liu, Y. (2019). Multi-scale analysis of fiber-matrix interfacial enhancement in hybrid structural composites with aligned zinc oxide nanowires. *Materials Research Express*.
140. Tao, Y.L., Fu, M., Zhao, A.L., He, D.W., and Wang, Y.S. (2010). The effect of seed layer on morphology of ZnO nanorod arrays grown by hydrothermal method. *Journal of Alloys and Compounds*, 489(1), 99-102.
141. Tynell, T. and Karppinen, M. (2014). Atomic layer deposition of ZnO: a review. *Semiconductor Science and Technology*, 29(4).
142. Rodriguez, M., Molina-Aldareguia, J.M., Gonzalez, C., and LLorca, J. (2012). A methodology to measure the interface shear strength by means of the fiber push-in test. *Composites Science and Technology*, 72(15), 1924-1932.
143. Hsueh, C.H. (1990). Interfacial Debonding and Fiber Pull-out Stresses of Fiber-Reinforced Composites. *Materials Science and Engineering a-Structural Materials Properties Microstructure and Processing*, 123(1), 1-11.
144. Rao, V., Herrerafranco, P., Ozzello, A.D., and Drzal, L.T. (1991). A Direct Comparison of the Fragmentation Test and the Microbond Pull-out Test for Determining the Interfacial Shear-Strength. *Journal of Adhesion*, 34(1-4), 65-77.
145. Haynes, W.M., *CRC handbook of chemistry and physics*. 2014: CRC press.

146. Khan, S.U. and Kim, J.-K. (2012). Improved interlaminar shear properties of multiscale carbon fiber composites with bucky paper interleaves made from carbon nanofibers. *Carbon*, 50(14), 5265-5277.
147. Bačáková, L., Starý, V., Kofroňová, O., and Lisá, V. (2001). Polishing and coating carbon fiber-reinforced carbon composites with a carbon-titanium layer enhances adhesion and growth of osteoblast-like MG63 cells and vascular smooth muscle cells in vitro. *Journal of Biomedical Materials Research: An Official Journal of The Society for Biomaterials, The Japanese Society for Biomaterials, and The Australian Society for Biomaterials and the Korean Society for Biomaterials*, 54(4), 567-578.
148. Tiwari, S. and Bijwe, J. (2014). Surface treatment of carbon fibers-a review. *Procedia Technology*, 14, 505-512.
149. Dilsiz, N. and Wightman, J. (1999). Surface analysis of unsized and sized carbon fibers. *Carbon*, 37(7), 1105-1114.
150. Yang, L., Cheng, S., Ding, Y., Zhu, X., Wang, Z.L., and Liu, M. (2011). Hierarchical network architectures of carbon fiber paper supported cobalt oxide nanonet for high-capacity pseudocapacitors. *Nano letters*, 12(1), 321-325.
151. Rao, M.V., Mahajan, P., and Mittal, R. (2008). Effect of architecture on mechanical properties of carbon/carbon composites. *Composite Structures*, 83(2), 131-142.
152. Pittman Jr, C., He, G.-R., Wu, B., and Gardner, S. (1997). Chemical modification of carbon fiber surfaces by nitric acid oxidation followed by reaction with tetraethylenepentamine. *Carbon*, 35(3), 317-331.
153. Li, J., Huang, Y., Xu, Z., and Wang, Z. (2005). High-energy radiation technique treat on the surface of carbon fiber. *Materials Chemistry and Physics*, 94(2-3), 315-321.
154. Wu, G. (2004). Oxygen plasma treatment of high performance fibers for composites. *Materials Chemistry and Physics*, 85(1), 81-87.
155. Park, S.-J. and Kim, B.-J. (2005). Roles of acidic functional groups of carbon fiber surfaces in enhancing interfacial adhesion behavior. *Materials Science and Engineering: A*, 408(1-2), 269-273.
156. Zhao, Z.-G., Ci, L.-J., Cheng, H.-M., and Bai, J.-B. (2005). The growth of multi-walled carbon nanotubes with different morphologies on carbon fibers. *Carbon*, 43(3), 663-665.
157. Fan, Z., Santare, M.H., and Advani, S.G. (2008). Interlaminar shear strength of glass fiber reinforced epoxy composites enhanced with multi-walled carbon nanotubes. *Composites Part A: Applied science and manufacturing*, 39(3), 540-554.
158. Zhu, J., Imam, A., Crane, R., Lozano, K., Khabashesku, V.N., and Barrera, E.V. (2007). Processing a glass fiber reinforced vinyl ester composite with nanotube enhancement of interlaminar shear strength. *Composites Science and Technology*, 67(7-8), 1509-1517.
159. Thostenson, E., Li, W., Wang, D., Ren, Z., and Chou, T. (2002). Carbon nanotube/carbon fiber hybrid multiscale composites. *Journal of Applied physics*, 91(9), 6034-6037.
160. Galan, U., Lin, Y., Ehlert, G.J., and Sodano, H.A. (2011). Effect of ZnO nanowire morphology on the interfacial strength of nanowire coated carbon fibers. *Composites Science and Technology*, 71(7), 946-954.
161. Malakooti, M.H., Patterson, B.A., Hwang, H.-S., and Sodano, H.A. (2016). ZnO nanowire interfaces for high strength multifunctional composites with embedded energy harvesting. *Energy & Environmental Science*, 9(2), 634-643.

162. Fei, J., Luo, D., Huang, J., Zhang, C., Duan, X., and Zhang, L. (2018). Growth of aligned ZnO nanorods on carbon fabric and its composite for superior mechanical and tribological performance. *Surface and Coatings Technology*, 344, 433-440.
163. Gan, X., Li, X., Gao, X., Zhuge, F., and Yu, W. (2010). ZnO nanowire/TiO2 nanoparticle photoanodes prepared by the ultrasonic irradiation assisted dip-coating method. *Thin Solid Films*, 518(17), 4809-4812.
164. Fard, M.Y., Chattopadhyay, A., and Liu, Y. (2012). Multi-linear stress–strain and closed-form moment curvature response of epoxy resin materials. *International Journal of Mechanical Sciences*, 57(1), 9-18.
165. Fard, M.Y., Liu, Y., and Chattopadhyay, A. (2011). Characterization of epoxy resin including strain rate effects using digital image correlation system. *Journal of Aerospace Engineering*, 25(2), 308-319.
166. Yekani Fard, M., Liu, Y., and Chattopadhyay, A. (2011). Analytical solution for flexural response of epoxy resin materials. *Journal of Aerospace Engineering*, 25(3), 395-408.
167. Fard, M.Y., Liu, Y., and Chattopadhyay, A. (2011). Nonlinear flexural behavior and moment curvature response of epoxy resin using digital image correlation technique. *Journal of Materials Science and Engineering*, 5(2), 212.
168. Yekani Fard, M., Liu, Y., and Chattopadhyay, A. (2012). A simplified approach for flexural behavior of epoxy resin materials. *The Journal of Strain Analysis for Engineering Design*, 47(1), 18-31.
169. Koo, B., Liu, Y., Chattopadhyay, A., and Dai, L. *Multiscale modeling of a mechanophore-embedded nanocomposite for damage initiation detection*. in *56th AIAA/ASCE/AHS/ASC Structures, Structural Dynamics, and Materials Conference*. 2015.
170. Hasan, Z., Chattopadhyay, A., Liu, Y., Johnston, J., and Heitland, C. *Analytical, numerical and experimental investigation on the use of nanocomposites in structural level components*. in *SAMPE Tech Seattle 2014 Conference*. 2014. Soc. for the Advancement of Material and Process Engineering.
171. Hasan, Z.F., Chattopadhyay, A., and Liu, Y. *Effect of viscoelastic interface on the behavior of nanocomposites*. in *54th AIAA/ASME/ASCE/AHS/ASC Structures, Structural Dynamics, and Materials Conference*. 2013.
172. Koo, B., Liu, Y., Zou, J., Chattopadhyay, A., and Dai, L. (2014). Study of glass transition temperature (Tg) of novel stress-sensitive composites using molecular dynamic simulation. *Modelling and Simulation in Materials Science and Engineering*, 22(6), 065018.
173. Zhang, J., Koo, B., Subramanian, N., Liu, Y., and Chattopadhyay, A. (2016). An optimized cross-linked network model to simulate the linear elastic material response of a smart polymer. *Journal of Intelligent Material Systems and Structures*, 27(11), 1461-1475.
174. Hasan, Z., Chattopadhyay, A., and Liu, Y. (2014). Multiscale approach to analysis of composite joints incorporating nanocomposites. *Journal of Aircraft*, 52(1), 204-215.
175. Hasan, Z., Chattopadhyay, A., and Liu, Y. (2014). An investigation into the performance of composite hat stringers incorporating nanocomposites using a multiscale framework. *Journal of Reinforced Plastics and Composites*, 33(15), 1375-1387.
176. Abshirini, M., Charara, M., Marashizadeh, P., Saha, M.C., Altan, M.C., and Liu, Y. (2019). Functional nanocomposites for 3D printing of stretchable and wearable sensors. *Applied Nanoscience*, 1-13.

177. Luo, W., Charara, M., Saha, M.C., and Liu, Y. (2019). Fabrication and characterization of porous CNF/PDMS nanocomposites for sensing applications. *Applied Nanoscience*, 9(6), 1309-1317.
178. Charara, M., Luo, W., Saha, M.C., and Liu, Y. (2019). Investigation of lightweight and flexible carbon nanofiber/poly dimethylsiloxane nanocomposite sponge for piezoresistive sensor application. *Advanced Engineering Materials*, 1801068.
179. Chowdhury, S.A., Saha, M.C., Patterson, S., Robison, T., and Liu, Y. (2019). Highly conductive polydimethylsiloxane/carbon nanofiber composites for flexible sensor applications. *Advanced Materials Technologies*, 4(1), 1800398.
180. Chavez, L.A., Wilburn, B.R., Ibave, P., Delfin, L.C., Vargas, S., Diaz, H., Fulgentes, C., Renteria, A., Regis, J.E., and Liu, Y. (2019). Fabrication and characterization of 3D printing induced orthotropic functional ceramics. *Smart Materials and Structures*.
181. Charara, M., Abshirini, M., Saha, M.C., Altan, M.C., and Liu, Y. (2019). Highly sensitive compression sensors using three-dimensional printed polydimethylsiloxane/carbon nanotube nanocomposites. *Journal of Intelligent Material Systems and Structures*, 30(8), 1216-1224.
182. Herren, B., Larson, P., Saha, M.C., and Liu, Y. (2019). Enhanced Electrical Conductivity of Carbon Nanotube-Based Elastomer Nanocomposites Prepared by Microwave Curing. *Polymers*, 11(7), 1212.
183. Chavez, L.A., Regis, J.E., Delfin, L.C., Garcia Rosales, C.A., Kim, H., Love, N., Liu, Y., and Lin, Y. (2019). Electrical and mechanical tuning of 3D printed photopolymer–MWCNT nanocomposites through in situ dispersion. *Journal of Applied Polymer Science*, 136(22), 47600.
184. Renteria, A., Diaz, J.A., He, B., Renteria-Marquez, I., Chavez, L.A., Regis, J.E., Liu, Y., Espalin, D., Tseng, T.-L.B., and Lin, Y. (2019). Particle size influence on material properties of BaTiO 3 ceramics fabricated using freeze-form extrusion 3D printing. *Materials Research Express*.
185. Renteria, A., Fontes, H., Diaz, J.A., Regis, J.E., Chavez, L.A., Tseng, T.-L.B., Liu, Y., and Lin, Y. (2019). Optimization of 3D printing parameters for BaTiO3 piezoelectric ceramics through design of experiments. *Materials Research Express*, 6(8), 085706.
186. Abshirini, M., Charara, M., Liu, Y., Saha, M., and Altan, M.C. (2018). 3D printing of highly stretchable strain sensors based on carbon nanotube nanocomposites. *Advanced Engineering Materials*, 20(10), 1800425.
187. Chowdhury, S., Olima, M., Liu, Y., and Saha, M. *Carbon nanofiber and PDMS based nanocomposite with sensing functions*. in *ASME 2016 International Mechanical Engineering Congress and Exposition*. 2016. American Society of Mechanical Engineers Digital Collection.
188. Liu, Y., Rajadas, A., and Chattopadhyay, A. (2012). A biomimetic structural health monitoring approach using carbon nanotubes. *Jom*, 64(7), 802-807.
189. Zou, J., Liu, Y., Shan, B., Chattopadhyay, A., and Dai, L.L. (2014). Early damage detection in epoxy matrix using cyclobutane-based polymers. *Smart Materials and Structures*, 23(9), 095038.
190. Luo, W., Liu, Y., and Saha, M. *CNT Bucky Paper Enhanced Sandwich Composites for In-Situ Load Sensing*. in *ASME 2017 international mechanical engineering congress and exposition*. 2017. American Society of Mechanical Engineers Digital Collection.

191. Shang, W. and Liu, Y. *Strain Sensing Using Hybrid Nanocomposite Membrane*. in *ASME 2016 International Mechanical Engineering Congress and Exposition*. 2016. American Society of Mechanical Engineers Digital Collection.
192. Liu, Y., Mohanty, S., and Chattopadhyay, A. *A Gaussian Process based prognostics framework for composite structures*. in *Modeling, Signal Processing, and Control for Smart Structures 2009*. 2009. International Society for Optics and Photonics.
193. Liu, Y., Mohanty, S., and Chattopadhyay, A. *Prediction of fatigue damage and residual useful life for composite structures using passive sensing*. in *7th International Workshop on Structural Health Monitoring: From System Integration to Autonomous Systems, IWSHM 2009*. 2009. DEStech Publications.
194. Kim, S.B., Liu, Y., Liu, K., and Chattopadhyay, A. *An Integrated Effort for the SHM of On-Orbit Satellite Boom Structures*. in *51st AIAA/ASME/ASCE/AHS/ASC Structures, Structural Dynamics, and Materials Conference 18th AIAA/ASME/AHS Adaptive Structures Conference 12th*. 2010.
195. Liu, Y., Kim, S.B., and Chattopadhyay, A. *Structural health monitoring of boom architectures for on-orbit satellites using system identification techniques*. in *51st AIAA/ASME/ASCE/AHS/ASC Structures, Structural Dynamics, and Materials Conference 18th AIAA/ASME/AHS Adaptive Structures Conference 12th*. 2010.
196. Liu, Y., Kim, S.B., Chattopadhyay, A., and Doyle, D. *Damage Localization in Complex Composite Panels Using Guided Wave Based Structural Health Monitoring System*. in *ASME 2011 Conference on Smart Materials, Adaptive Structures and Intelligent Systems*. 2011. American Society of Mechanical Engineers.
197. Wang, S., Tran, T., Xiang, L., and Liu, Y. *Non-Destructive Evaluation of Composite and Metallic Structures using Photo-Acoustic Method*. in *AIAA Scitech 2019 Forum*. 2019.
198. Wang, S., Xiang, L., Liu, Y., and Liu, H. *Photo-Acoustic Based Non-Contact and Non-Destructive Evaluation for Detection of Damage Precursors in Composites*. in *ASME 2018 International Mechanical Engineering Congress and Exposition*. 2018. American Society of Mechanical Engineers Digital Collection.
199. Liu, Y., Fard, M.Y., Kim, S.B., Chattopadhyay, A., and Doyle, D. *Damage detection in composite structures using Lamb wave analysis and time-frequency approach*. in *Sensors and Smart Structures Technologies for Civil, Mechanical, and Aerospace Systems 2011*. 2011. International Society for Optics and Photonics.
200. Liu, Y., Johnston, J., and Chattopadhyay, A. *Non-Destructive evaluation of composite adhesive kissing bond*. in *ASME 2013 International Mechanical Engineering Congress and Exposition*. 2013. American Society of Mechanical Engineers Digital Collection.
201. Liu, Y. and Sodano, H.A. *An investigation into active piezoelectric nanocomposites for distributed energy harvesting*. in *Active and Passive Smart Structures and Integrated Systems 2008*. 2008. International Society for Optics and Photonics.
202. Lin, Y., Liu, Y., and Sodano, H.A. (2009). Hydrothermal synthesis of vertically aligned lead zirconate titanate nanowire arrays. *Applied Physics Letters*, 95(12), 122901.
203. Liu, Y., Yekani Fard, M., and Chattopadhyay, A. *A Statistical Approach to Investigate Temperature Effects on Guided Wave Based Structural Health Monitoring*. in *53rd AIAA/ASME/ASCE/AHS/ASC Structures, Structural Dynamics and Materials Conference 20th AIAA/ASME/AHS Adaptive Structures Conference 14th AIAA*.